2012

The effect of inorganic fillers on the properties of wood plastic composites

Birm June Kim
Louisiana State University and Agricultural and Mechanical College

THE EFFECT OF INORGANIC FILLERS ON THE PROPERTIES OF WOOD PLASTIC COMPOSITES

A Dissertation

Submitted to the Graduate Faculty of the
Louisiana State University and
Agricultural and Mechanical College
in partial fulfillment of the
requirements for the degree of
Doctor of Philosophy

In

The School of Renewable Natural Resources

by
Birm June Kim
B.S., Kookmin University, February 1997
M.S., Seoul National University, February 2004
May 2012

ACKNOWLEDGEMENTS

Many people contributed to the successful completion of this dissertation.

First of all, I cordially appreciate my committee chair, Dr. Qinglin Wu for his guidance, advice, encouragement and support throughout my PhD program. His talent and diligence have thoroughly motivated me and will shine on me in my future career.

I also greatly appreciate my committee members, Dr. Cornelis F. de Hoop, Dr. Ioan I. Negulescu, Dr. Sun Joseph Chang, Dr. Sunggook Park, and Dr. W. David Constant. Their suggestions and advices were invaluable and constructive in my research work and dissertation. It has been an honor and privilege for me to have them on my committee.

I acknowledge my laboratory fellows and friends, Dr. Chengjun Zhou, Dr. Xia Guan, Mr. Jingquan Han, Mr. Runzhou Huang, Mr. Kai Chi and Dr. Peng Li for their help on experiments. Special thanks go to Dr. Fei Yao and Dr. Yanjun Xu, my former laboratory fellows, for their suggestions and discussions on my research.

I am grateful to my parents, Sang-Eon Kim and Gi-Joo Kim for their love, care and support. Also, I appreciate that my parents-in-law, Jae-Heui Park and Sook-Hee Jun for their love, concern and encouragement.

Last but not least, I am heartily indebted to my wife, Sun-Young Park for her patience, devotion, sacrifice, and endless love. She is the one who should get the credit for each and every piece of success that I have achieved. She deserves it.

Financial support from USDA-NIFA Biomass Initiative Program (Award Number: 68-3A75-6-508) and the National Nature Science Foundation of China (Award Number: 31010103905) is greatly appreciated.

TABLE OF CONTENTS

LIST OF TABLES

LIST OF FIGURES

NOMENCLATURE

ANOVA: analysis of variance

A-TL: averaged sound transmission loss

CC: calcium carbonate

CTE: coefficient of thermal expansion

DSC: differential scanning calorimetry

DTG: derivative thermal gravimetric

FTIR: fourier transform infrared

GBP: ground bamboo particle

GF: glass fiber

HDPE: high density polyethylene

IM: impact strength

LDPE: low density polyethylene

MA: maleic anhydride

MAPE: maleic anhydride grafted polyethylene

MOE: modulus of elasticity

MOR: modulus of rupture

M-region: mass controlled region

NCC: natural calcium carbonate

NF: natural fiber

NFPC: natural fiber/polymer composite

PCC: precipitated calcium carbonate

PP: polypropylene

PVC: poly (vinyl chloride)

RBF: refined bamboo fiber

R_{FE}: experimental resonance frequency

R_{FS1}: stiffness-1 resonance frequency

R_{FS2}: stiffness-2 resonance frequency

$R_{S1\text{-}M\text{-}IP}$: intersection point from stiffness-1 to mass law predictions

$R_{S2\text{-}M\text{-}IP}$: intersection point from stiffness-2 to mass law predictions

R-PP/PE: recycled PP/PE

SEM: scanning electron microscope

S-region: stiffness controlled region

TG: thermogravimetric

TGBP: silane treated GBP

TL: sound transmission loss

TRBF: silane treated RBF

TS: thickness swelling

V-HDPE: virgin HDPE

WA: water absorption

WF: wood fiber or wood flour

WPC: wood plastic composite

XPS: X-ray photoelectron spectroscopy

XRD: X-ray diffraction

ABSTRACT

The effect of inorganic fillers including precipitated calcium carbonate (PCC), glass fiber (GF), and nano-clay on properties of structured WPCs was investigated.

In PCC-bamboo-polymer hybrid composites, tensile and flexural moduli were improved with increasing PCC content. After silane treatment of bamboo, RBF-filled hybrid composites showed better mechanical properties compared to those of GBP-filled hybrid composites. The hybrid composites showed 3-4 times higher modulus than those of PCC-filled composites at high PCC levels.

Various property differences were observed between weak- and strong-core coextruded systems with shell composition changes. While the weak-core systems showed improved flexural strengths compared to their core-only control, the strong-core systems had lowered flexural strengths. In both systems, impact strengths increased at low shell filling levels but decreased at high shell filling levels. Impact fracture types varied with core quality and shell filling composition. Coextruded composites with treated PCC-filled shell showed better water absorption (WA) property compared to core-only controls and coextruded composites with high WF-filled shell. Plastic-only shell increased overall coefficient of thermal expansion (CTE) of coextruded composites, but filled shells led to the CTE decreases of coextruded composites. GF in shell behaved as an effective reinforcement for coextruded composites. The comparisons of flexural property among different core systems show that GF reinforcements were optimized at high GF loadings in a shell layer and GF alignments in the shell layer also played an important role. In coextruded composites with different shell thicknesses, the flexural property enhanced with the increase of shell bending modulus and strength at a given shell thickness. When the flexural property of shell was less than that of core, the increase of shell thickness led to reduced

flexural property. On the other hand, when the flexural property of shell was higher than that of core, the opposite was true.

In sound transmission loss (TL) testing, the stiffness and surface density were major factors influencing the sound insulation property of materials. The experimental TL results showed that the addition of clay or PCC and/or wood fiber (WF) fillers led to the increases of general resonance frequencies and TL in filled composites. However, at high filling levels, composite stiffness decreases led to TL reduction. The experimental TL curves of filled HDPE and WPCs were well approximated with the combined TL predictions from their corresponding stiffness-1 and stiffness-2 TL for S-region and mass law TL for M-region.

CHAPTER 1 INTRODUCTION

1.1 BACKGROUND

Wood/natural fiber plastic composites (WPCs) have attracted considerable attention in recent years. Many emerging applications for WPCs include decking, building, automobile, and infrastructure (Klyosov 2007; Selke and Wichman 2004). Polyethylene (PE), polyvinylchloride (PVC) and polypropylene (PP) hold a major share of resins used in WPC. Compared with traditional glass fiber and mineral fillers, wood fillers are known to be less expensive, lighter, sustainable, and less abrasive to processing machines. To enhance product performance, significant effort has been made to study WPC's properties as affected by raw material compositions, wood-plastic interfacial bonding, and composite processing parameters (Lu, Wu, and McNabb 2000; Mohanty, Misra, and Drzal 2001).

WPC is the combination form of raw materials such as fillers (organic and inorganic), plastic, and additives (Nwabunma and Kyu 2008). Among the raw materials, fillers are solid materials added to plastics mainly to reduce cost and improve properties (Kroschwitz 1990; Whelan 1994). Typically, fillers are inexpensive, thus make the filled plastic composites less expensive. Also, the fillers can lead to improved mechanical properties of filled composites by restricting molecular mobility of plastic matrices (Fitzgerald, Ferrar, and Binga 1998) through morphology changes (Okamoto et al. 1996). Therefore, the proper selection and use of filler combinations are very important in balancing the cost and performance of WPC.

In general, fillers are divided into organic and inorganic fillers. Organic fillers include wood, jute, and agriculture fibers. Inorganic fillers include minerals such as calcium carbonate (CC), talc, and mica and synthetic fibers like glass, ceramic and carbon fibers. The effect of inorganic fillers on the composite property strongly depends on the size, shape, content, surface

characteristics, aspect ratio, and dispersion of the fillers (Chan et al. 2002). Usually, the addition of inorganic fillers into polymeric materials enhances the mechanical properties (mainly, stiffness) and dimension stability of filled composites (Nwabunma and Kyu 2008; Wypych 2010). CC, talc, and mica are quite common inorganic fillers used in plastic industry and replace the much more expensive plastic. Among the CCs, precipitated calcium carbonate (PCC) has a more even and smaller size. PCC filled PP showed more significant effects on the brittleness, ductility and toughness than talc and mica (Bramuzzo, Savadori, and Bacci 1985). PCC of sugar origin is considered as waste and therefore, its new value-added applications in WPC are needed. Glass fibers (GFs) and various nano-scale fillers (e.g., montmorillonite, graphite nanoflake, carbon nanotube, etc) have been reported to enhance strength and barrier property of filled plastic composites (Bramuzzo, Savadori, and Bacci 1985; Gong et al. 2004; Jiang et al. 2003). For WPC applications, the use of high strength fillers is often cost-prohibitive. However, the application of these materials at critical locations for structured WPC can lead to significant property enhancement while maintaining competitive costs.

Coextruded wood plastic composite with a core-shell structure has been recently developed and used to enhance performance characteristics of WPC (Jin and Matuana 2010; Stark and Matuana 2007). By proper combination of constituting layers, one can achieve a balance of such properties as light weight, high strength, high stiffness, wear resistance, biological resistance, unusual thermal expansion characteristics, appearance, etc (Jin and Matuana 2010; Kim and Wu 2012; Stark and Matuana 2007; Yao and Wu 2010). Fundamental understanding of the interactions between shell and core layer with different structure (e.g., thickness) and material combinations is, however, needed to achieve desired product performance. The incorporation of fillers in a shell layer of coextruded WPCs has positively

affected the mechanical properties of core-shell structured composites. However, cost and performance effective shells are still needed to achieve desired composite performance.

Various sound barrier materials including concrete, brick, metal, plastic, wood and composites have been used to reduce noise levels. Among the materials, viscoelastic polymer materials show great potential for damping sound and vibration. However, most polymer materials have lower elastic modulus and surface density, leading to poor sound insulating performances when solely used as a sound barrier (Wang et al. 2011). WPCs, as new generation green composites, offer advantages in relatively light weight, excellent recyclability, low toxicity and high thermal stability. Thus, their application as sound barrier uses can offer a competitive alternative to the conventional sound barriers. For this purpose, acoustic properties of structured WPCs, influenced by composite formulations need to be fully understood.

1.2 OBJECTIVES

The objectives of the research described in this work are:

1) To investigate combined influence of PCC content, bamboo fiber type, and surface silane treatment on the properties of filled bamboo plastic composites;

2) To elucidate the effect of treated PCC and WF loadings in the shell layer on the mechanical, WA and CTE properties of coextruded WPCs with two different core systems;

3) To evaluate the effect of various GF contents in a shell layer and shell thickness changes on the mechanical properties of coextruded WPCs in combination with three core systems (low, moderate, and strong); and

4) To develop an experimental procedure for studying sound insulation properties of mineral-filled solid plastic composites and WPCs using an impedance tube method, and to

investigate the effect of mineral type and loading levels on transmission loss (TL) properties of the composites.

1.3 ORGANIZATION OF DISSERTATION

Chapter 1 provides an overall introduction of this research and the structure of this dissertation.

Chapter 2 investigates the mechanical and WA properties of recycled-PP/PE composites reinforced with different PCC content, bamboo fiber type and fiber surface treatment.

Chapter 3 studies the effect of treated PCC and WF loadings in the shell layer on the mechanical, WA and CTE properties of coextruded WPC with two different core systems.

Chapter 4 discusses the effect of GF contents in a shell layer and shell thickness changes on the flexural and impact properties of coextruded WPCs in combination with three core systems (low, moderate, and strong).

Chapter 5 presents sound insulation property of HDPE composites and WPCs filled with different mineral types and loading levels.

Chapter 6 provides overall conclusions of this dissertation.

1.4 REFERENCES

Bramuzzo, M., A. Savadori, and D. Bacci. 1985. Polypropylene Composites - Fracture-Mechanics Analysis of Impact Strength. *Polymer Composites* 6: 1-8.

Chan, C.M., J.S. Wu, J.X. Li, and Y.K. Cheung. 2002. Polypropylene/calcium carbonate nanocomposites. *Polymer* 43: 2981-92.

Fitzgerald, J.J., W.T. Ferrar, and T.D. Binga. 1998. Fatigue-resistant silicone elastomer formulations. *Journal of Applied Polymer Science* 70: 1633-41.

Gong, F.L., M. Feng, C.G. Zhao, S.M. Zhang, and M.S. Yang. 2004. Thermal properties of poly(vinyl chloride)/montmorillonite nanocomposites. *Polymer Degradation and Stability* 84: 289-94.

Jiang, H.H., D.P. Kamdem, B. Bezubic, and P. Ruede. 2003. Mechanical properties of poly(vinyl chloride)/wood flour/glass fiber hybrid composites. *Journal of Vinyl & Additive Technology* 9: 138-45.

Jin, S., and L.M. Matuana. 2010. Wood/plastic composites co-extruded with multi-walled carbon nanotube-filled rigid poly(vinyl chloride) cap layer. *Polymer International* 59: 648-57.

Kim, B.-J., and Q.L. Wu. 2012. Mechanical and Physical Properties of Core-Shell Structured Wood Plastic Composites: Effect of Shells with Hybrid Mineral and Wood Fillers. *Composite Part B, In review*.

Klyosov, A.A. 2007. *Wood-plastic composites*. Hoboken, New Jersey: John Wiley & Sons Inc.

Kroschwitz, J.I. 1990. *Concise Encyclopedia of Polymer Science and Engineering*, 1st ed: Wiley-Interscience.

Lu, J.Z., Q.L. Wu, and H.S. Mcnabb. 2000. Chemical coupling in wood fiber and polymer composites: A review of coupling agents and treatments. *Wood and Fiber Science* 32: 88-104.

Mohanty, A.K., M. Misra, and L.T. Drzal. 2001. Surface modification of natural fibers and performance of the resulting biocomposites: An overview. *Comp Interf.* 8: 313-43.

Nwabunma, D., and T. Kyu. 2008. *Polyolefin composites*: John Wiley & Sons Inc.

Okamoto, M., Y. Shinoda, T. Okuyama, A. Yamaguchi, and T. Sekura. 1996. Synthesis and crystallization behaviour of an intercalated compound of poly(ethylene terephthalate) and mica. *Journal of Materials Science Letters* 15: 1178-9.

Selke, S.E., and I. Wichman. 2004. Wood fiber/polyolefin composites. *Composites Part a-Applied Science and Manufacturing* 35: 321-6.

Stark, N.M., and L.M. Matuana. 2007. *Coating WPCs using co-extrusion to improve durability*. In *Conference for Coating Wood and Wood Composites: Designing for Durability*, 1-12. Seattle, WA,.

Wang, X., F. You, F.S. Zhang, J. Li, and S.Y. Guo. 2011. Experimental and Theoretic Studies on Sound Transmission Loss of Laminated Mica-Filled Poly(vinyl chloride) Composites. *Journal of Applied Polymer Science* 122: 1427-33.

Whelan, T. 1994. *Polymer Technology Dictionary*. London, UK: Chapman & Hall.

Wypych, G. 2010. *Handbook of fillers*, 3th ed: ChemTec Publishing.

Yao, F., and Q.L. Wu. 2010. Coextruded Polyethylene and Wood-Flour Composite: Effect of Shell Thickness, Wood Loading, and Core Quality. *Journal of Applied Polymer Science* 118: 3594-601.

CHAPTER 2 PERFORMANCE OF BAMBOO PLASTIC COMPOSITES WITH HYBRID BAMBOO AND PRECIPITATED CALCIUM CARBONATE FILLERS[1]

2.1 INTRODUCTION

Natural fibers have been widely used as reinforcing fillers in plastic composites due to low cost, light weight and recyclability.(Hristov, Lach, and Grellmann 2004; Mohanty, Misra, and Drzal 2001) Bamboo fiber is one of the traditionally used natural fibers due to its fast growth, abundant availability and good mechanical properties from longitudinally aligned fiber structure.(Han et al. 2008; Shin and Yipp 1989; Takaya and Tadashi 1970) It is considered as one of the alternatives for wood resources and the use of bamboo fiber in composites can help save wood resources.(Han et al. 2008) However, bamboo fibers are more brittle compared to other natural fibers.(Okubo, Fujii, and Yamamoto 2004) Therefore, to enhance their reinforcing effect in plastic composite, certain treatments of original bamboo fiber are needed. Alkali (Cantero et al. 2003; Gassan and Bledzki 1999) and acid (Winandy, Stark, and Horn 2008) based processes comprised most of current fiber pre-treatments, but the use of chemical agents and high energy consumption of the process can lead to significant environmental problems and high costs. Heat treatment with or without refining has also been introduced as natural fiber treatment options. For instance, it was shown that high temperature steam treatment improved dimensional stability of wood products through chemical modification of wood components.(Giebeler 1983; Inoue and Norimoto 1991) Thermomechanical pulping through steam aided refining process showed lower energy cost and increased fiber strength.(Vena 2005) While pre-treatments show improved properties of natural fibers, the pre-treated fibers still have hydrophilic characteristics different from hydrophobic plastics. Thus, to increase the compatibility between fiber and plastic

[1] Reprint in part with permission from Polymer Composites
Kim, B.J., F. Yao, G. Han, Q. Wu. 2012. Performance of bamboo plastic composite with hybrid bamboo and precipitated calcium carbonate fillers. *Polymer Composites* 33: 68-78.

matrix, various coupling agents have been used.(Lu, Wu, and Mcnabb 2000) Maleic anhydride (MA) grafted polymers are most widely utilized coupling agents. These MA copolymers lead to the compatibility increase of treated fibers with plastic matrix through ester linkages and hydrogen bonds between fiber and anhydride groups,(Felix and Gatenholm 1991; Lu, Negulescu, and Wu 2005) readily improved mechanical properties. The use of silane cross-linking agents has also been tried in the composites. Nachtigall et al.(Nachtigall, Cerveira, and Rosa 2007) tested the properties of polypropylene (PP) / wood fiber (WF) composites with same concentration of silane and MA coupling agent. The result suggested that composites with silane treatment showed better tensile strength, lower water absorption and more homogeneous morphology than the composites made with MA. Kim et al.(Kim et al. 2011) further investigated the effect of various silane coupling agents for PP with NaOH pre-treated WF and the whole silane treated WF filled composites showed significantly improved tensile strength, flexural strength and water absorption property compared to untreated WF filled composite.

Calcium carbonate (CC) is one of the most abundant and stable minerals, generally divided into natural calcium carbonate (NCC) and precipitated calcium carbonate (PCC). While NCC is acquired from quarrying in mines, PCC is manufactured by chemical processes.(Katz and Milewski 1987) In plastic manufacturing, the use of PCC as a filler or an extender is prevalent (Katz and Milewski 1987). The size, shape and content of PCC can affect mechanical properties of composites by modifying micro morphology of base plastics.(Bramuzzo, Savadori, and Bacci 1985; da Silva et al. 2002; Maiti and Mahapatro 1991; Misra, Deshmane, and Yuan 2007) Bramuzzo et al.(Bramuzzo, Savadori, and Bacci 1985) tested mechanical properties of PP composites with several inorganic fillers and reported that PCC showed more significant effect on brittleness, ductility and toughness of PP than other fillers. Maiti et al.(Maiti and Mahapatro

1991) investigated tensile properties of i-PP/PCC composite and showed modulus increase and strength decrease with the increase of PCC loading. da Silva et al.(da Silva et al. 2002) reported that when a small amount of PCC was added to the PP matrix, an increase in impact strength was observed. But, at high PCC loadings, the impact strength was decreased. They mentioned that this result was due to the difference of PCC dispersion in plastic matrix. Deshmane et al.(Misra, Deshmane, and Yuan 2007) evaluated the difference in impact behavior from neat HDPE to CC-HDPE composites and identified the reinforcement of composites through observing changes of structure and mechanical behaviors processed under similar conditions. In their investigations, they reported that the nucleating effect of CC reduced the spherulite size of base polymer, which led to some deleterious effects on yield stress.

Several commercial wood plastic composite (WPC) deck boards contain a certain amount of CC (e.g., Geo Deck^{TM} by LDI Composites) and talc (e.g., Timber Tech^{TM} by Timber Tech Company).(Klyosov 2007) The use of mineral fillers in the product can help replace much more expensive plastic, increase stiffness of the filled products, and render the plastic more flame resistant. For example, it was shown that 12-32% (w/w) filling ranges of CC with a 7-μm median particle size increased the flexural modulus of HDPE-based WPC up to 64%. Also, the flexural strength of 200-mesh CC (27.5%, w/w) and 325-mesh CC (27.5%, w/w) filled PP composite with 40-mesh wood (27.5%, w/w) showed an increased trend from 38.6-44.8 to 45.5-51.5 MPa, respectively.(Klyosov 2007) However, the use of PCC in WPC has not been reported (e.g., PCC from sugar making process).(Echeverria and Holst 2005)

In this research, PCC of sugar origin and bamboo fiber were used as fillers for natural fiber plastic composites from recycled polypropylene and polyethylene (R-PP/PE) resin. The

objectives of the research were to investigate combined influence of PCC content, bamboo fiber type and silane treatment on the properties of PCC filled bamboo plastic composites.

2.2 EXPERIMENTAL

2.2.1 Materials and Preparation

R-PP/PE resin, ground bamboo particle (GBP, ≤ 20 mesh), thermo-mechanically refined bamboo fiber (RBF, ≤ 20 mesh) and PCC were used as raw materials. Originally, R-PP/PE (about 95% PP and 5% PE) was a commingled plastic in a fluffy form and it was pelletized using a twin-screw extrusion machine before being blended with other raw materials. GBP was prepared from bamboo flakes through grinding and screening using a granulator with a 20 mesh screen. RBF was produced by refining bamboo chips at 160°C for 10 min using a KRK-2503 steam-aided disc refining system (Kumagai Riki Kogyo Co., Tokyo, Japan). Silane coupling agent (Z-6094) from the DOW Corning Co. (Midland, MI, USA) was utilized to treat GBP and RBF. The composition of silane was aminoethyl-aminopropyl-trimethoxysilne (> 60 wt%) and the density of this organo-silane was 1.02 g/cm^3.

Silane treatments of GBP and RBF were made by immersion methods. GBP and RBF were firstly oven-dried at 85°C for 24 hr to reach moisture content level less than 2%. They were immersed in an aqueous solution (methanol:water = 9:1) including silane coupling agent (3 % of the weight of bamboo fiber) at 25°C for 1 hr. Before treatments, the silane aqueous solution was pre-hydrolyzed for over 30min. After immersion, silane treated bamboo fiber was dried at 85°C for 24 hr again. The treated fiber was stored in plastic bags prior to uses. PCC was obtained from Domino Sugar Company (New Orleans, LA, USA). It was dried at 85°C for 24 hr and screened with a 100-mesh screen.

2.2.2 Composite Manufacturing

A CW Brabender Intelli-Torque Twin-Screw Extruder **(**CW Brabender Instruments, South Hackensack, NJ) was used to blend R-PP/PE, bamboo fiber and PCC hybrid composites.

R-PP/PE and PCC were blended first as a base material (50 wt% of plastic and 50 wt% of PCC). After that, the pellets were diluted in the variation of PCC (6, 12, 18 wt%, respectively) and re-compounded with bamboo fiber (40 wt%) in the blends of R-PP/PE and PCC (60 wt%) and then extruded in the second step. The blending temperature profile was 155°C, 175°C, 180°C, 180°C, and 170°C from the feeding zone to die and the extruder rotation speed was 90 rpm. The extruded blends were pelletized and then dried in an oven at 85°C for 24 hr.

Standard test samples were made through a Battenfeld 35-Ton Plus Injection Molding Machine (Wittmann Battenfeld GmbH, Kottingbrunn, Austria) at an injection temperature of 175°C.

2.2.3 Material Characterizations

Thermal properties of bamboo fiber and PCC were measured using TA Q-50 thermo gravimetric analyzer (TGA: TA Instruments, New Castle, DE). Samples were heated from 25°C to 600°C for bamboo fibers and from 25°C to 875°C for PCC at a heating rate of 10°C /min under nitrogen flow.

FT-IR analyses of bamboo fibers were performed using a Nicolet 650 analyzer (Nicolet Instrument Corporation, Madison, WI) to investigate the changes in the compositions of GBP and RBF before and after treatments. Specimens were prepared as KBr pellets (bamboo fiber: KBr = 1 : 10) and then analyzed in the range of 525–4000 cm^{-1}. The acquired FT-IR data were from the averages of 64 scans.

The morphologies of PCC and composites were analyzed by a Hitachi S-3600N VP Scanning Electron Microscope (SEM) (Hitachi Ltd., Tokyo, Japan). The samples were coated with Pt to improve the surface conductivity before observation and observed at an acceleration voltage of 15 kV.

The surface area of PCC was acquired from the multipoint Brunauer, Emmett and Teller (BET) method based on the isothermal adsorption of nitrogen. An Autosorb-1 Surface Area and Pore Size Analyzer (Quantachrome Instruments, Boynton Beach, FL) was used. Dried PCC particles were degassed first and then measured using nitrogen gas.

The specific gravity of PCC was tested with a water pycnometer according to the ASTM D854-02. Beside, the oil absorption property of PCC was carried out according to the ASTM D281-95.

X-ray Diffraction (XRD) analysis was performed using a Rigaku MiniFlex X-ray Diffractometer (Rigaku Corporation, Tokyo, Japan) to investigate the characteristics of PCC. This was measured over a range of 2θ from 10° to 70° and tested with CuKα (λ=1.5405Å) at 25°C in a reflection mode. The scanning rate and step size were 2°/min and 0.01°, respectively.

Tensile and flexural tests of manufactured composite samples were carried out using a Model 5582 Advanced Mechanical Testing System (Instron Inc., Norwood, MA). Tensile strengths were tested according to the ASTM D 638-99 and type I specimens of a dog-bone shape were used. Flexural strengths were measured according to the ASTM D 790-03. Notched izod impact strengths were measured with Tinius Olsen 92T Impact Tester (Tinius Olsen, Horsham, PA) according to the ASTM D 256-05. Five replicate samples were used for each test.

For water absorption (WA) test, samples of a nominal size (30×12×3 mm) were prepared from the injection molded plates and tested by measuring the weight of samples after 1- to 10-

week water immersion. The samples were removed from water bath at the end of each week. The WA was calculated using:

$$WA(\%) = \left(\frac{W_a - W_b}{W_b} \right) \times 100 \quad (2.1)$$

where W_a and W_b are sample weight (g) after and before soaking, respectively. Four samples were used to get average value for each test.

2.3 RESULTS AND DISCUSSION

2.3.1 Basic Properties of Bamboo Filler

Figure 2.1(a) and Figure 2.1(b) show the thermo-gravimetric (TG) and derivative thermal gravimetric (DTG) curves for RBF and GBP. The DTG curves of the two fibers represent different trends. RBF shows one cellulose peak at 340°C with a broad tail of lignin. On the other hand, GBP shows a main cellulose peak at 350°C and one shoulder of hemicellulose at 300°C with a tail of lignin.(Brebu and Vasile 2010; Yao et al. 2008) To obtain the amount of each component in bamboo fibers, deconvolutions for DTG curves of RBF and GBP were carried out by using Gaussian fitting technique. (Hughes and Sexton 1988)

Table 2.1 shows the components and their percentage amount, acquired from the deconvoluted DTG curves of GBP and RBF in the 150-600°C temperature range. It can be seen that no change in holocellulose-1 (cellulose) contents was observed, but there were some changes in lignin and holocellulose-2 (hemicellulose) contents between RBF and GBP. These changes are related to the fiber disc refining process with steam at high temperature and pressure.(Dwianto et al. 1996; Okubo, Fujii, and Yamamoto 2004; Salmen, Yin, and Berglund 2011; Winandy, Stark, and Horn 2008) Dwianto et al.(Dwianto et al. 1996) showed the initiation of hemicellulose degradation in lignocellulosic fibers from 150^{o}C and subsequent increases of cellulose crystallinity.

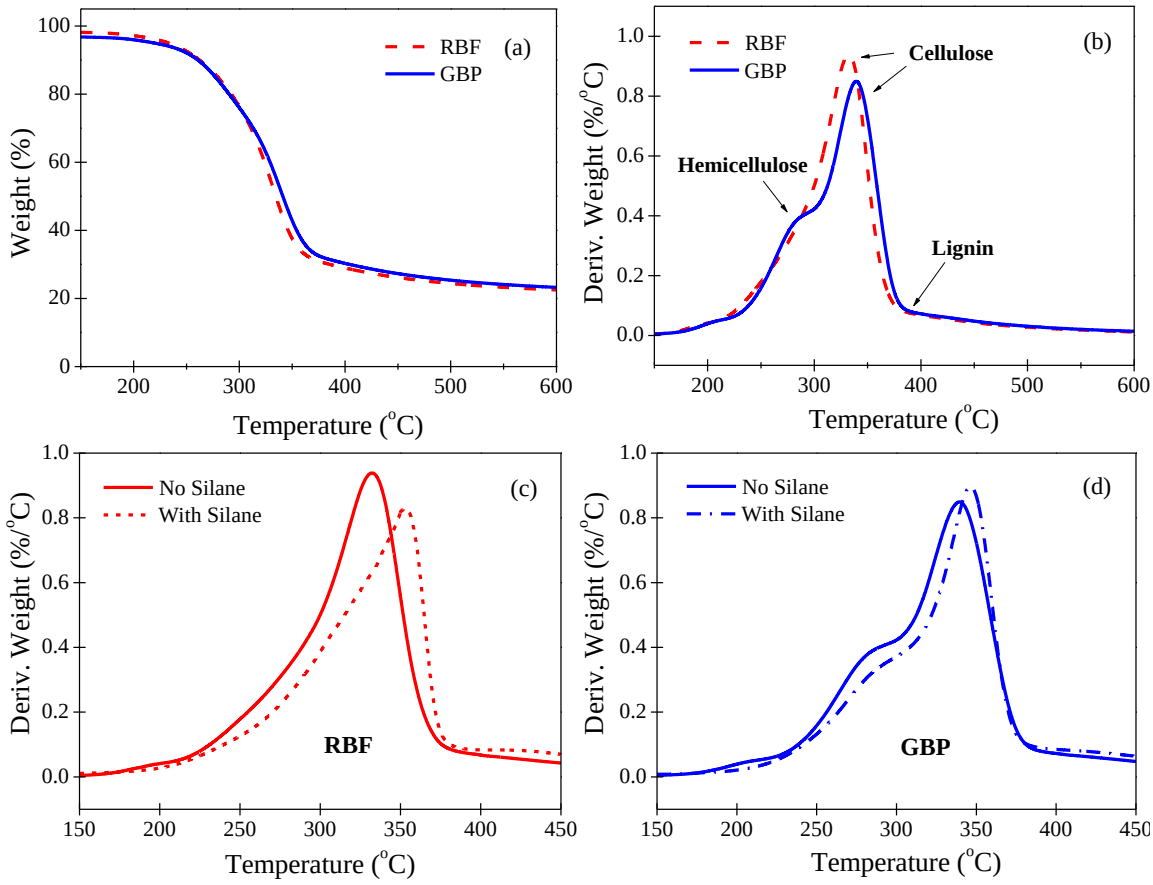

Figure 2.1 Thermogravimetric data of bamboo filler. (a) and (b): TG and DTG curves of raw RBF and GBP; (c) and (d): DTG comparison between RBF and GBP before and after silane treatment.

Table 2.1 Chemical compositions estimated from deconvoluted DTG curves for both GBP and RBF

Fiber type	Components (%)				Total (%)
	Hollocellulose-1	Hollocellulose-2	Lignin	Ash	
GBP	28.71	25.97	15.03	20.29	100
RBF	28.81	27.87	14.21	19.11	100

Also, Y Yin et al.(Salmen, Yin, and Berglund 2011) suggested that the decreases of hemicelluloses after steaming process were observed at 160^{o}C and above. Considering the published researches, the deconvoluted peak of hemicellulose in RBF might include some portion of cellulose. Comparison of deconvoluted peak temperatures of GBP and RBF (273.69°C and 277.67°C for holocellulose-2; 316.64°C and 309.11°C for holocellulose-1, respectively) allowed the determination of the cellulose portion, which is included in holocellulose-2 of RBF. The increase of holocellulose content after refining process played a significant role in the thermal stability of bamboo fibers treated with silane coupling agent. As shown in Figure 2.1(c) and Figure 2.1(d), the increase of DTG peak temperature is bigger from RBF to silane treated RBF (TRBF) (from 339.56 to 358.22°C) than from GBP to silane treated GBP (TGBP) (from 342.69 to 350.86°C). This result indicates that the refining process in RBF helped develop more silane crosslinks on the fiber surfaces.

Measured FTIR data is shown in Figure 2.2(a). The peak at 1739 cm^{-1} is assigned to the O=C–OH group of the glucuronic acid unit and the decrease of this peak indicates a split-off of the carbonyl group in hemicelluloses after steam assisted refining.(Salmen, Yin, and Berglund 2011; Sgriccia, Hawley, and Misra 2008) The comparison between RBF and GBP shows that small amount of hemicelluloses was decomposed in RBF. Among GBP, TGBP and RBF, any further remarkable differences were not shown. However, TRBF showed more critical differences. The increased intensities of the peaks at 1604 cm^{-1} and at 1510 cm^{-1} indicate the existence of silane crosslinks on the surface of TRBF after silane treatment and these changes probably resulted from the traces of NH_2 in silane coupling agent (Belgacem et al. 2004).

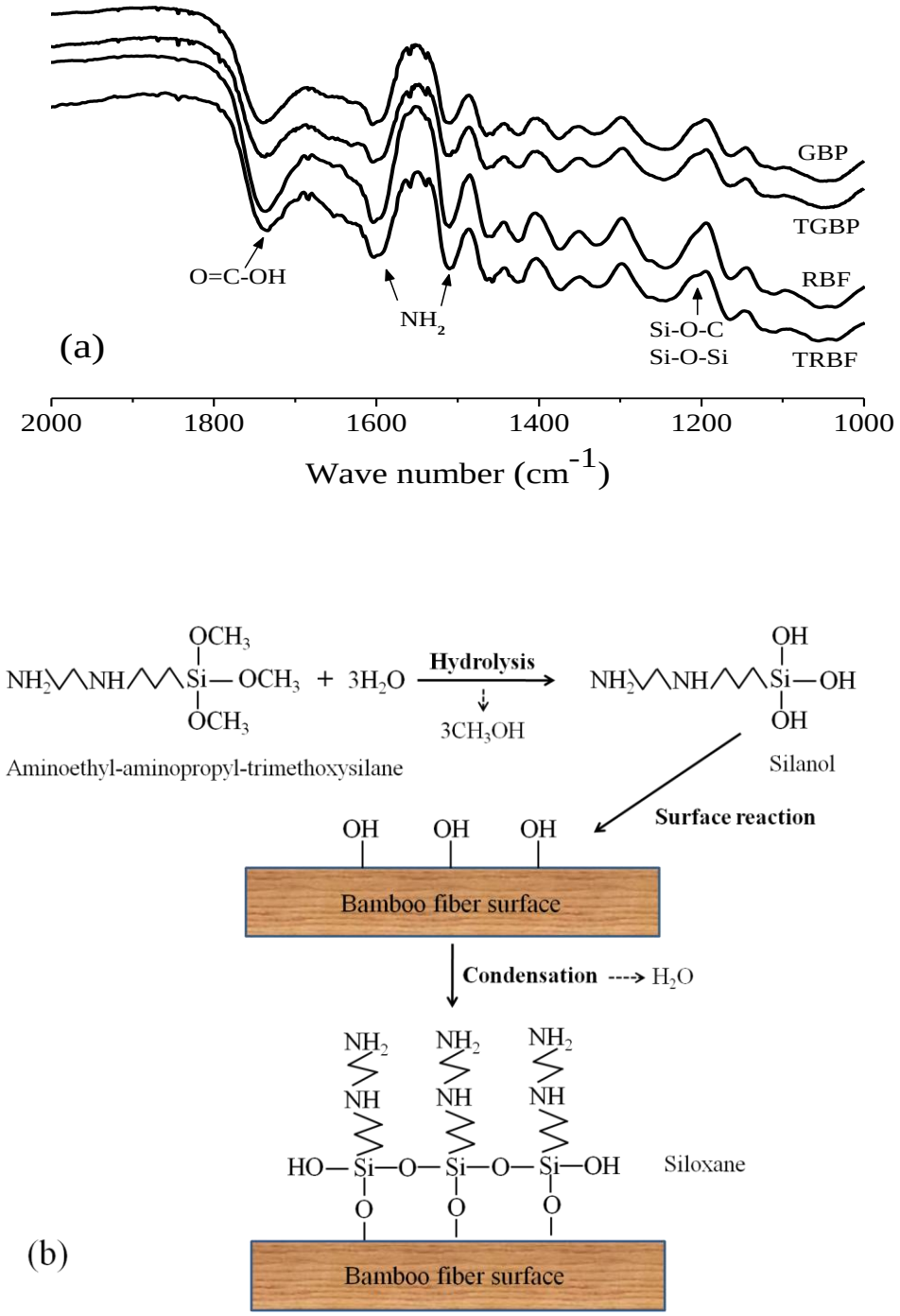

Figure 2.2 FT-IR spectra (a) of RBF and GBP before and after silane treatment and schematic diagram (b) of bamboo fiber surfaces chemically modified by silane treatment.

Besides, the small peak shown around 1203 cm^{-1}, arranged as Si-O-C or Si-O-Si band was associated with silane crosslinks.(Lee et al. 2009) Above results suggest that the silane coupling agent more effectively interacted with RBF than with GBP.

Figure 2.2(b) shows the schematic diagram transforming the hydrophilic bamboo fiber surface to hydrophobic surface by silane coupling reaction. Through silanization, hydrolysis of silane, condensation between silanols, and bond formation between siloxane and bamboo fibers were consecutively achieved.(Lee et al. 2009)

2.3.2 Basic Properties of PCC

Figure 2.3(a) shows a SEM micrograph of PCC particles at the dry state and the averaged individual particle size estimated from SEM micrograph amounts to 1.16μm. However, as shown in this figure, individual cubic PCC particles were agglomerated together and these agglomerated forms of PCC with measured mean particle size of 8.75μm were detected by the particle size analysis using laser diffraction technique in Figure 2.3(b).

Besides, surface area, specific gravity and oil absorption of the PCC were 8.685 m^2/g, 2.56 g/cm^3, and 19.8 g/100g, respectively. The property ranges of commercial CC, commonly used in plastics or WPCs are 2-24 m^2/g, 2.7–2.9 g/cm^3 and 13-21 g/100g for surface area, specific gravity and oil absorption, respectively.(Wypych 2010b) Hence, the relatively large surface area of PCC was related with smaller particle size and the somewhat reduced specific gravity of PCC presumably resulted from impurities.

The XRD patterns of PCC are given in Figure 2.4(a). Through the comparison of XRD peaks of the PCC samples with the Joint Committee on Powder Diffraction Standards (JCPDS) data for three phases (calcite, aragonite and vaterite) of CC,(Tai and Chen 2008) it can be seen

that most PCC was calcite, which is thermally stable compared with other CC phases including aragonite and vaterite. Also, the clear peaks of calcite indicate relative purity of the PCC.

Thermo-gravimetric analysis (TGA) data of the PCC is shown in Figure 2.4(b). It can be seen that a small amount of weight loss (%) occurred around 280°C and a drastic loss happened between 600 and 740°C. The loss at the higher temperature range was presumably weight loss of CO_2 ($CaCO_3 \rightarrow CaO + CO_2$). The theoretical value of CO_2 loss is 44 % for 100 % pure CC. From the TGA data, the weight loss of CO_2 was 41.99 %. Therefore, the calculated purity of PCC (purity = measured weight loss / 44 × 100) was 95.43%.(Dweck 2010) The impurity was organic matter from sugar processing. Derivative thermo-gravimetric (DTG) curve of PCC further indicates the weight loss range of the PCC. The first low and broad peak at 283.40°C was due to the decomposition of impurities included in PCC. The second high and sharp peak at 734.14°C was the mass loss of CO_2 gas from decomposition of PCC.

2.3.3 Mechanical and Morphological Properties of Bamboo-PP/PE Composites

Figure 2.5 shows the flexural strength and modulus of GBP and RBF filled composites with and without silane treatment.

For flexural strength (Figure 2.5(a)), GBP composite (GBP-C) showed a higher value than that of RBF composite (RBF-C). However, after silane treatment, the strength of TRBF composite (TRBF-C) became much higher than that of TGBP composite (TGBP-C). This result shows that after silane treatment, less lignin and more holocellulose contents of RBF induced more silane crosslinks,(Winandy, Stark, and Horn 2008) which led to the increase of flexural strength through the enhanced adhesion and compatibility with polymer matrix.

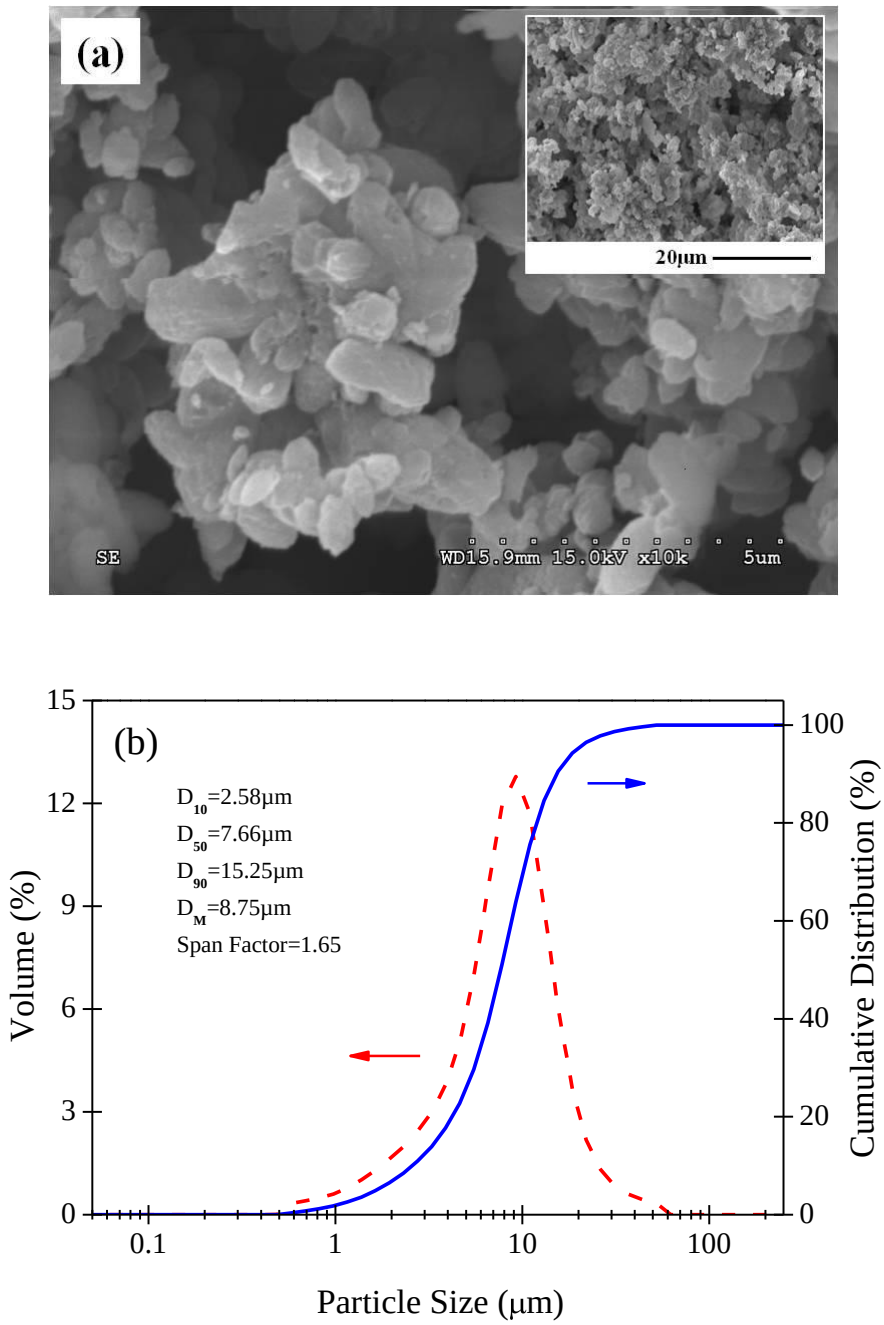

Figure 2.3 Raw PCC morphology and particle size data. (a): SEM micrograph of PCC particles; (b): measured particle size distribution based on the laser diffraction technique.

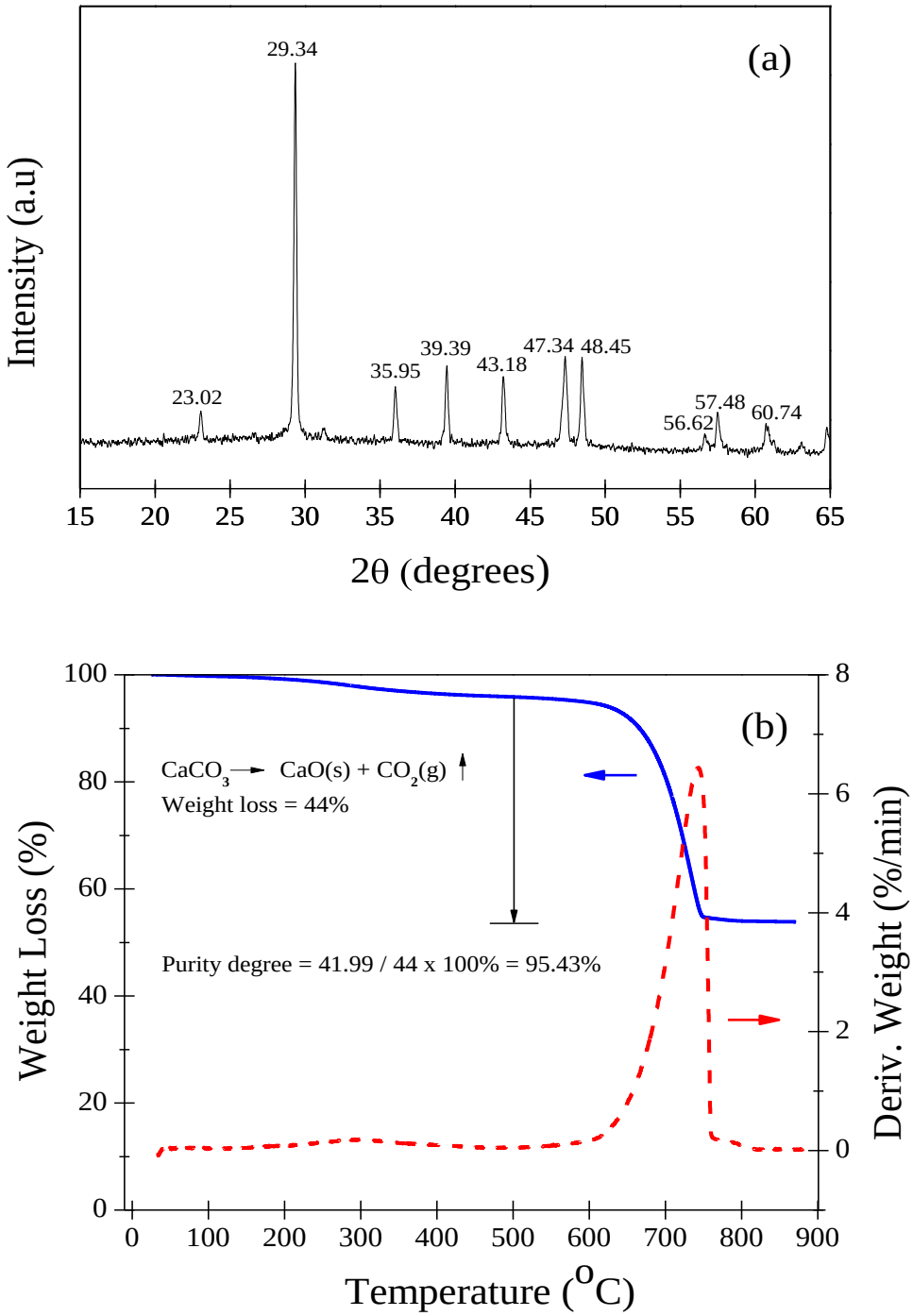

Figure 2.4 Measured XRD pattern (a) and thermal decomposition data (b) of the PCC filler.

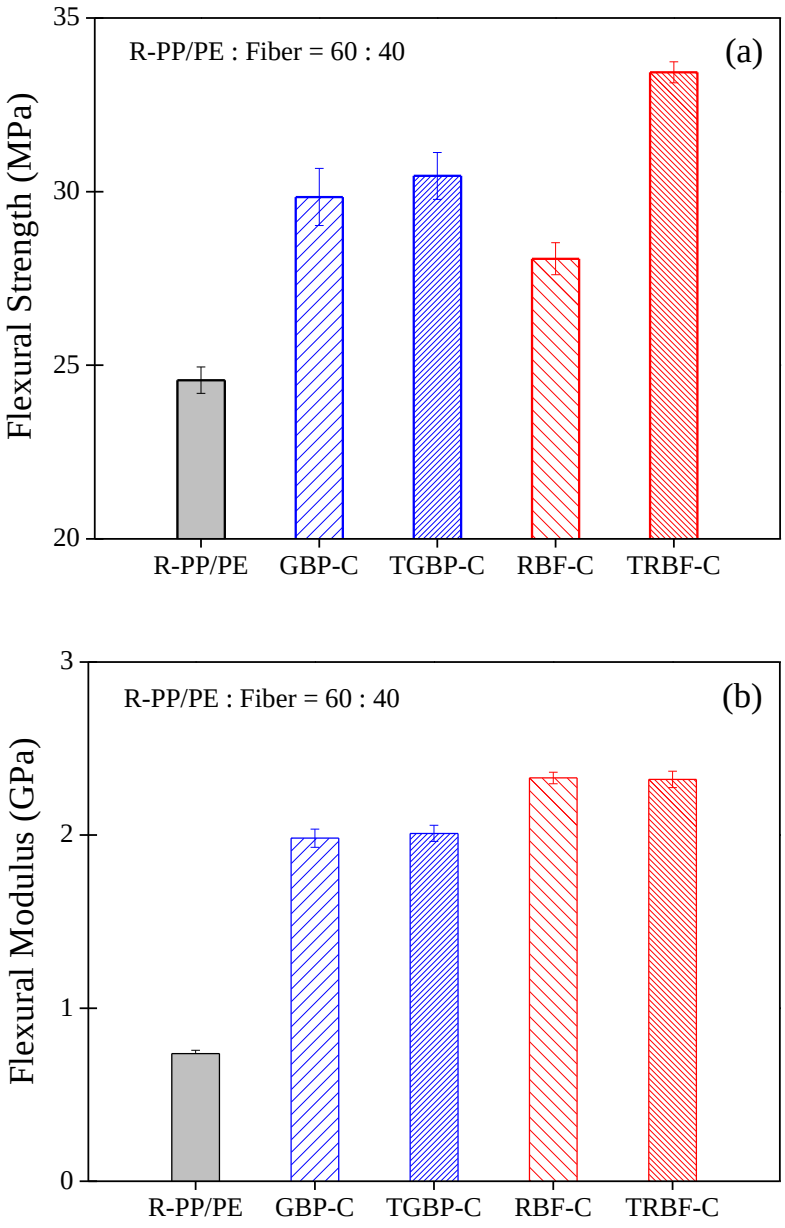

Figure 2.5 Comparison of measured flexural strength (a) and modulus (b) for R-PP/PE resin and bamboo-PCC-PP/PE composites.

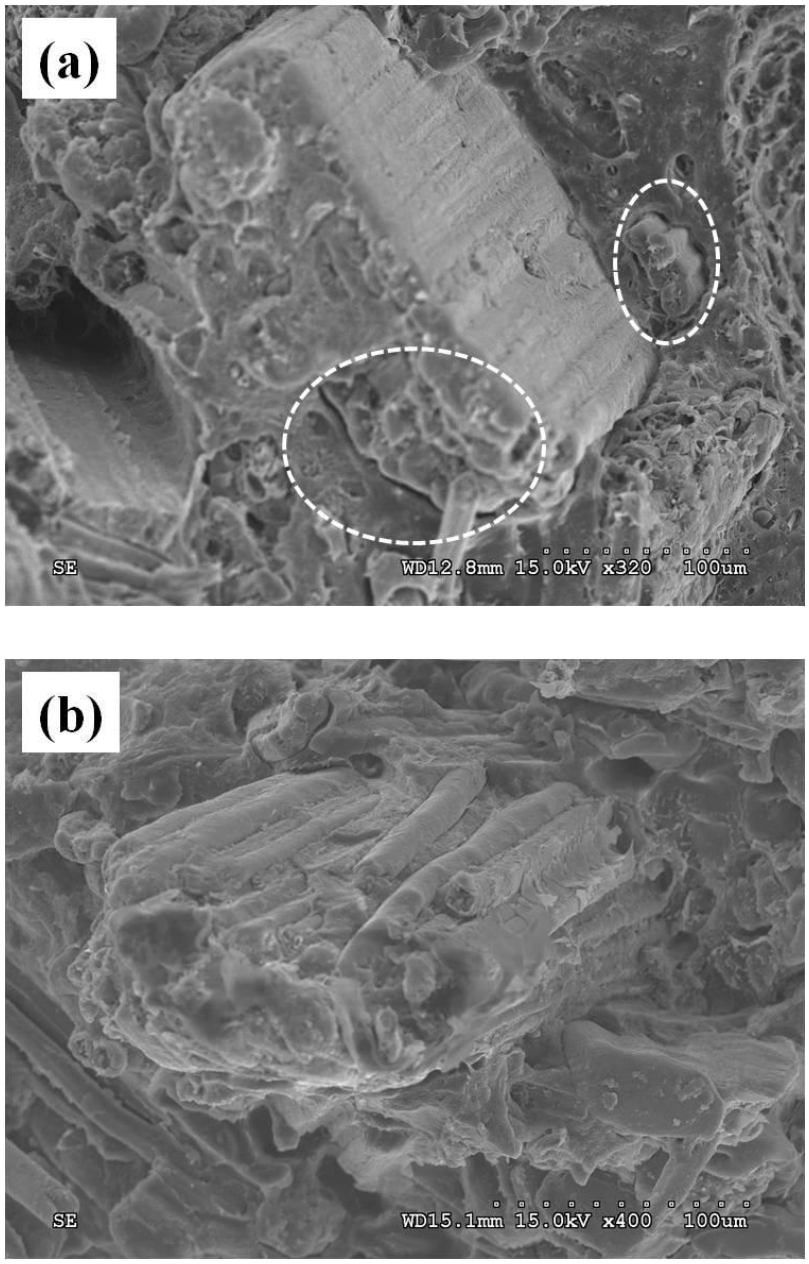

Figure 2.6 SEM micrographs of the impact fractured surfaces of TGBP (a) and TRBF (b) composites.

For flexural modulus (Figure 2.5(b)), the difference between GBP-C and RBF-C seemed to be due to the holocellulose content in bamboo fiber and an obvious effect of silane treatment was not observed.

Also, the increased adhesion after silane treatment was verified from SEM images of TGBP composite (TGBP-C) and TRBF composite (TRBF-C) as shown in Figure 2.6. Interfacial gaps between fibers and polymer are clearly seen in TGBP-C (Figure 2.6(a)). On the other hand, enhanced interfacial adhesions are observed in TRBF-C (Figure 2.6(b)).

Moreover, from these micrographs, the different fiber surfaces between RBF and GBP were also seen. The surface of TGBP was relatively smooth with no individual fibers. TRBF had a rough surface showing exposed individual fibers or fiber bundles. Similar results were observed in the comparison of SEM micrographs between dry ground and steam exploded rice husks (Donaldson, Wong, and Mackie 1988; Park et al. 2004).

According to Stark and Rowlands,(Stark and Rowlands 2003) the steam-aided disc refining system led to the increase of fiber surface area and aspect ratio. Thus, it can be explained that the significantly improved adhesion and compatibility between TRBF and plastic matrix was resulted from the increased silane cross-links on its exposed fibers with the increase of fiber surface area and aspect ratio.

2.3.4 Mechanical and Morphological Properties of PCC-PP/PE Composites

Figure 2.7 shows measured flexural, tensile and impact properties of the composites as a function of PCC content. The flexural strength (Figure 2.7(a)) varied little from 0 to 10 wt% PCC contents, but increased somewhat at the 15 wt% PCC content level. The highest increase was shown at the 30% PCC content. The graph of flexural modulus showed similar features. The tensile strength (Figure 2.7(b)) slightly decreased as PCC content increased and the tensile

modulus showed a slight increase. The notched impact strength (Figure 2.7(c)) decreased as a function of PCC content (a 63% reduction at the 30% PCC level). The above results indicate that the use of PCC led to decreased toughness for the blends of R-PP/PE with PCC.

Figure 2.8 shows the impact fractured surfaces of the blends of R-PP/PE with PCC**.** The distribution and aggregation of PCC in the polymer matrix can be observed from Figure 2.8. The neat R-PP/PE (Figure 2.8(a)) demonstrated clearly fractured features full of fibrils. The R-PP/PE blended with 7 wt% PCC (Figure 2.8(b)) had some well dispersed PCC particles in the polymer matrix (estimated mean particle diameter = 1.25 ± 0.43 μm). For the R-PP/PE blended with 30 wt% PCC (Figure 2.8(c)), some aggregated PCC particles were seen in the polymer matrix (estimated mean particle diameter = 1.66 ± 1.24 μm). The data suggested that high shear forces during compounding helped separate the agglomerated PCC particles (Figure 2.3). At higher PCC loading levels (e.g., 30 wt%), some agglomeration still existed, leading to larger observed particles. Overall, the separated PCC particles may still be too large to positively affect toughness of the resultant composites.(Bryant and Wiebking 2002)

The observed mechanical properties of PCC-filled composite are in an argument of general trend for mineral-filled plastic composites. For example, it was reported that the use of talc, CC and Biodac® (a mineral-filled cellulosic material) in low density polyethylene led to a significant increase in tensile modulus (200%, 77% and 130% for talc, CC and Biodac®, respectively) and decrease in toughness (42%, 58% and 86% for talc, CC and Biodac®, respectively) at the 30% loading level.(Klyosov 2007)

2.3.5 Properties of PCC-Bamboo-PP/PE Composites

The mechanical properties of PCC-bamboo-PP/PE composites are summarized in Table 2.2. For the flexural strength of composites, the increased extents were not significantly different

until the 12 wt% PCC content level. However, a somewhat increased feature was observed at the 18 wt% PCC content. The flexural strengths of GBP filled composites with PCC were slightly higher compared to those of RBF filled composites with PCC. After silane treatment, there was little change for the flexural strengths of GBP filled composites with PCC regardless of PCC content. This probably means that more lignin and less holocellulose contents in GBP with relatively low fiber aspect ratio led to the decrease of silane crosslinks. (Gregorova et al. 2009; Stark and Rowlands 2003) For RBF filled composites with PCC, over 15% increases of flexural strengths were observed after the silane treatment in the whole range of PCC content, indicating that less lignin and more holocellulose contents in RBF led to the increase of flexural strengths by improved silane coupling.(Gregorova et al. 2009; Inoue and Norimoto 1991; Stark and Rowlands 2003) On the other hand, impact strengths decreased as PCC content increased as a result of the early fractures from the lack of toughening effect due to the size of PCC.

Impact fractured SEM images of GBP filled composites with 6 and 18 wt% PCC contents are shown in Figure 2.9. In the 6 wt% PCC reinforced composite (Figure 2.9(a)), PCC particles were evenly dispersed. However, the 18 wt% PCC reinforced composite (Figure 2.9(b)) demonstrated frequent advents of PCC aggregations with the poor interfacial adhesions between fiber and polymer matrix.

The enhanced moduli of variously treated bamboo filled composites as a function of PCC content are shown in Figure 2.10. The flexural and tensile moduli of GBP and RBF filled composites with PCC had similar values from 12 to 18 wt% PCC contents. However, the values of TGBP and TRBF filled composites with PCC featured the continuous increases. The different trends of measured modulus among the above composites are attributed to the aggregation and dispersion of PCC in bamboo-plastic matrix.

For GBP and RBF filled composites with PCC, the small changes of flexural and tensile modulus from 12 to 18 wt% PCC contents indicate that the aggregated PCC particles prevented from shortening the ligament thickness and led to a faster initiation of fracture (Fu, Wang, and Shen 1993; Fu and Wang 1993; Thio et al. 2002).

Table 2.2 Mechanical properties of PCC-bamboo-PP/PE composites

System[a]	PCC[a] (wt%)	Tensile modulus[b] (GPa)	Flexural modulus (GPa)	Flexural strength (MPa)	Impact strength (kJ/m^2)
R-PP&PE/GBP	0	2.43 (0.19)B	1.98 (0.05)B	29.84 (0.82)B	4.33 (0.15)A
	6	2.39 (0.15)B	1.94 (0.04)B	29.79 (0.38)B	4.10 (0.17)B
	12	2.84 (0.17)A	2.42 (0.03)A	30.52 (0.61)B	3.63 (0.10)C
	18	2.88 (0.13)A	2.44 (0.04)A	31.40 (0.55)A	3.40 (0.20)D
R-P&PE/TGBP	0	2.58 (0.06)D	2.01 (0.05)D	30.45 (0.67)A	4.29 (0.24)A
	6	2.77 (0.28)C	2.19 (0.04)C	30.96 (0.29)A	3.69 (0.27)B
	12	2.83 (0.08)B	2.52 (0.07)B	30.94 (0.67)A	3.36 (0.26)C
	18	3.18 (0.19)A	2.82 (0.06)A	30.90 (0.38)A	3.22 (0.15)C
R-PP&PE/RBF	0	2.63 (0.24)B	2.33 (0.03)C	28.07 (0.46)C	3.74 (0.17)A
	6	2.88 (0.25)B	2.52 (0.07)B	28.49 (0.27)BC	3.11 (0.16)B
	12	3.51 (0.24)A	2.95 (0.05)A	29.69 (0.37)AB	2.69 (0.08)C
	18	3.64 (0.13)A	2.98 (0.17)A	29.17 (0.99)A	2.38 (0.05)D
R-PP&PE/TRBF	0	2.75 (0.24)C	2.32 (0.05)D	33.44 (0.31)B	3.15 (0.06)A
	6	2.74 (0.15)C	2.57 (0.03)C	33.60 (0.25)B	2.87 (0.10)B
	12	3.21 (0.07)B	2.85 (0.04)B	33.89 (0.33)B	2.82 (0.05)B
	18	3.48 (0.18)A	3.12 (0.17)A	34.58 (0.81)A	2.71 (0.02)C

[a] R-PP&PE: recycled polypropylene and polyethylene; GBP: ground bamboo particle; TGBP: silane treated bamboo particle; RBF: refined bamboo fiber; TRBF: silane treated bamboo fiber. R-PP&PE to bamboo fiber ratio was 60 to 40 wt%. PCC was based on total composite weight.
[b] Means with the same letter for each category are not significantly different at the 95% confidence level; numbers in parenthesis are standard deviations.

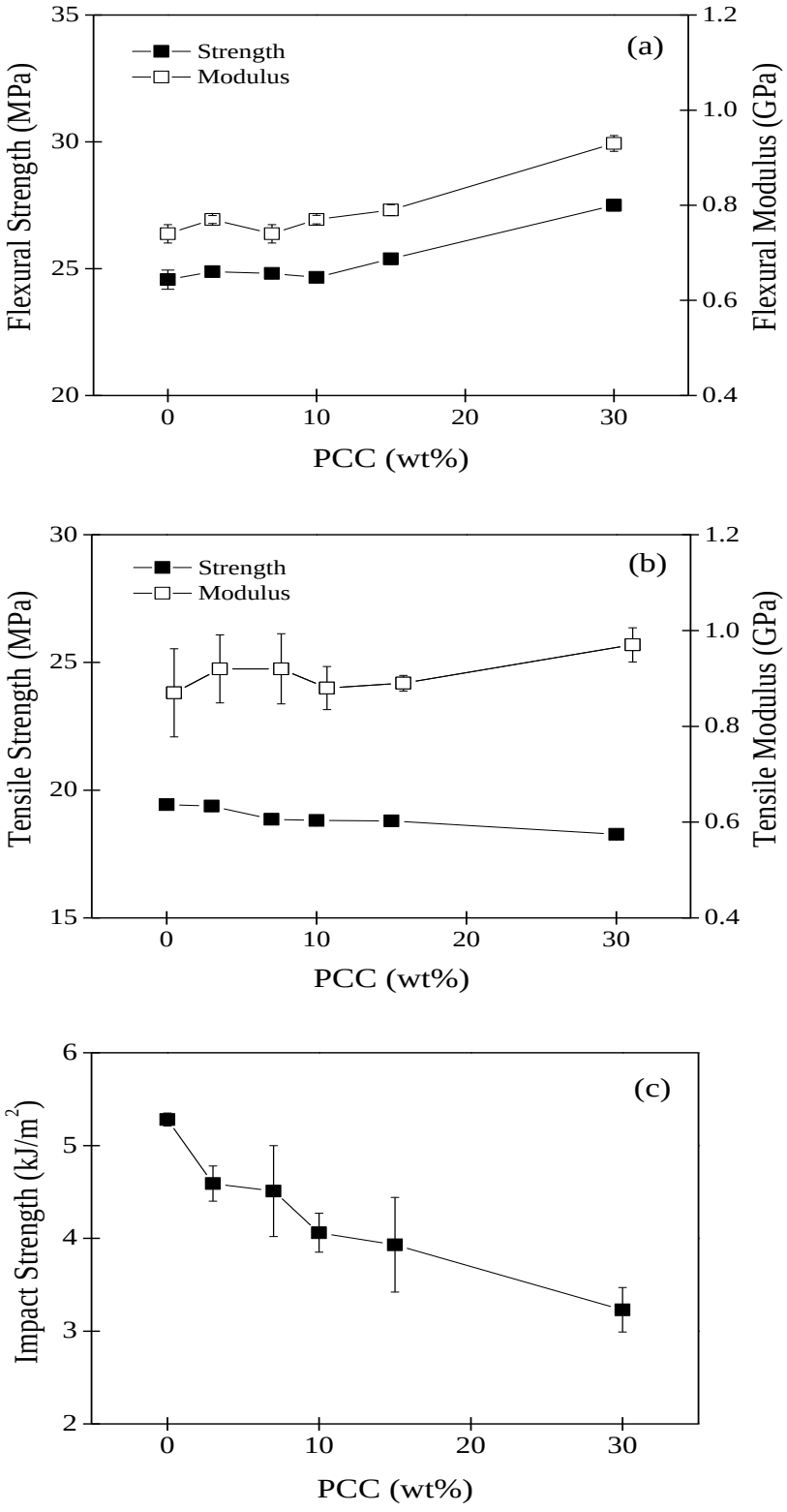

Figure 2.7 Comparison of flexural (a), tensile (b) and impact (c) properties of PCC-filled composites as a function of PCC content.

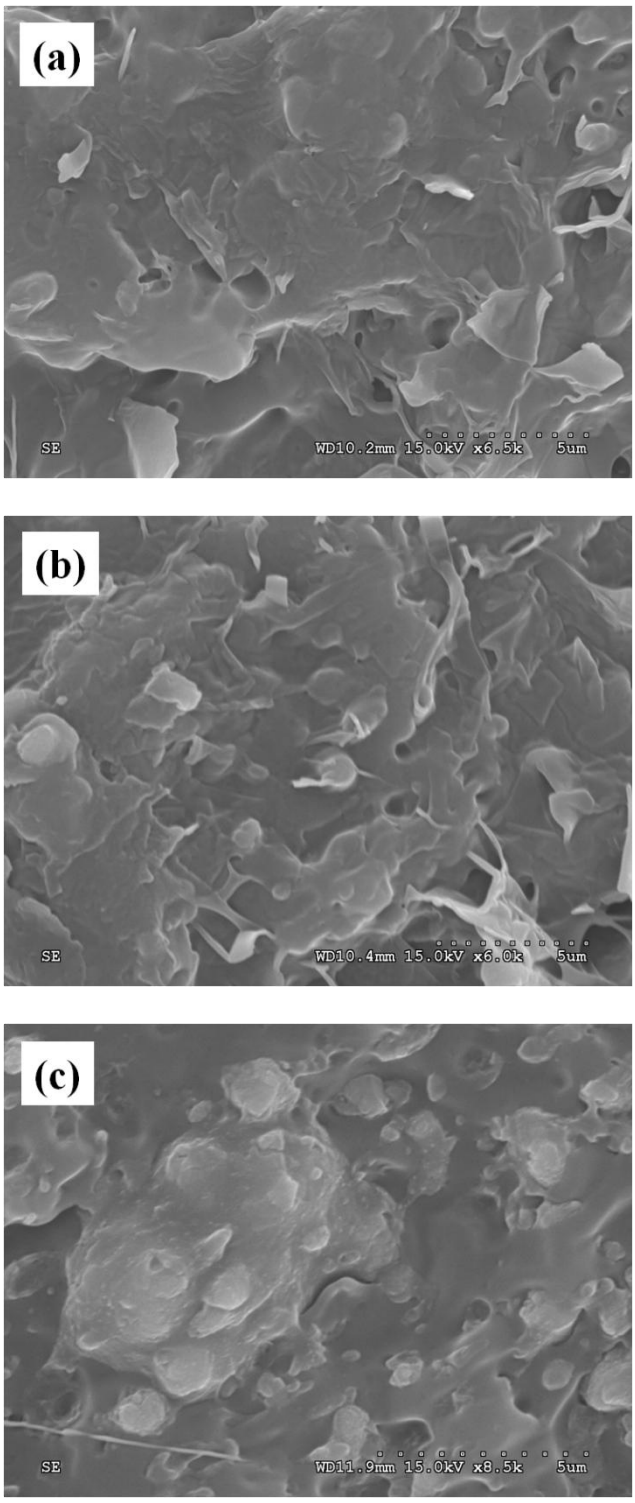

Figure 2.8 SEM micrographs of the impact fractured surfaces of R-PP/PE and PCC blends. (a): R-PP/PE; (b): R-PP/PE and PCC (7 wt%); (c): R-PP/PE and PCC (30 wt%).

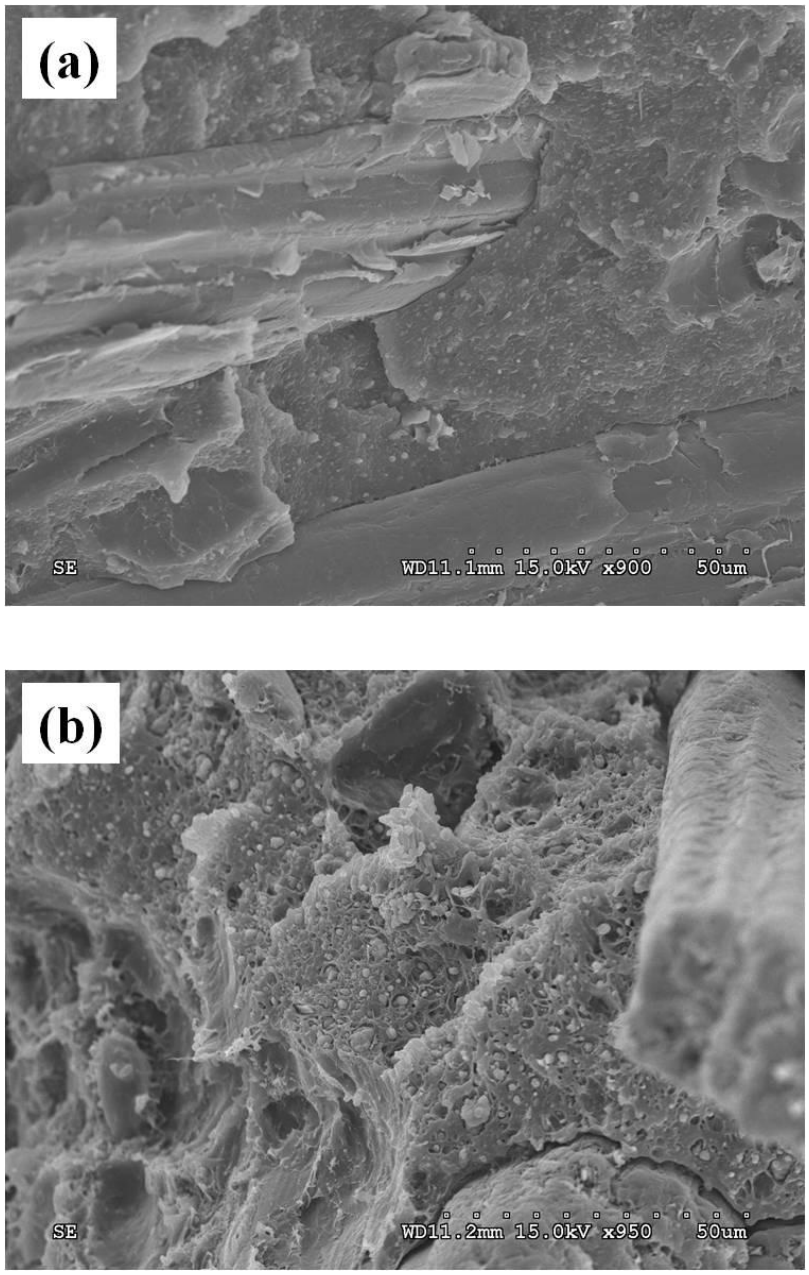

Figure 2.9 SEM micrographs of the impact fractured surfaces of PCC-GBP-PP/PE composites: (a) 6 wt% PCC and (b) 18 wt% PCC.

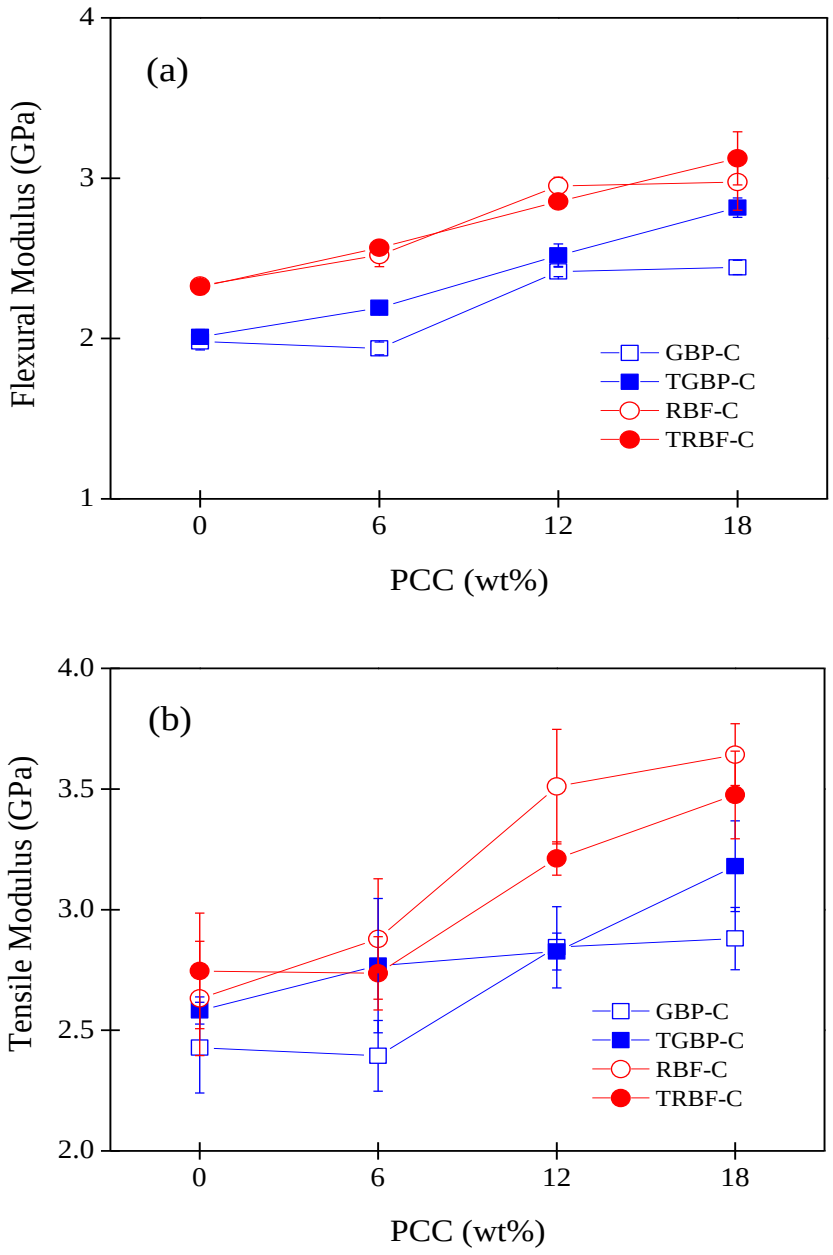

Figure 2.10 Comparison of flexural modulus (a) and tensile modulus (b) of PCC-GBP and PCC-RBF composites before and after silane treatment as a function of PCC content.

For TGBP and TRBF filled composites with PCC, the remaining silanols, which were not cross-linked with bamboo fibers might react with the surface of PCC, leading to the improved dispersion and decreased aggregation of PCC in composites and the large modulus changes from 12 to 18 wt% PCC contents.

Table 2.3 shows measured water absorption (WA) values as a function of time among different composites with and without PCC. The addition of PCC (18 wt%) into bamboo-plastic matrix gave rise to a slight increase of WA properties. The WA values of composites with PCC were about 1-2% higher compared to those of composites without PCC after 10 weeks water immersion. It is noticed that WA values in this experiment were from 2.37-3.27% at the 18 wt% PCC level after a two-week water immersion, while other previous research data for the WA values of CC filled WPC showed 7.1-9.0% at 10-20% CC levels (Klyosov 2007). This discrepancy is presumably due to the differences in manufacturing methods, base resins, composite density, and fibers (wood versus bamboo). The WA increases of PCC filled composites seemed to be related to mainly the interfacial gap from poor compatibility between hydrophilic PCC and polymer. Among variously treated bamboo filled composites, it is observed that TRBF filled composites had the lowest WA values, while RBF filled composites had the highest values. This fact indicates that the moisture uptakes in composites are related to the WA properties of respective fibers and compatibility between fibers and plastic matrix.

Two-way ANOVA test data on WA in the variation of immersion time are shown in Table 2.4. The ANOVA results showed that both fiber type and PCC content had a significant influence on WA of the composites. For the combined effect of fiber type and PCC content on WA, a significant interaction was observed after 1-week water immersion at the 95% confidence

level. However, after that, interactions between fiber type and PCC content on WA were not significant.

Table 2.3 WA (%) of variously treated bamboo-PP/PE composites with and without PCC.

PCC (wt%)	Fiber type[a]	WA (%) at time interval[a]				
		1 week	2 weeks	3 weeks	4 weeks	10 weeks
0	GBP	2.13 (0.28)	3.01 (0.54)	3.78 (0.74)	4.45 (0.95)	6.42 (1.34)
	RBF	2.02 (0.14)	3.07 (0.33)	4.03 (0.43)	4.83 (0.50)	7.30 (0.52)
	TGBP	1.83 (0.26)	2.42 (0.44)	3.06 (0.56)	3.52 (0.69)	5.52 (1.24)
	TRBF	1.32 (0.02)	2.03 (0.20)	2.41 (0.04)	2.87 (0.09)	4.57 (0.31)
18	GBP	2.37 (0.44)	3.27 (0.86)	4.24 (1.21)	5.57 (0.97)	7.81 (1.05)
	RBF	2.92 (0.31)	4.47 (0.66)	5.86 (0.79)	7.02 (0.85)	8.91 (0.06)
	TGBP	1.89 (0.26)	2.87 (0.45)	3.88 (0.33)	4.52 (0.55)	6.72 (0.69)
	TRBF	1.63 (0.14)	2.37 (0.28)	3.10 (0.38)	3.78 (0.48)	6.15 (0.77)

[a] GBP: ground bamboo particle; RBF: refined bamboo fiber; TGBP: silane treated bamboo particle; TRBF: silane trated bamboo fiber; the numbers in parenthesis are standard deviations

Table 2.4 Two-way ANOVA tests of the effect of fiber and PCC on WA of R-PP/PE composites at different time intervals.

Variables	Water absorption at time interval[a]				
	1 week	2 weeks	3 weeks	4 weeks	10 weeks
Fiber	< 0.0001	< 0.0001	< 0.0001	< 0.0001	< 0.0001
PCC	0.0004	0.0024	0.0004	< 0.0001	< 0.0001
Fiber × PCC	0.0197	0.1174	0.1876	0.2434	0.9606

[a] The values shown are *p*-values of 2-way ANOVA tests. The *p*-values smaller than 0.05 indicate significant influences of the corresponding treatments on WA at the 95% confidence level.

2.4 CONCLUSIONS

The differences in chemical composition and surface morphology between RBF and GBP led to more effective silane crosslinking on the RBF surfaces. Dry PCC particles showed an agglomerated form, and compounding PCC with R-PP/PE resin helped separate it to smaller individual particles. Measured flexural strength and flexural modulus of PCC-only-filled composites increased significantly from 15 to 30% PCC content levels, while the tensile and impact strength of composites decreased with the addition of PCC.

For composites with hybrid bamboo and PCC fillers, tensile and flexural moduli were improved with the increase of PCC content. After silane treatment of the bamboo filler, RBF filled composites showed noticeably increased mechanical properties compared to those of GBP filled composites. For modulus values, PCC-bamboo-polymer composites were 3-4 times higher than those of PCC-polymer composites at high PCC levels.

2.5 REFERENCES

Belgacem, M.N., M. Abdelmouleh, S. Boufi, A.P. Duarte, A. Ben Salah, and A. Gandini. 2004. Modification of cellulosic fibres with functionalised silanes: development of surface properties. *International Journal of Adhesion and Adhesives* 24: 43-54.

Bramuzzo, M., A. Savadori, and D. Bacci. 1985. Polypropylene Composites - Fracture-Mechanics Analysis of Impact Strength. *Polymer Composites* 6: 1-8.

Brebu, M., and C. Vasile. 2010. Thermal Degradation of Lignin - a Review. *Cellulose Chemistry and Technology* 44: 353-63.

Bryant, W.S., and H.E. Wiebking. 2002. *The effect of calcium carbonate size and loading level on the impact performance of rigid PVC compounds containing varying amounts of acrylic impact modifier.* In *ANTEC*, 173-7.

Cantero, G., A. Arbelaiz, F. Mugika, A. Valea, and I. Mondragon. 2003. Mechanical behavior of wood/polypropylene composites: Effects of fibre treatments and ageing processes. *Journal of Reinforced Plastics and Composites* 22: 37-50.

da Silva, A.L.N., M.C.G. Rocha, M.A.R. Moraes, C.A.R. Valente, and F.M.B. Coutinho. 2002. Mechanical and rheological properties of composites based on polyolefin and mineral additives. *Polymer Testing* 21: 57-60.

Donaldson, L.A., K.K.Y. Wong, and K.L. Mackie. 1988. Ultrastructure of Steam-Exploded Wood. *Wood Science and Technology* 22: 103-14.

Dweck, J. 2010. *An introduction to thermal analysis: fundamentals and main techniques*. In *MACSTU-LSU*. Baton Rouge, LA.

Dwianto, W., F. Tanaka, M. Inoue, and M. Norimoto. 1996. *Crystallinity Changes of Wood by Heat or Steam Treatment*. In *The 46th Annual Meeting of Japan Wood Research Society*, 47-9. Kumamoto.

Echeverria, A.A., and M.R. Holst. 2005. *Use of precipitated calcium carbonate (PCC) originating from sugar as a raw material in the ceramic industry.* US.

Felix, J.M., and P. Gatenholm. 1991. The Nature of Adhesion in Composites of Modified Cellulose Fibers and Polypropylene. *Journal of Applied Polymer Science* 42: 609-20.

Fu, Q., G. Wang, and J. Shen. 1993. Polyethylene toughened by CaCO3 particle: Brittle-ductile transition of CaCO3-toughening HDPE. *J Appl Polym Sci* 49: 673-7.

Fu, Q., and G.H. Wang. 1993. Effect of Morphology on Brittle-Ductile Transition of Hdpe/Caco3 Blends. *Journal of Applied Polymer Science* 49: 1985-8.

Gassan, J., and A.K. Bledzki. 1999. Possibilities for improving the mechanical properties of jute epoxy composites by alkali treatment of fibres. *Composites Science and Technology* 59: 1303-9.

Giebeler, E. 1983. Dimensional Stabilization of Wood by Moisture-Heat-Pressure-Treatment. *Holz Als Roh-Und Werkstoff* 41: 87-94.

Gregorova, M.H., R. Wimmer, B. Saake, and A. C. 2009. Poly(lactide acid) Composites Reinforced with Fibers Obtained from Different Tissue Types of Picea stichensis. *Journal of Applied Polymer Science* 114: 2616-23.

Han, G., Y. Lei, Q. Wu, Y. Kojima, and S. Suzuki. 2008. Bamboo-Fiber Filled High Density Polyethylene Composites: Effect of Coupling Treatment and Nanoclay. *Journal of Polymers and the Environment* 16: 123-30.

Hristov, V.N., R. Lach, and W. Grellmann. 2004. Impact fracture behavior of modified polypropylene/wood fiber composites. *Polymer Testing* 23: 581-9.

Hughes, A.E., and B.A. Sexton. 1988. Curve Fitting Xps Spectra. *Journal of Electron Spectroscopy and Related Phenomena* 46: 31-42.

Inoue, M., and M. Norimoto. 1991. Heat treatment and steam treatment of wood. *Wood Ind.* 49: 588–92.

Katz, H.S., and J.V. Milewski. 1987. *Handbook of fillers for plastics.* New York: Van Nostran Reinhold Co

Kim, T.-W., S.-Y. Lee, S.-J. Chun, G.-H. Doh, and K.-H. Paik. 2011. Effect of silane coupling on the fundamental properties of wood flour reinforced polypropylene composites. *Journal of Composite Materials* 45: 1595-605.

Klyosov, A.A. 2007. *Wood-plastic composites*. Hoboken, New Jersey: John Wiley & Sons Inc.

Lee, S.Y., S.J. Chun, G.H. Doh, I.A. Kang, S. Lee, and K.H. Paik. 2009. Influence of Chemical Modification and Filler Loading on Fundamental Properties of Bamboo Fibers Reinforced Polypropylene Composites. *Journal of Composite Materials* 43: 1639-57.

Lu, J.Z., I.I. Negulescu, and Q.L. Wu. 2005. Maleated wood-fiber/high-density-polyethylene composites: Coupling mechanisms and interfacial characterization. *Composite Interfaces* 12: 125-40.

Lu, J.Z., Q.L. Wu, and H.S. McNabb. 2000. Chemical coupling in wood fiber and polymer composites: A review of coupling agents and treatments. *Wood and Fiber Science* 32: 88-104.

Maiti, S.N., and P.K. Mahapatro. 1991. Mechanical-Properties of I-Pp/Caco3 Composites. *Journal of Applied Polymer Science* 42: 3101-10.

Misra, R.D.K., C. Deshmane, and Q. Yuan. 2007. On the fracture characteristics of impact tested high density polyethylene-calcium carbonate nanocomposites. *Materials Science and Engineering a-Structural Materials Properties Microstructure and Processing* 452: 592-601.

Mohanty, A.K., M. Misra, and L.T. Drzal. 2001. Surface modification of natural fibers and performance of the resulting biocomposites: An overview. *Comp Interf.* 8: 313-43.

Nachtigall, S.M.B., G.S. Cerveira, and S.M.L. Rosa. 2007. New polymeric-coupling agent for polypropylene/wood-flour composites. *Polymer Testing* 26: 619-28.

Okubo, K., T. Fujii, and Y. Yamamoto. 2004. Development of bamboo-based polymer composites and their mechanical properties. *Composites Part a-Applied Science and Manufacturing* 35: 377-83.

Park, B.D., S.G. Wi, K.H. Lee, A.P. Singh, T.H. Yoon, and Y.S. Kim. 2004. X-ray photoelectron spectroscopy of rice husk surface modified with maleated polypropylene and silane. *Biomass & Bioenergy* 27: 353-63.

Salmen, L., Y.F. Yin, and L. Berglund. 2011. Effect of Steam Treatment on the Properties of Wood Cell Walls. *Biomacromolecules* 12: 194-202.

Sgriccia, N., M.C. Hawley, and M. Misra. 2008. Characterization of natural fiber surfaces and natural fiber composite. *Composites : Part A* 39: 1632-7.

Shin, F.G., and M.W. Yipp. 1989. Analysis of the mechanical properties and microstructure of bamboo-epoxy composites. *J Mater Sci* 24: 3483-90.

Stark, N.M., and R.E. Rowlands. 2003. Effect of Wood Fiber Characteristics on Mechanical Properties of Wood/Propylene Composites. *Wood and Fiber Science* 35: 167-74.

Tai, C.Y., and C.K. Chen. 2008. Particle morphology, habit, and size control of CaCO3 using reverse microemulsion technique. *Chemical Engineering Science* 63: 3632-42.

Takaya, N., and Y. Tadashi. 1970. *Structural Observation on Wood and Bamboo by X-ray.* In *The 20th and 21st Meetings of Japan Wood Research Society*, 1-12. Tokyo.

Thio, Y.S., A.S. Argon, R.E. Cohen, and M. Weinberg. 2002. Thoughening of isotactic polypropylene with CaCO3 particles. *Polymer* 43: 3661-74.

Vena, P.F. 2005. *Thermomechanical pulping (TMP) Chemithermomechanical pulping (CTMP) and Biothermomechanical pulping (BTMP) of Bugweed (Solanum Mauritianum) and Pinus Patula*. 82: The University of Stellenbosch.

Winandy, J.E., N.M. Stark, and E. Horn. 2008. *Wood Plastic Composites Using Thermomechanical Pulp Made From Oxalic Acid-Pretreated Red Pine Chips.* In *7th Global WPC and Natural Fibre Composites Congress and Exhibition.* Germany.

Wypych, G. 2010. *Handbook of fillers*, 3rd ed. Ontario, Canada: ChemTec Publishing.

Yao, F., Q.L. Wu, Y. Lei, W.H. Guo, and Y.J. Xu. 2008. Thermal decomposition kinetics of natural fibers: Activation energy with dynamic thermogravimetric analysis. *Polymer Degradation and Stability* 93: 90-8.

CHAPTER 3 MECHANICAL AND PHYSICAL PROPERTIES OF CORE-SHELL STRUCTURED WOOD PLASTIC COMPOSITES: EFFECT OF SHELLS WITH HYBRID MINERAL AND WOOD FILLERS

3.1 INTRODUCTION

Coextrusion generally consists of two or more extruders combined with one die to produce multiple-layer products (Rosato 1998). By combining molten multiple plastic layers with various properties into one profile, optimization of product performance is possible (Giles, Wagner, and Mount 2005). Water resistance, air entrapment, oxygen barrier, and increased toughness are some of the advantages of coextruded products (Giles, Wagner, and Mount 2005; Rosato 1998). For example, coextrusion method has been applied to produce packaging films for maintaining content freshness, pipes requiring high mechanical properties, and other specialty products (Doshi, Charrier, and Dealy 1988; Kim et al. 1984).

Coextrusion in wood plastic composite (WPC) was first reported with a combination of WPC core and pure plastic shell layer. Stark and Matuana (Stark and Matuana 2007) investigated moisture uptake, flexural properties and weathering performance between non-coextruded and coextruded WPC with a pure high density polyethylene (HDPE) or pure polypropylene (PP) shell. In their research, coextruded WPC demonstrated much reduced moisture uptake than non-coextruded WPC and there were almost no differences in flexural properties between them. They further studied the effects of a stabilized shell layer blended with HDPE and additives including a compatibilizer, a photostabilizer and a nanosized titanium dioxide (TiO_2) on the coextruded WPC after weathering tests (Stark and Matuana 2009). The coextruded WPC with a stabilized shell layer showed better water resistance properties and the combination of a compatibilizer and a photostabilizer improved composite lightening by a synergistic effect. The individual use of TiO_2 or a photostabilizer showed a noticeably enhanced color stability for each capped WPC.

However, a simultaneous use of both additives had a deleterious effect on color stability. Jin and Matuana (Jin and Matuana 2008) studied the improvements of water resistance through the application of a pure HDPE plastic shell onto an extruded WPC core. The water absorption (WA) and thickness swelling (TS) properties of coextruded WPC were better than those of non-coextruded WPC without a shell.

The application of a pure plastic shell with a relatively low modulus over a WPC core negatively affected overall composite modulus. Jin and Matuana (Jin and Matuana 2010) reported a study using a PVC shell layer on a PVC-wood flour (WF) core. Increased flexural strength and decreased flexural modulus were observed for the coextruded composites. It was pointed out that high strength and low stiffness characteristics of PVC led to the decrease of composite flexural modulus. To acquire a simultaneous enhancement of both flexural modulus and flexural strength, they used carbon nano-tube (CNT) in a shell layer, in combination with two core compositions (40% versus 60% WF) and two processing conditions (low versus high temperature). The combination of a CNT-filled PVC shell and a high temperature processed WPC core showed better flexural strength and flexural modulus. However, the use of high-cost CNTs was not cost-effective for WPC products. Yao and Wu (Yao and Wu 2010) investigated the coextruded WPC using the combinations of recycled PE core compositions (weak and strong) and a virgin PE shell with different WF contents and shell thicknesses. In the comparison of mechanical properties between weak and strong core systems, coextruded composites with a weak core showed much higher percentage increases in flexural and impact strength than those with a strong core. At the same shell thickness, less WF loading in the shell led to highly increased impact strength, but there were almost no changes in flexural modulus. On the other hand, the increase of impact strength and the decrease of flexural modulus were observed with

increased shell thickness. Thus, they suggested that good flexural modulus of coextruded WPC resulted from the combination of a thinner shell and a higher modulus core.

The addition of mineral fillers into polymeric materials enhances their physical and mechanical properties (Nwabunma and Kyu 2008; Wypych 2010a). Among the mineral fillers, precipitated calcium carbonate (PCC) from chemical processes (Bleakley and Jones 1993; Liu et al. 2006; Porter and Wilson 1999; Rothon 1999; Wypych 2010a) has characteristics of very fine and regular particle size (Xanthos 2005). Thus, its uses in plastic composites have led to improved mechanical properties (Patnaik 2003; Zuiderduin et al. 2003). However, the fine size of PCC conversely causes its aggregations in composites, leading to a deleterious effect on the properties of PCC filled composites (Lam et al. 2009). Hence, to decrease this deleterious effect, surface treated PCC has been used. Lam *et al*. (Lam et al. 2009) investigated the effect of modified PCC in PP matrix through optical and thermal analysis. Nanosized PCC (n-PCC) and nanosized surface modified PCC (ns-PCC) filled PP composites were prepared. The initial decomposition temperature of ns-PCC/PP composites was higher than that of n-PCC/PP composites at the same filling ratio, indicating that the reinforcing effect of ns-PCC was increased by surface treatment. J. Cayer-Barrioz *et al.* (Cayer-Barrioz et al. 2006) studied the interfacial adhesion between polyamide 66 (PA66) and PCC (untreated PCC; 3wt% stearic acid treated PCC; amino acid treated PCC). Dynamic mechanical analysis (DMA) demonstrated the effects of the surface treated PCC through the G" peak shifts by +13K for the amino acid treatment and +6K for the stearic acid treatment. Moreover, environmental scanning electron microscope analysis confirmed the differences of adhesions among PCC filled composites. Kim *et al.* (Kim et al. 2012) investigated that technical feasibility of using PCC of sugar origin as a reinforcing filler for bamboo fiber plastic composite. It was shown that air-dry PCC particles

were in an agglomerated form made of individual cubic particles of about 1.2 micron in diameter. Compounding with plastic resin helped separate the PCC to smaller individual particles. The use of PCC led to a significant increase of flexural strength and flexural modulus of PCC filled composites after 10 wt% PCC loading level. For bamboo filled composites with PCC, tensile modulus and flexural modulus were improved with the increase of PCC content and with use of surface treated bamboo filler. The use of raw and treated PCC in coextruded WPC (e.g., in the shell layer to modify overall composite properties) has not been reported.

The objectives of this study were to elucidate the effect of TPCC and WF loadings in the shell layer on the mechanical, water absorption and thermal expansion properties of coextruded WPC with two different core systems.

3.2 EXPERIMENTAL

3.2.1 Materials and Preparation

Fluffy form of recycled-PP/HDPE resin from a local plastic recycling company was pelletized using a twin-screw extruder before blending with other raw materials. Virgin HDPE (HGB 0760) was provided by ExxonMobile Chemical Co. (Houston, TX, USA). Pine WF (20 mesh particle size) was supplied by American Wood Fibers Inc. (Schofield, WI, USA). PCC was obtained from Domino Sugar Co. (New Orleans, LA, USA) and screened to pass an 100-mesh screen. MAPE (Epolene^{TM} G2608) from Eastman Chemical Co. (Madison, TN, USA) and silane coupling agent (Z-6094) from the DOW Corning Co. (Midland, MI, USA) were utilized to increase the compatibility between fillers and plastic matrix. Lubricant (TPW 306) from Struktol Co. (Stow, OH, USA) was used to improve the processing of WPC profile.

The silane treatment of PCC was made by an immersion method. Before treatment, PCC was dried at 80°C for 24 hr. After that, aqueous solution (ethanol:water = 90:10) including silane

coupling agents (1 wt%) was prepared and left at 25°C for 30 min to attain proper hydrolysis and condensation of silane. The PCC was then immersed in the solution to achieve proper silane surface treatments. Silane treated PCC was dried at 80°C for 24 hr again. The recycled PP/HDPE plastic and virgin HDPE were used as base resins for two core systems (i.e., weak core and strong core). Virgin HDPE was used to make shell material for both systems. Materials used for shell were compounded and pelletized at 165 (feeder), 175, 180, 170 and 180^{o}C (die) before the coextrusion process. TPCC was first compounded with virgin HDPE to form a 50/50 wt% master batch. The compounded master batch pellets were then compounded again with WF at target loading levels.

3.2.2 Coextruded WPC Manufacturing

The composites were formulated with two core types (i.e., weak and strong) in combination with two shell systems for each core type. The formulation for the weak- and strong-core systems were, respectively, R-PP/HDPE: WF: Lubricant: MAPE = 40: 50: 6: 4 wt% and V-HDPE: WF: Lubricant: MAPE = 40: 50: 6: 4 wt%. The two shell systems were a) TPCC (6, 12, and 18%) + WF (15%) + V-HDPE (79, 73, and 67%) and b) TPCC (12%) + WF (0, 5, 15, and 25%) + V-HDPE (88, 83, 73, and 63%).

The composites were manufactured with a pilot-scale coextrusion system (Yao and Wu 2010). This system consists of a Leistritz Micro-27 co-rotating parallel twin-screw extruder (Leistritz Corporation, Allendale, NJ) for core and a Brabender 32 mm conical twin-screw extruder (Brabender Instruments Inc., South Hackensack, NJ) for shell. A specially-designed die with a cross-section area of 13 x 50 mm and a target shell thickness of 1.0 mm was used. A vacuum sizer was used to maintain the targeted size. The coextruded profiles passed through a 2 m water bath with water spraying using a down-stream puller. Manufacturing temperatures for

core were controlled between 150 and 175^{o}C. Manufacturing temperature for shells varied from 150 to 170^{o}C in the variation of different shell formulations.

3.2.3 Characterization

X-ray photoelectron spectroscopy (XPS) was carried out using a Kratos Axis-165 high performance multi analysis (Kratos Analytical Ltd., Manchester, UK) to investigate atomic elements of treated PCC with a monochromatic MgKa source (1253.6 eV) at 15 kV and 20 mA. Oven dried PCC particles were mounted onto a holder and placed in a vacuum of 1–5 x 10^{-8} torr. FT-IR analysis was performed using a Bruker Tensor 27 system (Bruker Optics Corporation, Billerica, MA) to investigate the changes the compositions of PCC before and after silane treatment. Powder samples were directly placed on the top sample plate with the ZnSe crystal illuminated and then analyzed in the range of 525–4000 cm^{-1}. The acquired FT-IR data were the averages of 32 scans.

Three-point flexural test was conducted using a model 5582 Instron testing machine (Instron Co, Norwood, MA) at a crosshead speed of 6mm/min according to the ASTM D790. Tinius Olsen Mode 1892 impact tester (Tinius Olsen Inc., Horsham, PA) was used to test Izod impact strength without notching according to the ASTM D256, using samples with a 3-mm thickness. These samples were acquired by cross-cutting the extruded profiles such that the impact force on the test samples was perpendicular to the coextrusion direction. Five samples were used for each group. Type of impact facture failure (i.e., hinge versus complete) for each sample was recorded.

Water soaking properties including WA and TS were measured using samples of 254 × 50 × 12 mm in size according to the ASTM D7031-2004. WA and TS values were determined as:

$$WA(\%) = \left(\frac{W_a - W_b}{W_b} \right) \times 100 \tag{3.1}$$

$$TS(\%) = \left(\frac{T_a - T_b}{T_b} \right) \times 100 \tag{3.2}$$

Where, W_a and W_b are sample weights (g) after and before soaking; T_a and T_b are sample thickness (mm) after and before soaking. Three samples per group were used to get an average value for each test.

For the coefficient of thermal expansion (CTE) measurement of coextruded WPCs, samples of 63.5 × 50 × 12 mm in size were prepared and tested. Length measurements were done with an IDF-130E Mitutoyo digimatic indicator (Mitutoyo Corporation, Japen) of 0.01 mm accuracy along the long (i.e., extrusion) dimension of the extruding direction of respective samples (between the two opposing center points on the end surfaces). Samples were conditioned to reach equilibrium temperatures of-15^{o}C and then 60^{o}C prior to measurements at each temperature. CTE was calculated as:

$$CTE(\alpha) = \left(\frac{L_f - L_i}{L_i} \right) \Big/ (T_f - T_i) \tag{3.3}$$

Where, L_f and L_i are the final and initial measured sample lengths (mm); T_f and T_i are the final and initial measured temperature (^{o}C). Three samples were used to get an average CTE value for each group.

3.3 RESULTS AND DISCUSSION

3.3.1 Properties of Treated PCC

Figure 3.1 shows measured XPS spectra of untreated PCC (Figure 3.1(a)) and TPCC (Figure 3.1(b)).

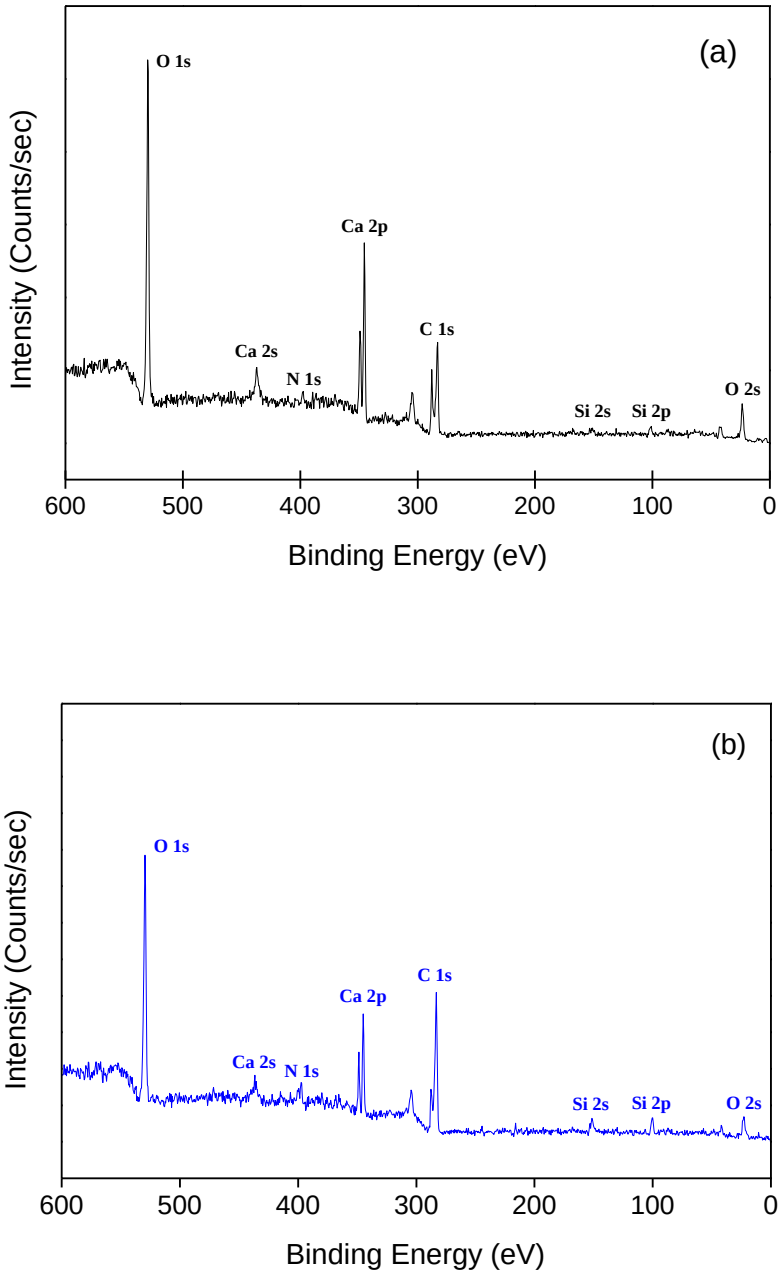

Figure 3.1 XPS spectra of untreated PCC (a) and treated PCC (b).

Table 3.1 Element composition, oxygen-carbon, and silicon-oxygen ratios of untreated PCC and TPCC from the XPS measurement.

Type	Element composition (%)					Element ratio	
	C_{1s}	O_{1s}	Ca_{2p}	Si_{2p}	N_{1s}	O/C	Si/O
Untreated PCC	48.92	38.66	8.76	2.11	1.54	0.79	0.05
TPCC	58.25	28.73	5.25	3.55	4.22	0.49	0.12

Before silane treatment, the magnitudes of silicon and nitrogen peaks in PCC were small. After treatment with the silane coupling agent (z-6094), these peak magnitudes were significantly increased. To acquire quantitative information of the element composition of PCC, the peak area of each electron from XPS spectra was standardized with a sensitivity factor.

The ratios of element composition (O/C and Si/O) resulted from the standardized process are shown in Table 3.1. Regardless of treatment conditions, the order of percentage composition was carbon (largest), oxygen, and calcium (smallest). However, for silicon and nitrogen, the order of percentage composition changed before and after the treatments. The silane treatment led to an increase of C1s electron from 48.92% to 58.25% and a decrease of O1s electron from 38.66% to 28.73%. The lower O/C and the higher Si/O ratios of silane treated PCC compared to untreated PCC demonstrated silane coupling agent attachment to the surface of PCC. There were 174 % increase of N_{1s} and 68 % increase of Si_{2p} electron, which showed the existence of silane element on treated PCC.

The silane deposition onto PCC is also observed in FT-IR spectra (Figure 3.2). For TPCC, the peak at 1040 cm^{-1} is assigned to Si-O-Si linkages considered as siloxan on the PCC. Beside, the peaks at 1100 cm^{-1} and 1080 cm^{-1} are associated with longer Si–O-Si structures (Abdelmouleh et al. 2004).

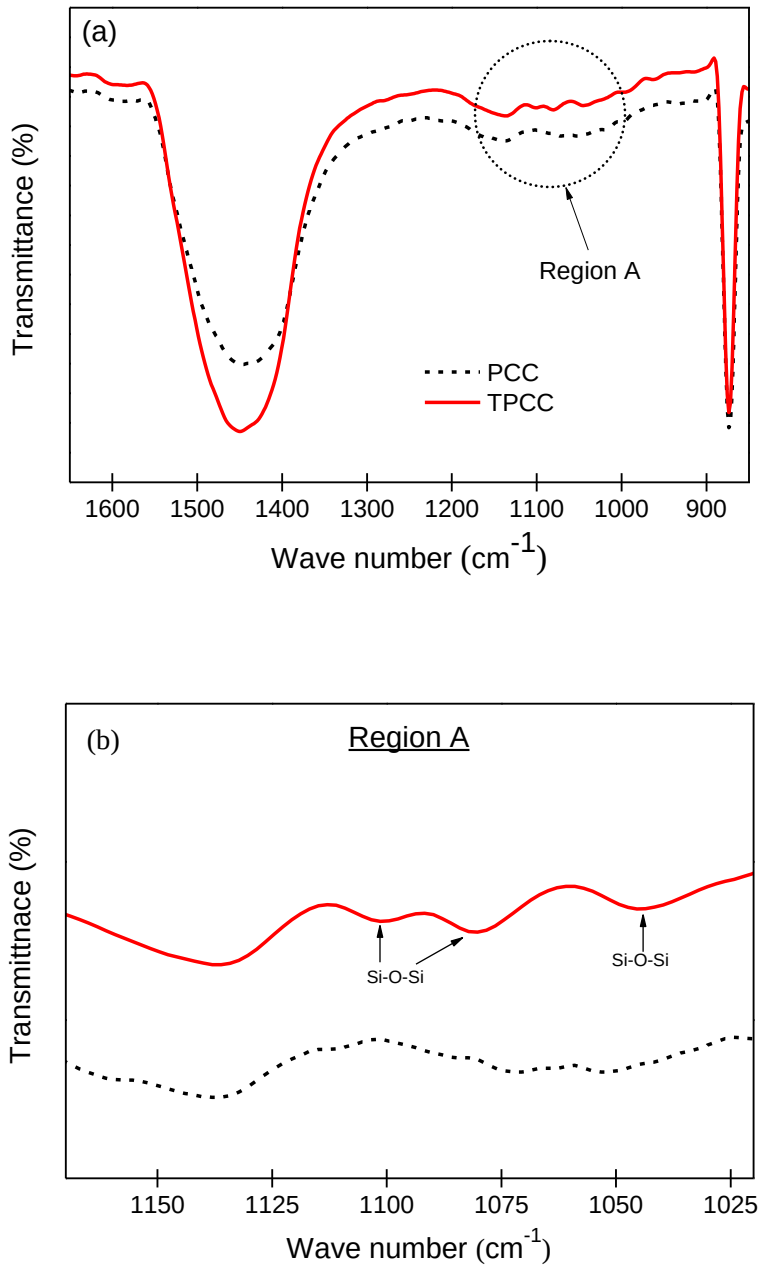

Figure 3.2 FT-IR spectra of PCC and TPCC (a: whole spectra and b: selected region).

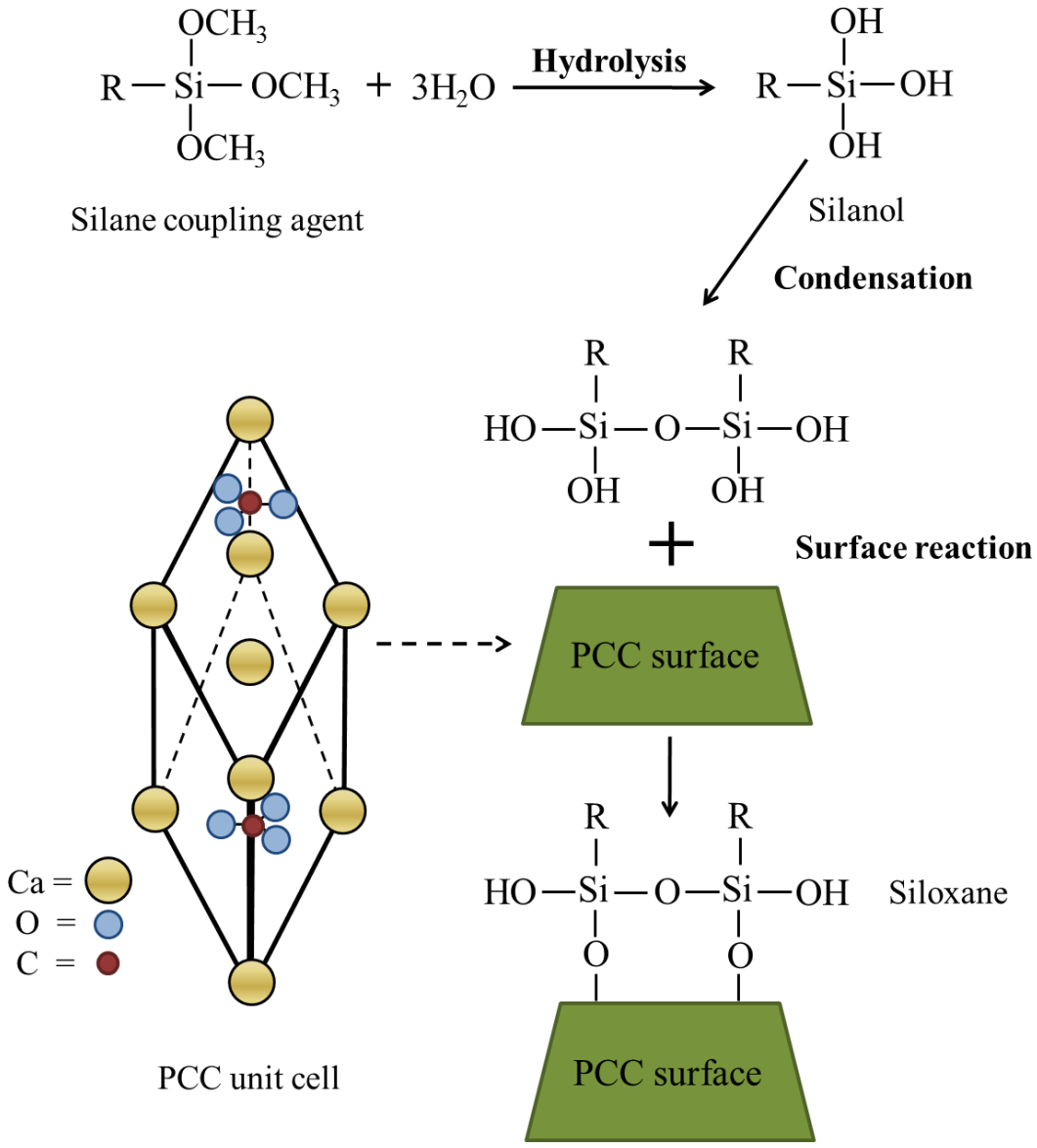

Figure 3.3 Schematic diagram of PCC surface chemically modified by silane treatment.

Figure 3.3 shows the schematic diagram illustrating the transformation of the hydrophilic PCC surface to hydrophobic surface by silane coupling reaction. Through silanization, hydrolysis of silane, condensation between silanols, and bond formation between siloxane and PCC surface were achieved in a consecutive manner.

3.3.2 Mechanical and Morphological Properties of Composites

Table 3.2 lists summarized data of measured flexural strength and modulus of coextruded WPCs with two core systems and various TPCC and WF contents in a shell layer. Figure 3.4 (a) and (b) show comparative charts of the two properties for various systems.

The flexural modulus for weak and strong cores was similar (2.75 GPa vs. 2.79 GPa). However, the flexural strength for the strong core was much higher than that of the weak core (34.5 MPa vs. 14.9 MPa). This was due to the fact that the strong core was made of virgin HDPE, while weak core was made of the recycled PP/HDPE.

For the composite flexural strength, the weak core system showed significant increases in relation to the strength value of weak core only. In this system, the shell layer made of filled virgin HDPE effectively prevented the deformation and subsequent crack occurrence of the composite due to its higher tensile strength. However, composites with the strong core system showed decreased overall strength compared with the corresponding core-only control. In this system, the core-only control had a relatively high strength. Hence, the interfaces between shell and core layers made of the same virgin HDPE and different filler contents played a dominant role in controlling flexural strengths regardless of TPCC loading.

For flexural modulus, both core systems had a decreased moduli compared to their respective core only controls. The extent of decrease was bigger in the weak core system than that in the strong core system. This is probably associated with the relatively poor compatibility

between shell and core plastics in the weak core system (Giles, Wagner, and Mount 2005; Rosato 1998). Beside, the somewhat enhanced flexural strength and modulus with the increase of TPCC contents presumably reflected the toughening effect of TPCC.

Table 3.2 Mechanical and thermal expansion properties of coextruded core-shell WPCs with various levels of TPCC and WF in the shell layer.

System[a]	PCC or wood in shell (wt%)	Flexural modulus[b] (GPa)	Flexural strength (MPa)	Impact strength (kJ/m^2)	CTE ($\times 10^{-5}/^{o}C$)
TPCC contents in WF shell (weak core)	No shell	2.75 (0.10)A	14.90 (1.02)B	2.42 (0.26)B	6.29 (0.03)A
	6	1.81 (0.18)B	20.57 (0.60)A	5.30 (0.98)A	6.35 (0.97)A
	12	1.95 (0.14)B	20.83 (1.30)A	5.01 (0.93)A	5.94 (0.89)A
	18	2.00 (0.14)B	21.34 (0.79)A	4.86 (0.47)A	6.01 (0.58)A
TPCC contents in WF shell (strong core)	No shell	2.79 (0.06)A	34.50 (0.59)A	6.05 (0.75)B	4.37 (0.69)B
	6	2.50 (0.23)B	30.11 (1.62)B	6.94 (1.11)A	6.13 (0.17)A
	12	2.54 (0.11)AB	30.93 (1.56)B	6.64 (1.01)A	5.32 (0.61)AB
	18	2.62 (0.14)AB	30.51 (0.98)B	5.96 (0.73)B	5.61 (0.63)A
WF contents in TPCC shell (weak core)	No shell	2.75 (0.10)A	14.90 (1.02)C	2.42 (0.26)E	6.29 (0.03)AB
	0	1.72 (0.10)C	19.49 (0.61)A	7.40 (1.65)A	7.32 (0.61)A
	5	1.78 (0.15)BC	19.69 (1.18)A	6.23 (1.25)B	5.92 (1.10)B
	15	1.95 (0.14)B	20.83 (1.30)A	5.01 (0.93)C	5.94 (0.89)B
	25	1.81 (0.20)BC	17.74 (2.01)B	3.61 (0.90)D	5.28 (0.78)B
WF contents in TPCC shell (strong core)	No shell	2.79 (0.06)A	34.50 (0.59)A	6.05 (0.75)B	4.37 (0.69)B
	0	2.31 (0.13)C	28.97 (1.25)C	8.17 (1.05)A	6.14 (0.89)A
	5	2.34 (0.09)C	29.34(0.81)BC	7.72 (1.04)A	6.24 (0.44)A
	15	2.54 (0.11)B	30.93 (1.56)B	6.64 (1.01)B	5.32 (0.61)AB
	25	2.21 (0.06)C	26.43 (0.40)D	5.26 (0.98)C	5.22 (0.73)AB

[a] Weak Core: R-PP/PE:WF:Lubricant:MAPE = 40:50:6:4; Strong Core: V-HDPE:WF:Lubricant: MAPE = 40:50:6:4

[b] Means with the same letter for each category are not significantly different at the 95% confidence level; numbers in parenthesis are standard deviations.

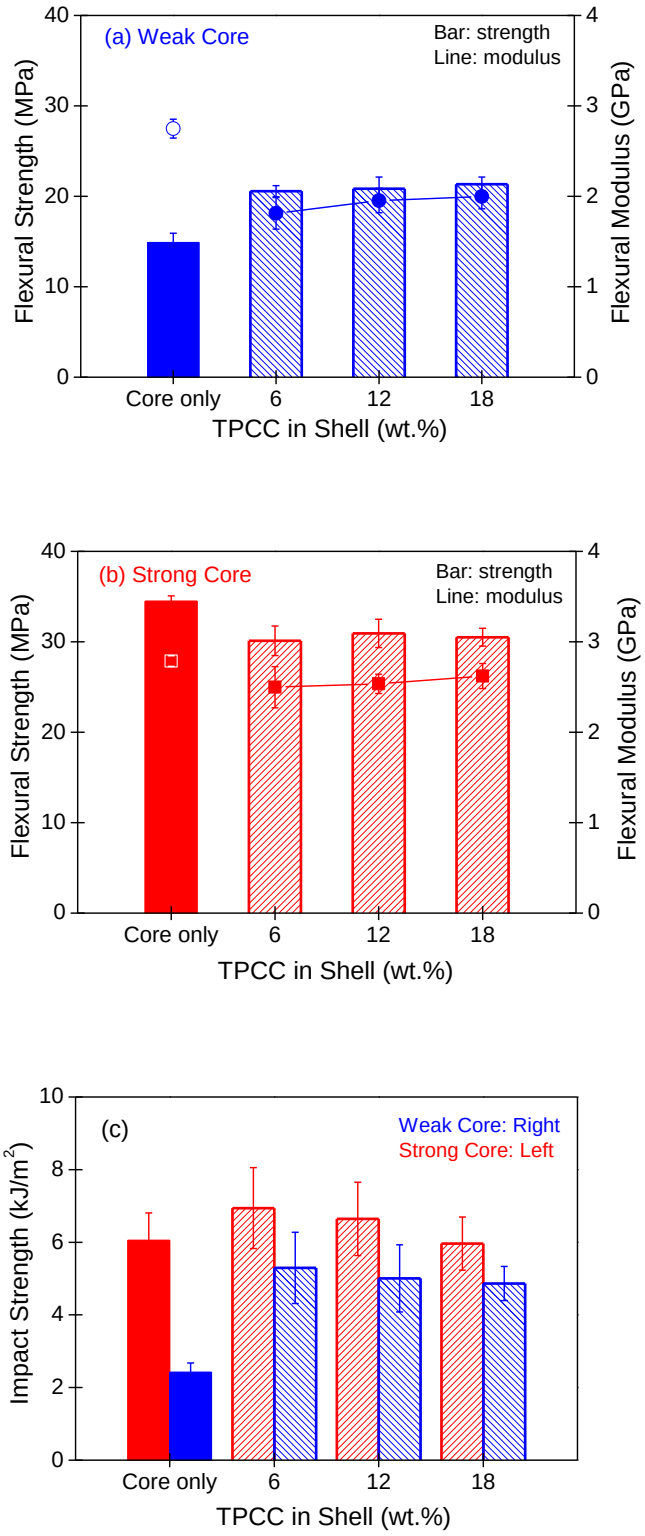

Figure 3.4 Flexural (a: weak core, b: strong core) and impact (c) properties of coextruded core-shell structured WPCs-effect of TPCC content in a 15% WF-filled shell.

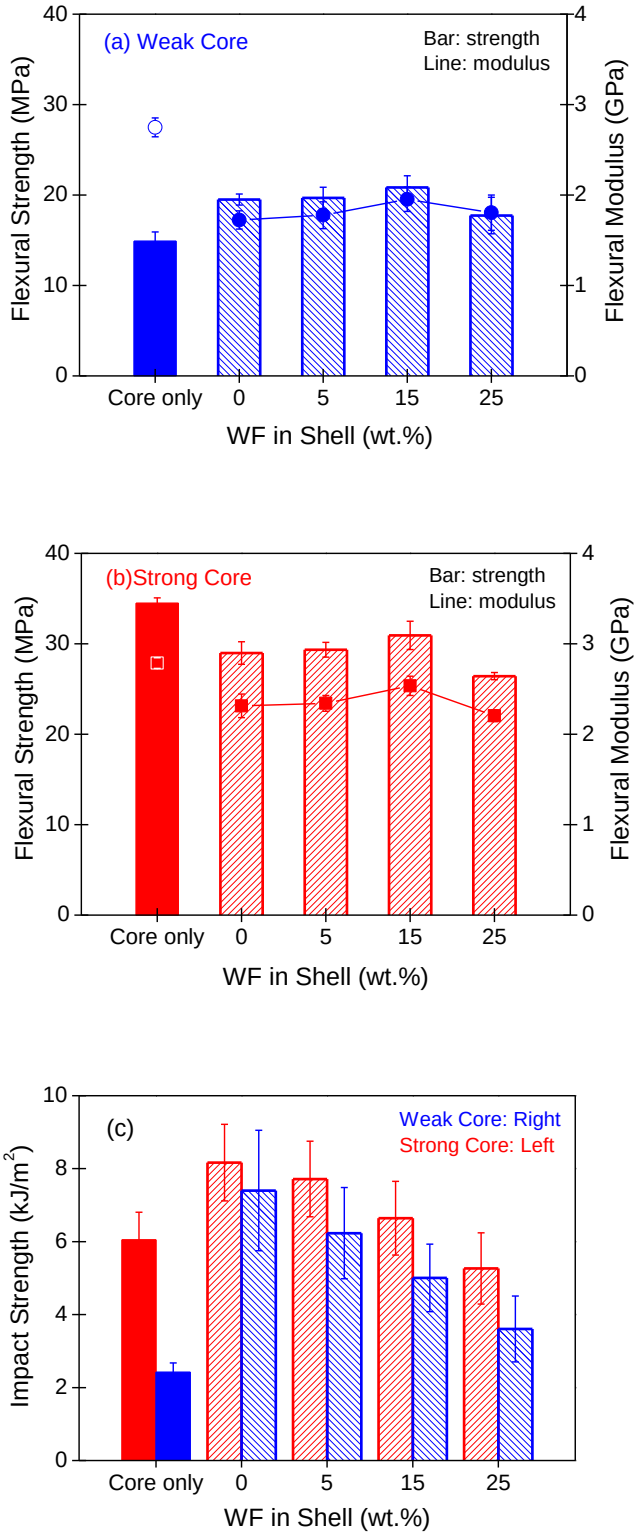

Figure 3.5 Flexural (a: weak core, b: strong core) and impact (c) properties of coextruded core-shell structured WPCs-effect of WF content in a 12% TPCC-filled shell.

Impact strengths of the coextruded WPCs are shown in Table 3.2 and Figure 3.4(c). As shown, the strength improvements were, respectively, 119% and 15% for weak and strong core systems. The more flexible and tougher shell layer made of virgin HDPE formed a more effective protection for the relatively brittle core layer in the weak core system. Thus, in coextruded WPC manufacturing, the combination of low-quality recycled plastic core and high quality virgin plastic shell can be a cost-effective choice with acceptable mechanical properties.

Flexural strengths for the coextruded WPCs with two core systems and various WF contents in a 12% TPCC filled shell are shown in Table 3.2 and Figure 3.5(a) and (b).

In the weak core system, the flexural strengths of coextruded WPCs were significantly higher than that of the core-only control. For the strong core system, coextruded WPCs showed lower strengths than that of their core-only control. Both coextruded WPC systems showed the slightly increased flexural strengths with increased WF content in the shell up to the 15% level. A similar trend was observed in flexural modulus of both coextruded systems. However, excessive WF loading in the shell layer (e.g., 25%) resulted in the reduction of flexural properties due to the poor WF dispersion and subsequent stress concentration. Impact strengths for both coextruded WPC systems are shown in Table 3.2 and Figure 3.5(c). A similar large increase in the impact strength of both core systems was observed in comparison with their respective core-only controls. The coextruded WPCs with TPCC only in shell showed the highest impact strength values among the coextruded WPCs. This is mainly related to the toughening effect of TPCC in a shell layer. However, as WF was added to the shell layer, the impact strengths of both systems were decreased, indicating that the addition of WF led to early initiation of cracks and failures in the shell layer due to its relatively bigger size and consequent cavity.

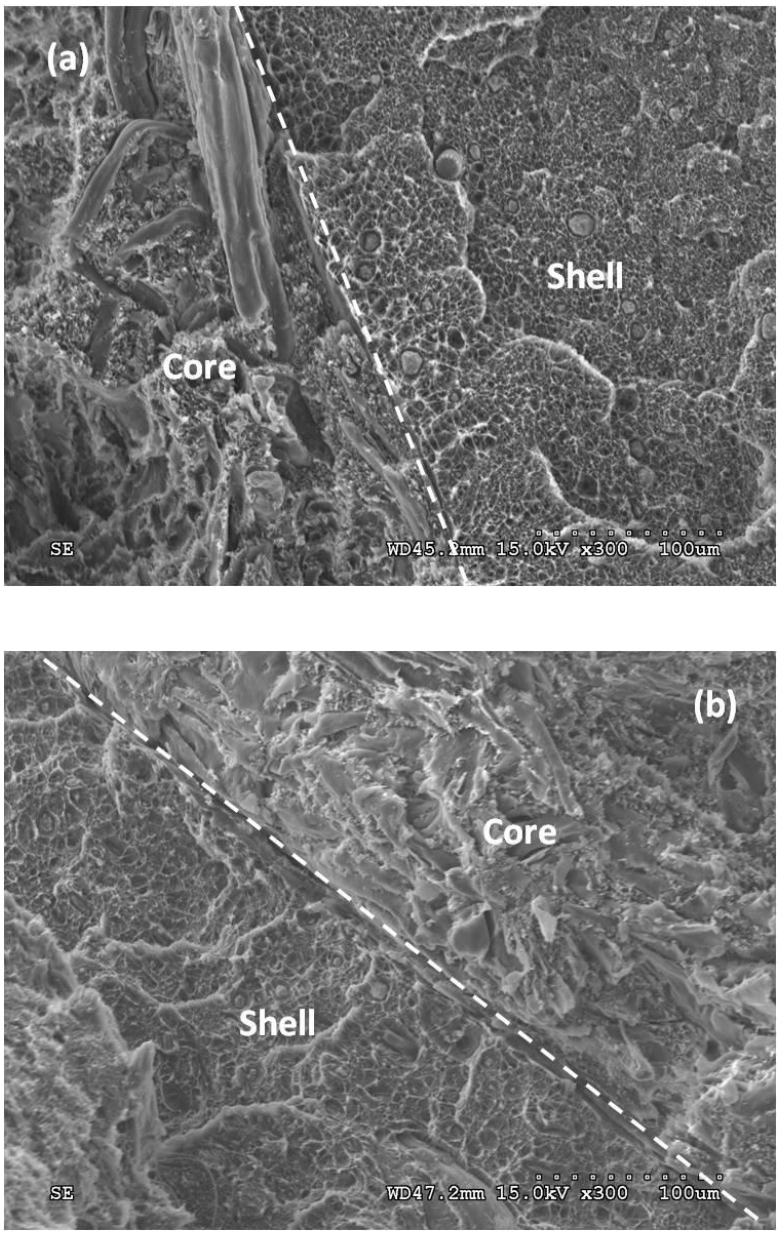

Figure 3.6 SEM micrographs of impact fractured surfaces of coextruded core-shell structured WPC: (a) weak core with TPCC-only filled shell layer; (b) weak core with TPCC and WF filled shell layer.

As a result, in the weak core system, the impact strength at the 25% WF filled shell showed the lowest value. Therefore, to acquire higher impact strength values in coextruded WPCs, the amount and size of WF in a shell layer should be adjusted and the combined use of smaller sized TPCC particle is encouraged.

Figure 3.6 shows SEM micrographs with magnified core-shell boundaries of the weak-core coextruded WPCs. Noticeable boundaries were observed in both SEM micrographs due to composition difference between WF-filled R-PP/PE core and TPCC- or TPCC/WF-filled HDPE shell.

The fractured surface of the coextruded WPC with TPCC-only filled shell (Figure 3.6(a)) showed clearly debonded small holes from the toughening effect of TPCC. On the other hand, the fractured surface of coextruded WPC with TPCC and 15% WF filled shell (Figure 3.6(b)) showed the irregularly debonded large holes with fracture propagation traces from the fast and extensive failures in the shell matrix indicating the weakened shell with large wood fiber presence.

3.3.3 Impact Fracture Type Comparison

Figure 3.7 shows a comparison of fracture type distributions (i.e., hinge versus complete) from impact tests of core-shell structured WPCs.

As shown, the fracture types varied with core quality (weak versus strong), composite structure, and filler compositions in the shell layer.

In the weak core systems (Figure 3.7(a) and (b)), while core-only controls had 100% complete-fracture mode, coextruded WPCs had much decreased complete-fracture percentage (conversely, much increased hinge fracture). The percentages of hinge fractures were 95, 70, and

65% at the TPCC levels of 6, 12, and 18% in a 12% WF filled shell layer; and 95, 90, 70, and 60% at the WF levels of 0, 5, 15, and 25% in a 15% TPCC filled shell layer.

For the strong core systems (Figure 3.7(c) and (d)), while core-only control had about 90% complete-fracture mode, coextruded WPCs had somewhat decreased complete fracture percentage. The percentages of hinge fractures were 40, 35, and 30% at the TPCC levels of 6, 12, and 18% in a 12% WF filled shell layer; and 40, 35, 35, and 30% at the WF levels of 0, 5, 15, and 25% in a 15% TPCC filled shell layer.

The observed impact fracture process in core-shell structured WPCs is systematically illustrated in Figure 3.8.

As shown, after an incident force impacted the front shell layer of coextruded WPCs, the shell layer absorbed some of the impact energy. The remaining impact force, which passed through the front shell layer, was absorbed by the core layer, and was lastly absorbed by the back shell layer.

In the weak core systems, when the impact force hit the shell surface of the coextruded WPC, more flexible and tougher shell layer made of virgin HDPE formed an effective protection for the relatively brittle core layer. However, the relatively poor compatibility between core and shell led to the unstable interfacial adhesion, which diverged the impact force.

The impact force was further distributed in the core layer and the force in the direction of loading was decreased to such an extent that it could not cause complete fracture of the back shell layer. While a core-only control showed a straight complete-fracture mode, coextruded WPCs had a much curved fracture line with hinged back shell from diverged impact forces in a core layer. Some apparent separation showing core-shell de-bonding was observed (Figure 3.8(a)). On the other hand, for the strong-core systems, the core and shell layers formed a

stronger bond resulting from the same HDPE resin and acted a whole system to resist the impact force. There was little diversion of the incident impact force, which caused complete fracture in the direction of impact loading (Figure 3.8(b)).

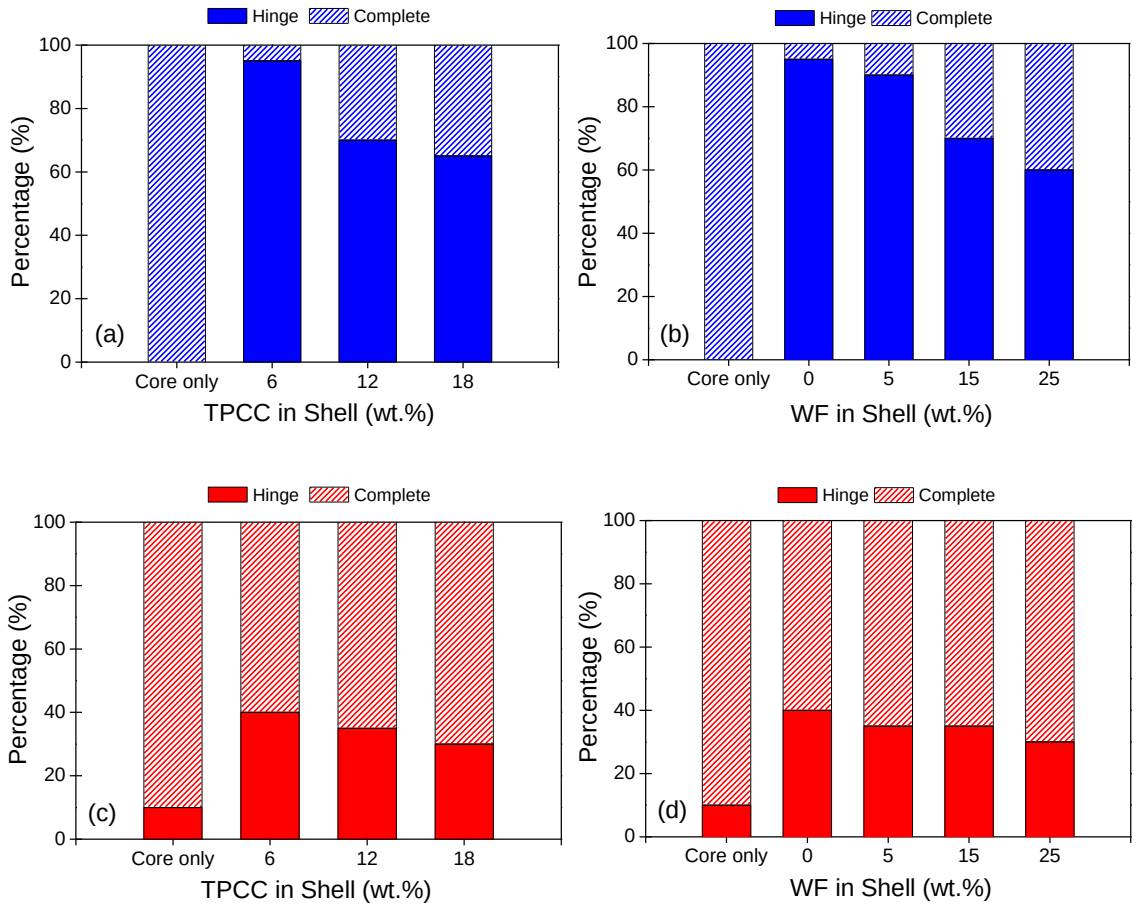

Figure 3.7 Fracture type distributions (hinge versus complete) from impact tests of coextruded core-shell structured WPCs. (a) and (b): weak core; (c) and (d): strong core.

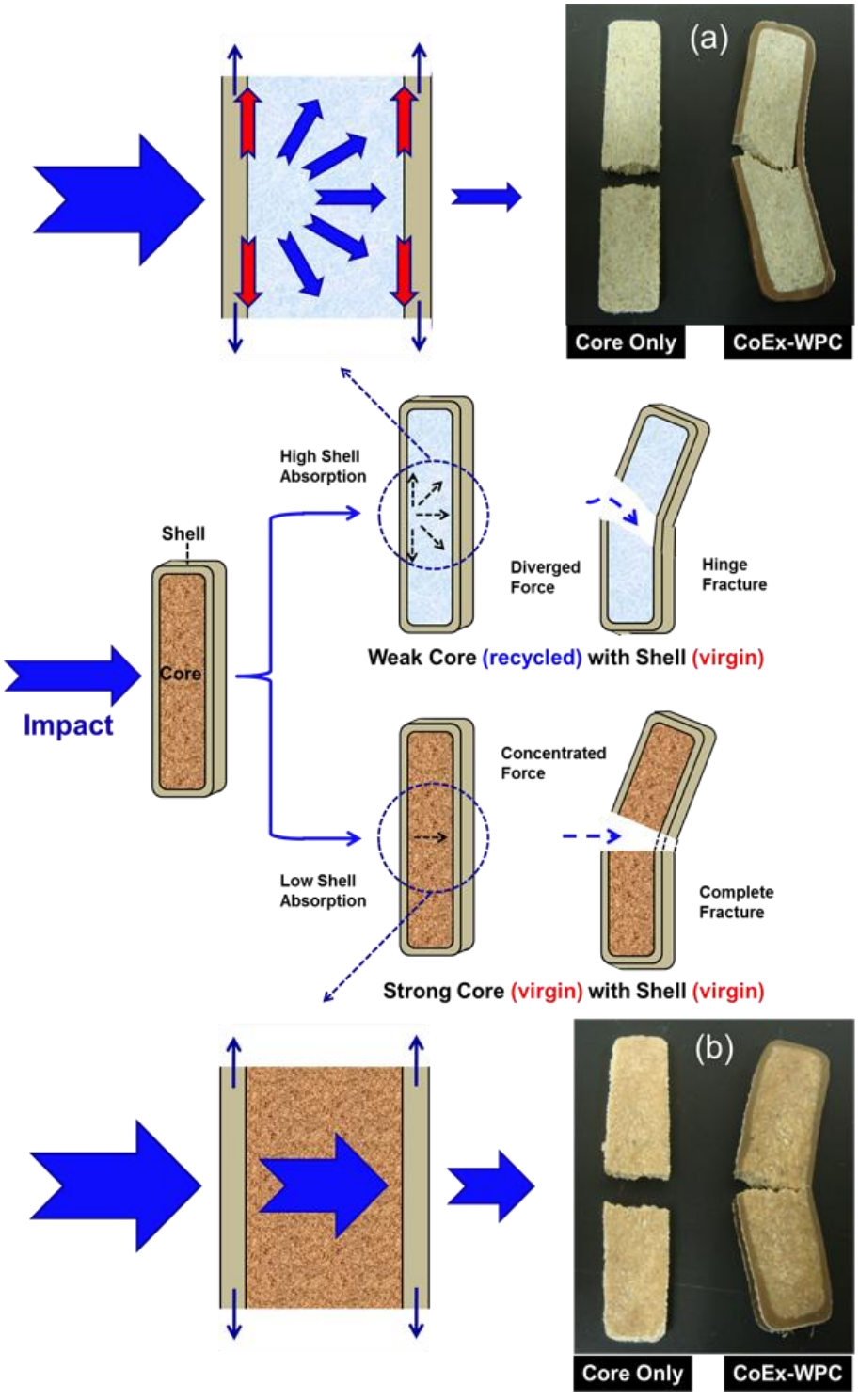

Figure 3.8 Schematic diagram showing impact fracture process of coextruded core-shell structured WPCs and photographs of typical impact fractured samples. (a): weak core system; (b): strong core system.

3.3.4 WA and TS Properties of Composites

The relationship between WA and TS for weak core and strong core systems in the variation of TPCC and WF content in a shell layer during 54 days of water immersion is shown in Figure 3.9.

For both core systems, it can be seen that the shell layer of coextruded WPCs prevented the core layer from excessive moisture uptake. Moreover, the comparison of WA and TS values between weak and strong core coextruded WPCs shows that the strong-core system had much better WA properties. This was due to the good bonding between WF and virgin HDPE in the strong core compared with a relatively poor bonding among different recycled materials in the weak core.

Increased loading of TPCC in the shell layer did not lead to any remarkable increases in WA and TS values of coextruded WPCs regardless of core qualities, as shown in Figure 3.9(a) and (b). This result is considerably ascribed to the improved dispersibility of TPCC and increased compatibility between TPCC and V-HDPE matrix in the shell layer. The relationship between WA and TS for weak- and strong-core systems in the variation of WF content in a shell layer is also shown in Figure 3.9(c) and (d). The water-proof effects of a shell layer were observed in both systems with the increased WF content in the shell layer. However, at the 25% WF level, WA and TS percentages of both systems were significantly increased. This was presumably related to the more WF loading and its hydrophilic property. Also, the high WF content in the shell layer induced cavities or gaps between WF and plastic matrix from the more aggregations of WF, consequently, leading to higher WA and TS values.

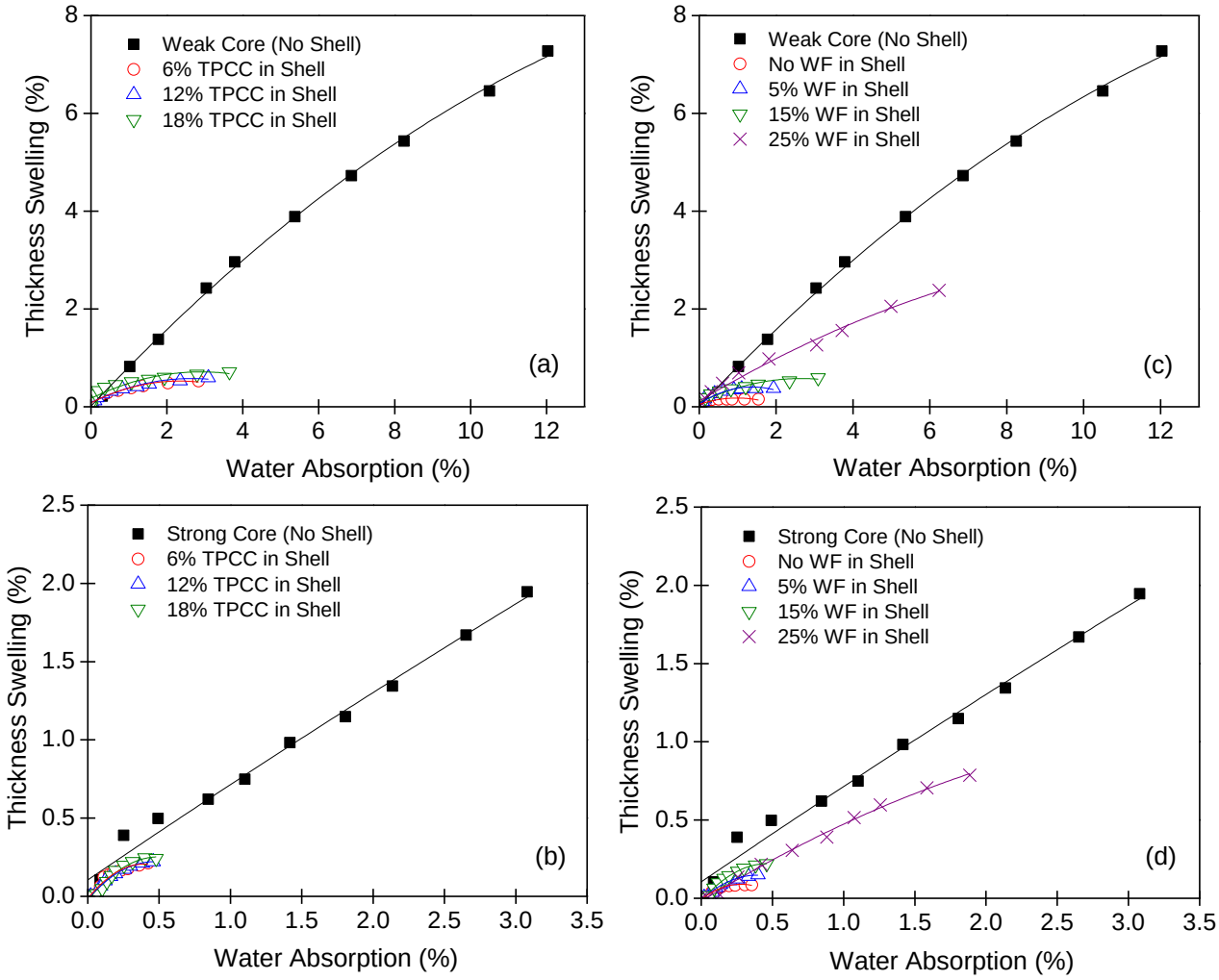

Figure 3.9 TS and WA properties of coextruded core-shell WPCs. (a): weak core and (b) strong core- effect of TPCC loading in a 15% WF-filled shell. (c): weak core and (d) strong core- effect of WF loading in a 12% TPCC-filled shell.

3.3.5 Thermal Expansion Properties of Composites

Table 3.2 lists the CTE values for coextruded WPCs with two different core systems in the variation of WF and PCC loading in a shell layer. For core-only controls, the weak core system had higher CTE values compared with the strong core system ($6.2\times10^{-5}/^{o}C$ vs. $4.2\times10^{-5}/^{o}C$) due to poor bonding between recycled plastics and wood fibers in the weak core system. Coextruded composites with 12% TPCC only in shell or the combination of 15% WF and 6% TPCC in shell showed increased CTE values. However, as filler amount in the shell layer increased, the CTE values of coextruded WPCs were reduced. Thus, a small amount of filler was not enough to offset the large CTE of the plastic matrix. As a result, coextruded WPCs with a larger portion of plastic in the shell layer would have increased CTE values.

The weak core system with recycled plastic core and virgin plastic shell at high filler loading in a shell layer showed smaller CTE values compared with core-only controls. Thus, a reinforced shell layer can help control overall thermal expansion properties of coextruded composites with a relatively poor core system. It seems that both wood and PCC fillers in the shell led to similar CTE values of the overall composites. From this result, it is found that the dimensional changes of the coextruded WPC can be significantly affected by filler loading and plastic quality in a shell layer.

3.4 CONCLUSIONS

Significant differences existed in mechanical, WA/TS and CTE properties between coextruded WPCs with weak and strong core systems as influenced by the shell compositions. In the weak core system with R-PP/HDPE, coextruded composites with a reinforced shell showed significantly improved flexural strengths compared to their core-only composite. In the strong core system made of V-HDPE, the flexural strengths of coextruded WPC were lowered

compared with the core-only composite. Impact strengths were significantly improved for both coextruded systems at low shell filling levels. High level of filler loading in the shell led to some decreases of impact strength in both coextruded systems. The types of impact fracture (i.e., hinge versus complete) varied largely with core quality and filler composition in the shell. WA/TS values of coextruded WPCs with high TPCC content in a shell layer were lower than those of core-only composites and coextruded WPCs with high wood content in the shell layer. The use of high percentage of plastic in a shell layer led to increased overall CTE values for coextruded WPCs. However, increased filler loading in the shell layer led to the decrease of CTE values for resultant coextruded WPC, especially, for the weak core system. Thus, the combination of a relatively weak core (e.g., made of recycled plastics) and a reinforced shell (e.g., with small sized inorganic particles) could be a cost-effective system for coextruded WPC manufacturing.

3.5 REFERENCES

Abdelmouleh, M., S. Boufi, M.N. Belgacem, A.P. Duarte, A. Ben Salah, and A. Gandini. 2004. Modification of cellulosic fibres with functionalized silanes: development of surface properties. *International Journal of Adhesion & Adhesives* 24: 43-54.

Bleakley, I.S., and T.R. Jones. 1993.*Precipitated calcium carbonate*. US.

Cayer-Barrioz, J., L. Ferry, D. Frihi, K. Cavalier, R. Seguela, and G. Vigier. 2006. Microstructure and mechanical behavior of polyamide 66-precipitated calcium carbonate composites: Influence of the particle surface treatment. *Journal of Applied Polymer Science* 100: 989-99.

Doshi, S.R., J.M. Charrier, and J.M. Dealy. 1988. A Coextrusion Process for the Manufacture of Short-Fiber-Reinforced Thermoplastic Pipe. *Polymer Engineering and Science* 28: 964-73.

Giles, H.F., J.R. Wagner, and E.M. Mount. 2005. *Extrusion: The definitive processing guide and handbook*: William Andrew Inc.

Jin, S., and L.M. Matuana. 2008. *Improving water resistance of wood-plastic composites through co-extrusion*. In *ANTEC*, 19-23. Milwaukee, WI.

Jin, S., and L.M. Matuana. 2010. Wood/plastic composites co-extruded with multi-walled carbon nanotube-filled rigid poly(vinyl chloride) cap layer. *Polymer International* 59: 648-57.

Kim, B.-J., F. Yao, G.H. Han, and Q. Wu. 2011. In-review. Performance of bamboo plastic composites with hybrid bamboo and precipitated calcium carbonate fillers. *Polymer Composites*.

Kim, Y.J., C.D. Han, B.K. Song, and E. Kouassi. 1984. Mechanical and Transport-Properties of Coextruded Films. *Journal of Applied Polymer Science* 29: 2359-82.

Lam, T.D., T.V. Hoang, D.T. Quang, and J.S. Kim. 2009. Effect of nanosized and surface-modified precipitated calcium carbonate on properties of CaCO(3)/polypropylene nanocomposites. *Materials Science and Engineering a-Structural Materials Properties Microstructure and Processing* 501: 87-93.

Liu, S.-T., M.J. Martin, W.C. Fultz, and P.D. Mcgill. 2006. *Precipitated calcium carbonate*. US.

Nwabunma, D., and T. Kyu. 2008. *Polyolefin composites*: John Wiley & Sons Inc.

Patnaik, P. 2003. *Handbook of inorganic chemicals*: McGraw-Hill Companies.

Porter, A.L., and W.J. Wilson. 1999. *Manufacture of precipitated calcium carbonate*. US.

Rosato, D.V. 1998. *Extruding plastics – A practical processing handbook*: Chapman & Hall.

Rothon, R.N. 1999. Mineral fillers in thermoplastics: Filler manufacture and characterisation. *Mineral Fillers in Thermoplastics I* 139: 67-107.

Stark, N.M., and L.M. Matuana. 2007. *Coating WPCs using co-extrusion to improve durability*. In *Conference for Coating Wood and Wood Composites: Designing for Durability*, 1-12. Seattle, WA,.

Stark, N.M., and L.M. Matuana. 2009. *Co-extrusion of WPCs with a clear cap layer to improve color stability*. In *4th Wood Fiber Polymer Composites International Symposium*, 1-13. Bordeaux, France.

Wypych, G. 2010. *Handbook of fillers*, 3th ed: ChemTec Publishing.

Xanthos, M. 2005. *Functional fillers for plastics*: Wiley-Vch Co.

Yao, F., and Q.L. Wu. 2010. Coextruded Polyethylene and Wood-Flour Composite: Effect of Shell Thickness, Wood Loading, and Core Quality. *Journal of Applied Polymer Science* 118: 3594-601.

Zuiderduin, W.C.J., C. Westzaan, J. Huetink, and R.J. Gaymans. 2003. Toughening of polypropylene with calcium carbonate particles. *Polymer* 44: 261-75.

CHAPTER 4 MECHANICAL PROPERTIES OF CO-EXTRUDED WOOD PLASTIC COMPOSITES WITH GLASS FIBER FILLED SHELL

4.1 INTRODUCTION

As a new generation green composite, coextruded wood plastic composite (WPC) with a core-shell structure has been recently developed and used to enhance performance characteristics of WPC (Jin and Matuana 2010; Stark and Matuana 2007). By proper combination of constituting layers one can achieve a balance of such properties as light weight, high strength, high stiffness, wear resistance, biological resistance, unusual thermal expansion characteristics, appearance, etc (Jin and Matuana 2010; Kim and Wu 2012; Stark and Matuana 2007; Yao and Wu 2010). Fundamental understanding of the interactions between shell and core layer with different structural (e.g., thickness) and material combinations is, however, needed to achieve desired product performance.

Early published work with WPC co-extrusion was done with unfilled plastic shell layers. Stark and Matuana (Stark and Matuana 2007) studied the moisture uptake of non-coextruded WPC and coextruded WPC with a high density polyethylene (HDPE) shell layer. It was shown that coextruded WPCs exhibited much reduced moisture absorptions than a non-coextruded WPC, leading to much needed water resistance improvement. Jin and Matuana (Jin and Matuana 2010) investigated flexural properties of coextruded WPCs using a PVC shell layer and reported that the addition of a pure plastic shell with a relatively low modulus over a WPC core negatively affected overall composite modulus in a core-shell structured material. Thus, to get a simultaneous improvement for both flexural modulus and flexural strength of coextruded WPCs, they considered the incorporation of carbon nano-tube (CNT) in a PVC shell layer. The addition of CNT filler in a shell layer led to some improvement of both flexural properties, but the use of

CNTs can lead to significant manufacturing cost increases. Hence, the attempts to improve the mechanical properties of coextruded WPCs using cheaper and more abundant fillers in a shell layer have been considered. Yao and Wu (Yao and Wu 2010) evaluated the coextruded WPC using the combinations of recycled PE (LDPE and HDPE) core compositions and a virgin HDPE shell with different shell thickness and wood fiber (WF) contents in a shell layer. In their experiment, coextruded WPCs with a weak core having more LDPE showed higher percentage improvements in flexural and impact strength compared with coextruded WPCs with strong core having less LDPE. At the same shell thickness, more WF contents in the shell led to the decrease of impact strength with no changes in flexural modulus. As the shell thickness increased, the increase of impact strength and the decrease of flexural modulus were observed. As a result, it was suggested that the better flexural modulus of coextruded WPC can be acquired from the combination of a thinner shell and a higher modulus core. More recently, Kim et al. (Kim and Wu 2012) studied the effects of silane treated precipitated calcium carbonate (TPCC) of sugar origin and WF filled shell layers on the properties of coextruded WPC with two different core systems (recycled PP/PE and virgin HDPE core). In this study, weak-core coextruded WPCs using a recycled PP/PE (over 90% of PP) core and a virgin HDPE shell showed significantly improved flexural strengths compared with core-only WPC regardless of filler content in a shell layer. However, strong-core coextruded WPCs made of the same virgin HDPE core and shell demonstrated relatively low strength increases in relation to core-only WPC and even showed strength reductions at high filler content in a shell layer. In impact strength, weak-core coextruded WPCs with different core-shell thermoplastics showed a 206% improvement at TPCC only in a shell layer. The incorporation of fillers in a shell layer of coextruded WPCs has somewhat positively affected the mechanical properties of core-shell structured composites.

However, cost and performance effective shells are still needed to achieve desired composite performance.

Short glass fibers (SGFs) have been used as a good reinforcing filler for WPC. Jiang et al. (Jiang et al. 2003) reported that impact strength of WPC using PVC and WF was considerably increased by adding SGF (a 60 % improvement in notched impact strength with 5 % SGF filled WPC). This improvement was due to the 3-dimensional network structure formed by the WF and SGF. It was suggested that the effectiveness of SGFs reinforcement was highly associated with SGF aspect ratio, SGF/WF composition, and PVC content. Jiang et al. (Jiang et al. 2007) applied a commingled unidirectional GF-polymer composite sheet (CUGPCS) to surface of WPC deck profile and achieved a good interfacial adhesion between CUGPC and WPC. Significantly increased bending modulus of rupture (MOR), modulus of elasticity (MOE), and strain at break were reported for the laminated WPC composites. However, manufacturing CUGPCS reinforced WPC with premade WPC boards requires additional processing steps and energy and long-term effectiveness of bonded surfaces has not been demonstrated. On the other hand, coextrusion technology making various properties of WPC highly tunable through fully capped shell in one step could be effective to achieve synergetic effects of SGF and WPC.

The objective of this study was to investigate the effects of various GF contents in a shell layer and shell thickness changes on the flexural and impact properties of coextruded WPC in combination with three core systems (low, moderate, and strong).

4.2 EXPERIMENTAL

4.2.1 Materials and Preparation

HDPE (AD60-007) and LDPE (LD103) were provided by ExxonMobile Chemical Co. (Houston, TX, USA). Pine WF (20 mesh particle size) was supplied by American Wood Fibers

Inc. (Schofield, WI, USA). Short GF reinforced HDPE pellets were provided by RTP Co. (Winona, MN, USA). The material was of the type RTP 707 CC UV Natural with glass fiber content of 40 % by the weight of total formulation. The fiber diameter was 0.014 mm and fiber length was 4 mm prior to compounding. The fibers were sized with a silane–based solution before compounding. UV (Type 6022) and coupling (Fusabond EMB 100D) agents were added to the GF-HDPE system during compounding. MAPE (Epolene^{TM} G2608) from Eastman Chemical Co. (Madison, TN, USA) was utilized to increase the compatibility between wood fillers and plastic matrix. Lubricant (TPW 306) from Struktol Co. (Stow, OH, USA) was also used to improve the processing of WPC profile. The mixtures of HDPE, LDPE and GF filled HDPE were used as base resins to make three core systems (i.e., weak, moderate and strong). HDPE and 40% GF filled HDPE or their mixtures were used to make a shell material as a function of GF content. Materials used for shell were used without pre-compounding to prevent further breakage of GF fibers.

4.2.2 Injection Molding of GF-HDPE Samples

Injection molding was used to make test samples for establishing shell properties. Experimental design included five blends with GF/HDPE ratios of 0:100, 10:90, 20:80, 30:70, and 40:60. Melt compounding was first performed using an intermesh, counter-rotating Brabender twin-screw extruder (Brabender Instruments, Hackensack, NJ) with a screw speed of 40 rpm. The temperature profile of barrels ranged from 150 to 175°C. The extrudates were air-cooled and then pelletized into granules. The granules were injection-molded into standard mechanical test specimens using a Batenfeld Plus 35 injection molding machine (Batenfeld, NJ, USA). The injection temperatures were 190 and 180 °C for HDPE/GF composites and virgin HDPE, respectively. All specimens were then conditioned for 72 hr at a temperature of 25 °C and

a relative humidity of 50% for later characterization.

4.2.3 Co-extruded WPC Manufacturing

The composites were formulated with three core types (i.e., weak, moderate and strong) in combination with different GF contents in shell and shell thickness changes for each core type. The formulations for the weak-, moderate- and strong-core systems were, respectively, LDPE: HDPE: WF: Lubricant: MAPE = 30: 10: 50: 6: 4 %, LDPE: HDPE: WF: Lubricant: MAPE = 10: 30: 50: 6: 4 %, and HDPE: GF: WF: Lubricant: MAPE = 50: 20: 25: 3: 2 %. Six GF content levels (i.e., 0, 10, 15, 20, 30, and 40 %) and five shell thicknesses (i.e., 0.8, 1.0, 1.2, 1.4, and 1.6 mm) were used to make different shells.

The composites were manufactured with a pilot-scale coextrusion system (Yao and Wu 2010). This system consists of a Leistritz Micro-27 co-rotating parallel twin-screw extruder (Leistritz Corporation, Allendale, NJ) for core and a Brabender 32 mm conical twin-screw extruder (Brabender Instruments Inc., South Hackensack, NJ) for shell. A specially-designed die with a cross-section area of 13 × 50 mm was used. A vacuum sizer was used to maintain the targeted size. The coextruded profiles passed through a 2 m water bath with water spraying using a down-stream puller. Manufacturing temperatures for core were controlled at 155 (feeder), 160, 165, 170, 170, 170, 160, 150, 140, 130, and 155^{o}C (die). Manufacturing temperature for shells varied from 150 to 165^{o}C in the variation of different shell formulations. Different shell thicknesses were achieved by controlling shell feeding rate and extrusion speed.

4.2.4 Mechanical Testing and Characterization

Three-point flexural test was conducted using a model 5582 Instron testing machine (Instron Co, Norwood, MA) at a crosshead speed of 6 mm/min according to the ASTM D790 to determine bending strength and modulus for both injection molded and extruded samples. Tinius

Olsen Mode 1892 impact tester (Tinius Olsen Inc., Horsham, PA) was used to test Izod impact strength according to the ASTM D256. The injection molded samples were notched prior to testing. For extruded material, test samples of 3-mm in thickness were acquired by cross-cutting the extruded profiles such that the impact force on the test samples was perpendicular to the coextrusion direction. These samples were tested without notching to preserve original core-shell structure. More than 5 samples were tested for each group. Type of impact facture failure (i.e., hinge versus complete) for each sample was recorded.

Composite morphologies were characterized by a Quanta 3D FEG Dual Beam Scanning Electron Microscope (SEM) with Focused Ion Beam (FIB) (FEI Company, Hillsboro, OR). The samples were coated with Pt to improve the surface conductivity before observation and observed at an acceleration voltage of 5 kV.

4.3 RESULTS AND DISCUSSION

4.3.1 Shell GF-HDPE Composite

4.3.1.1 Morphology

Typical SEM micrographs for 30% GF-filled HDPE composites are shown in Figure 4.1. Most GF fillers were aligned perpendicular to the fracture plane (i.e., along the injection molding flow direction). Certain filler pullouts happened during fracture process as indicated by the circular voids on the fracture plane. The remaining GF fillers appeared to be well-bonded to the matrix, indicating effect of surface coupling treatments of the GFs prior to mixing with the plastic matrix.

4.3.1.2 Mechanical Property

Flexural property (MOE and MOR) and impact strength of GF filled shell-only composites are summarized in Table 4.1 and the data are plotted in Figure 4.2(a).

Flexural moduli of GF filled composites exhibited an increasing trend with increased filler loadings. The neat HDPE showed a flexural modulus of 0.85 GPa and for 40% GF filled composite, the modulus was increased to 5.8 GPa. The increase of flexural modulus was attributed to the enhanced interfacial interaction between the GF filler and polymer matrix and the high aspect ratios of GF fillers in the plastic matrix also helped it (DiBenedetto 2001; Rothon 1999; Wypych 2010a; Xanthos 2005).

In flexural strength, GF-filled composites showed significant strength increases with increased GF loadings. At the 40% GF loading level, the strength was 3.94 times higher than that of the neat resin. It can be concluded that GF filler alignments as shown in the SEM micrographs (Figure 4.1) also played an important role in determining the flexural strength of the composites (Fu and Lauke 1996)

Figure 4.2(b) illustrates the notched Izod impact strengths of GF-filled composites in the variation of GF content.

The neat HDPE had an impact strength of 28.57 kJ/m^2 and when the GF filler was added to the system, the strength was significantly decreased. At the 10% GF loading level, the impact strength was 9.63 kJ/m^2 and the reduced impact strength of GF-filled composites may be due to the decrease of ductility and toughness by the incorporation of fillers, restricting the molecular chain movement of the plastic matrix (Nunez et al. 2003). In GF-filled composites, the impact strength increased with further increase of GF loading beyond the 10% level. Since GFs were well bonded to the plastic matrix, the perpendicularly aligned GF fillers to the impact testing direction (Figure 4.1) could help absorb the impact force, leading to enhanced impact strength.

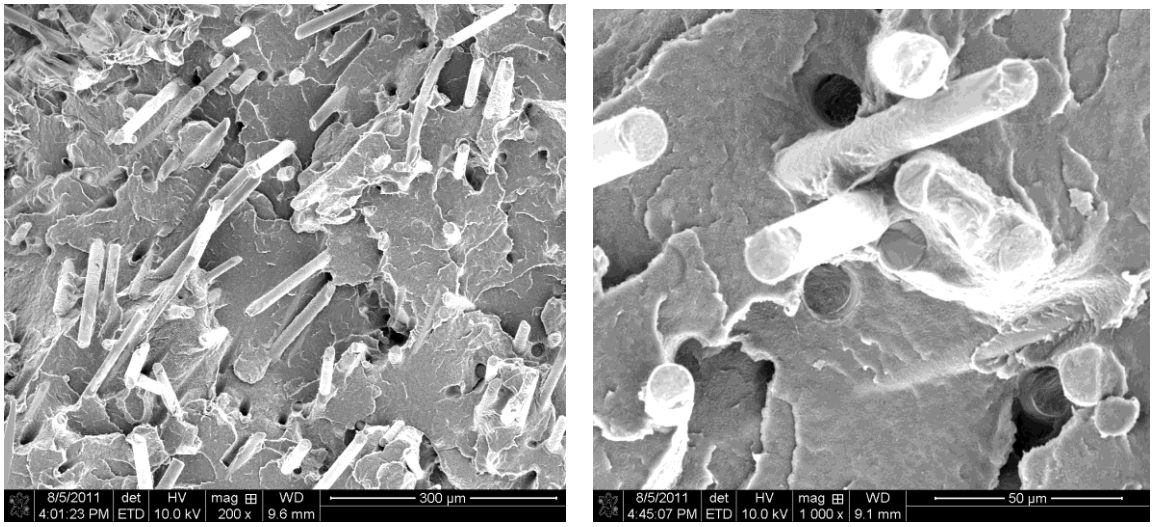

Figure 4.1 SEM micrographs of impact fractured surfaces of 30% GF filled HDPE composites.

Table 4.1 Mechanical properties of core-only WPCs with different core quality (weak, moderate, and strong) and shell-only composites with various GF content.

Composite Type	Material Make-up	Property		
		MOE[a] (GPa)	MOR (MPa)	IM (kJ/m^2)
Shell	GF/HDPE: 0:100	0.85 (0.06)	21.83 (0.96)	28.57 (2.04)
	GF/HDPE: 10:90	1.31 (0.03)	29.22 (0.18)	9.62 (0.37)
	GF/HDPE: 20:80	2.34 (0.33)	40.92 (0.58)	10.37 (0.37)
	GF/HDPE: 30:70	3.57 (0.08)	57.80 (0.69)	11.94 (0.16)
	GF/HDPE: 40:60	5.78 (0.19)	85.93 (1.59)	14.55 (0.34)
Core	Weak	2.16 (0.05)	22.32 (0.54)	5.39 (0.42)
	Moderate	3.23 (0.07)	31.04 (0.41)	3.52 (0.26)
	Strong	4.45 (0.30)	48.82 (1.52)	4.60 (0.60)

[a] The numbers in parenthesis are standard deviations.

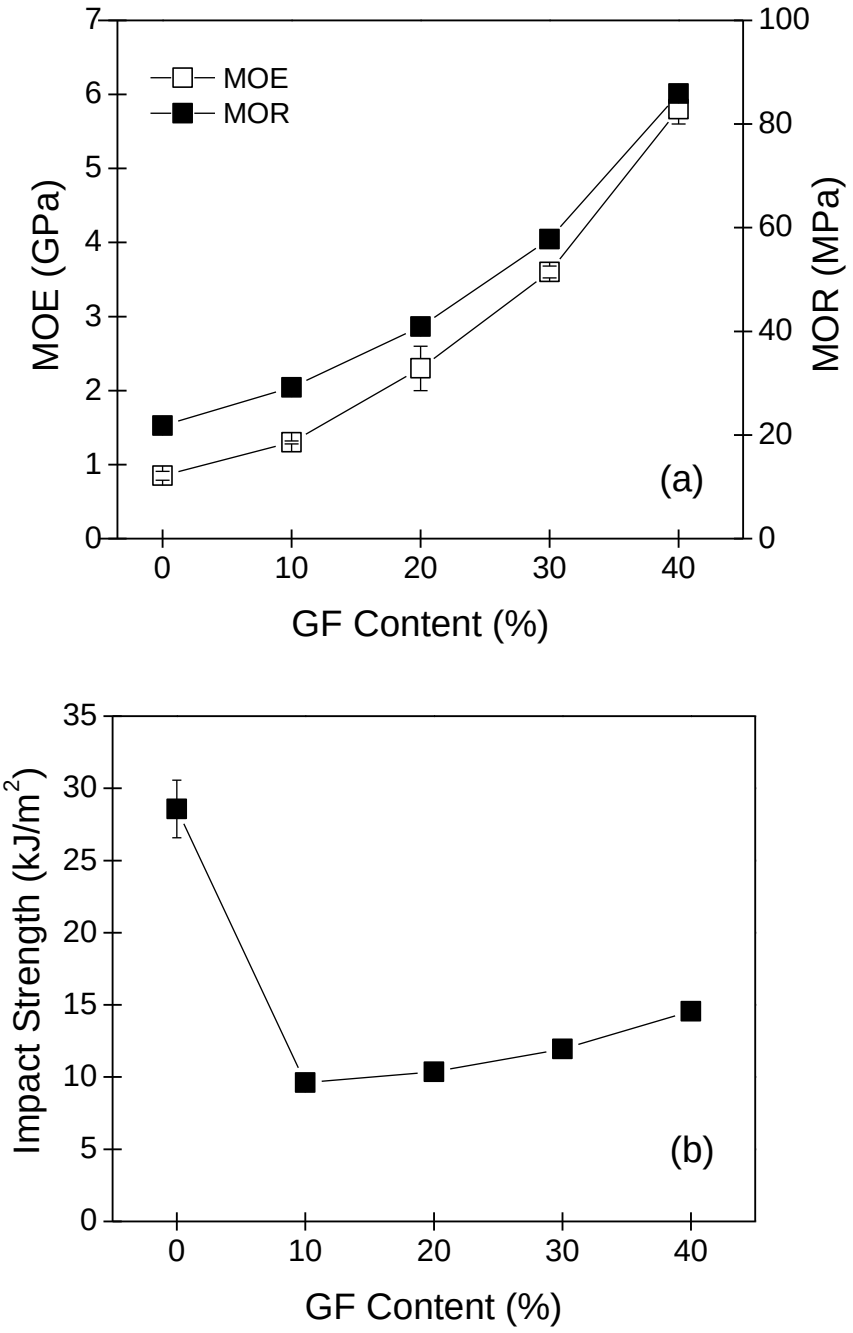

Figure 4.2 Flexural properties (a) and impact strength (b) of GF filled shell-only composites.

4.3.2 Extruded Core-only Composites

4.3.2.1 Morphology

SEM micrographs from impact fractured core-only WPCs with three different core systems (i.e., weak, moderate, and strong) are shown in Figure 4.3. For weak- and moderate-core WPCs (shown in Figure 4.3(a) and (c)), well distributed WF fillers in plastic matrix are seen in both composites. But, more magnified images (Figure 4.3(b) and (d)) show somewhat different fracture features between the two composites. As shown in Figure 4.3(b), for weak-core WPC, broken WF filler still covered with plastic indicates that more flexible LDPE in the matrix prevented the WFs from being cleanly pulled-out. However, for moderate core WPC with HDPE (Figure 4.3(d)), relatively clean surfaces of WFs without plastic covering are observed. For strong-core WPC (Figure 4.3(e)), well-dispersed WF and GF fillers are apparent and the close-up micrograph (Figure 4.3(f)) indicates good interfacial adhesion between fillers (both GF and WF) and plastic matrix. Thus, it can be possibly said that more coupling agent (and lubricant) included in the strong-core WPC effectively improved the dispersibility and adhesion of fillers in plastic matrix (Tselios et al. 1999).

4.3.2.2 Mechanical Property

Figure 4.4(a) and (b) summarize measured flexural properties (MOE and MOR) and impact property of core-only WPCs with three different core systems (i.e., weak, moderate, and strong, respectively). HDPE has more rigid and tougher characteristics compared with LDPE due to its macromolecular properties (Charles 2000). Hence, in WPC matrix containing more HDPE, better flexural modulus and strength are expected. The MOE and MOR values were increased in the order of weak, moderate, and strong core.

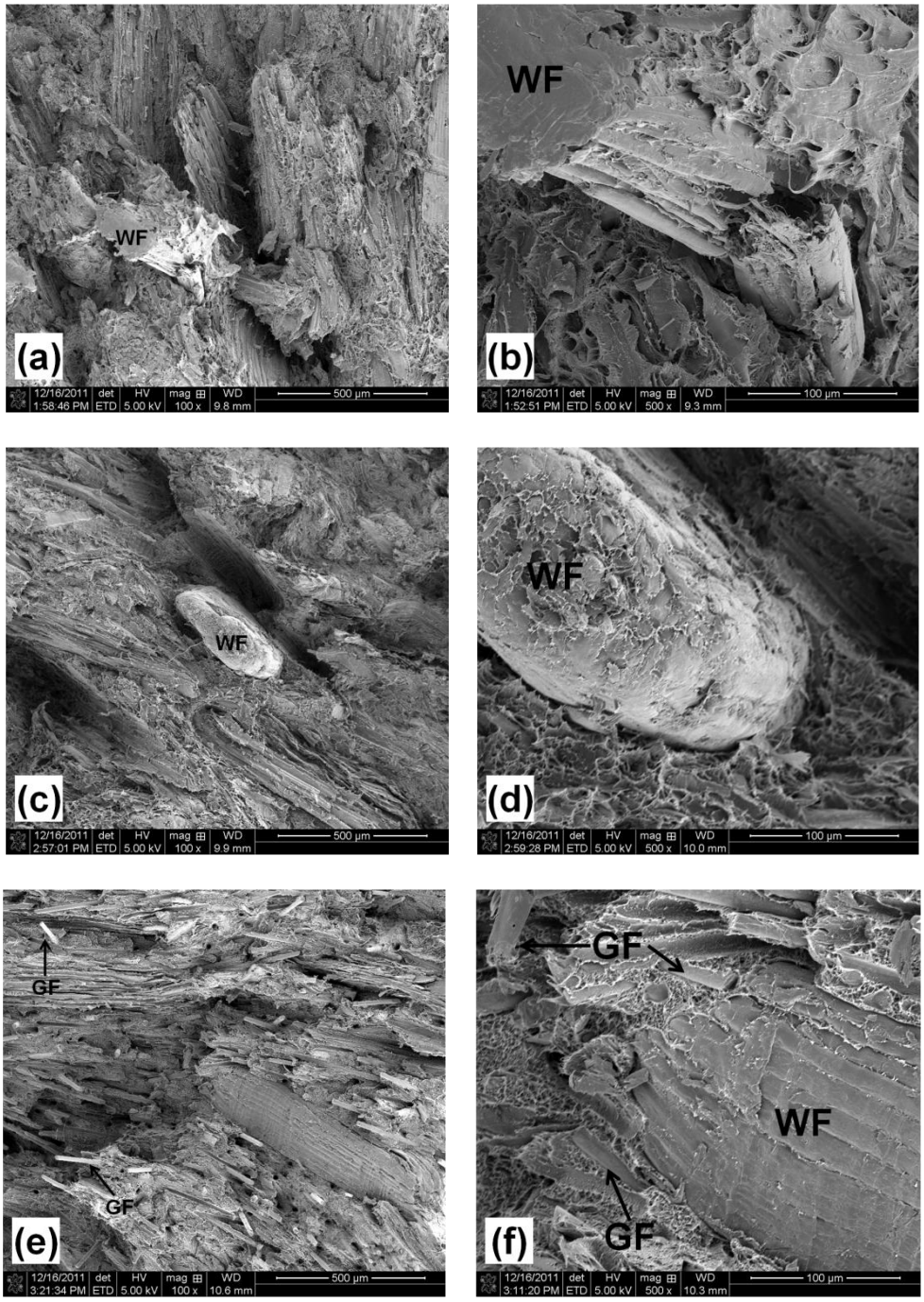

Figure 4.3 SEM micrographs of core-only WPCs: weak core (a and b), moderate core (c and d) and strong core (e and f).

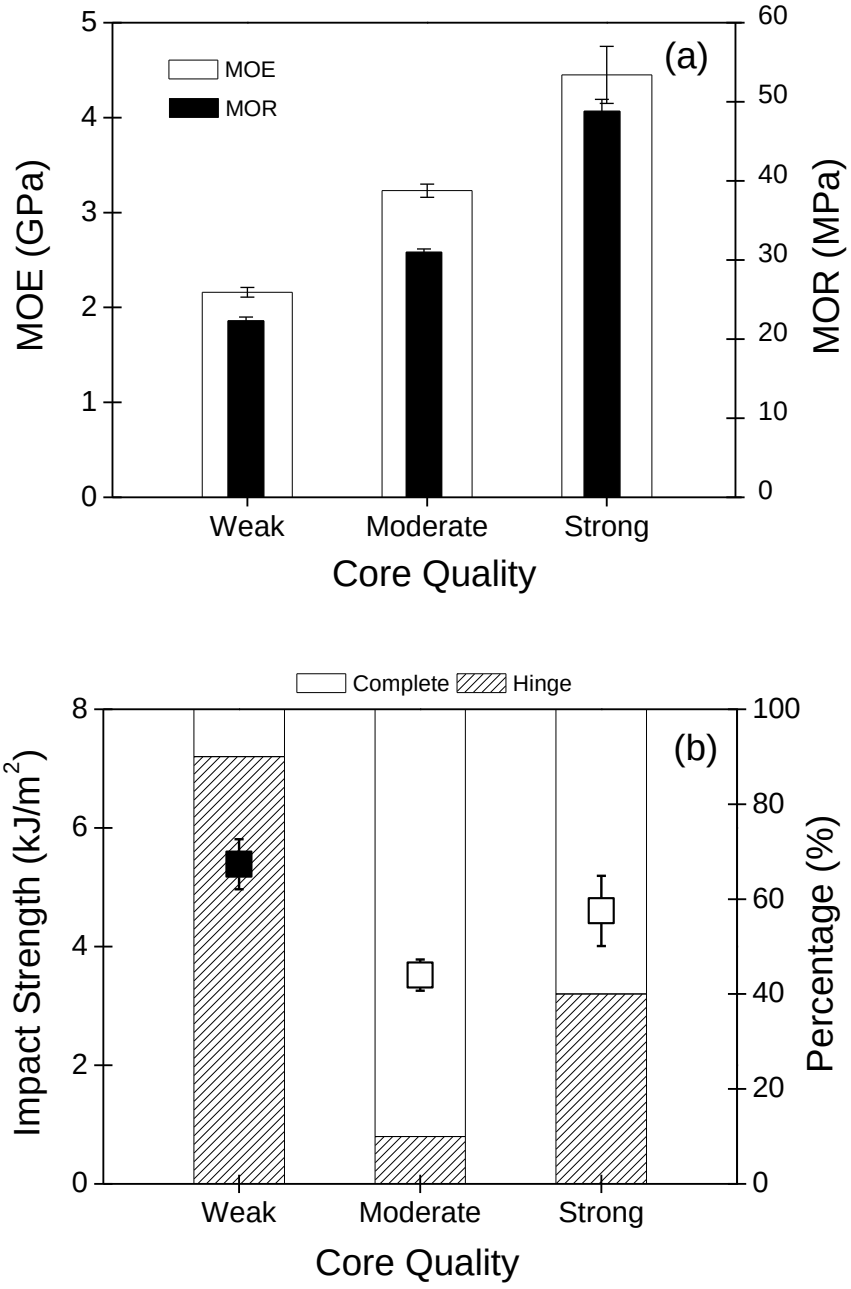

Figure 4.4 Flexural properties (a) and impact strength with percentage of breaking types (b) for extruded core-only WPCs (weak, moderate, and strong core).

The weak- and moderate-core WPCs included 50% WF, while the strong-core WPC had 25% WF and 20% GF. The MOE and MOR values of core-only composites are significantly higher in the strong-core system than those in weak- and moderate-core systems. This indicates that the incorporation of GF in WPC matrix led to the remarkably improved flexural properties due to its high fiber strength and high aspect ratios (Ghaus and Hamid 2008; Shakeri and Raghimi 2010; Thwe and Liao 2002; Tungjitpornkull, Chaochanchaikul, and Sombatsompop 2007; Velmurugan and Manikandan 2007). Moreover, the GF fiber direction (perpendicular to flexural test direction) in extruded composites affected the strength improvements of the strong core WPC (Fu and Lauke 1996).

Impact strength values were from high to low in the order of weak, strong, and moderate core systems. This result seems to indicate that weak-core WPC with more flexible LDPE (75% LDPE in plastic) absorbed more impact energy than strong-core WPC and moderate-core WPC using HDPE-only and less LDPE (25% LDPE in plastic), respectively.

As shown in Figure 4.4(b), the impact fracture types varied with different core quality. Weak core WPC showed 90% hinge-fracture mode. On the other hand, strong- and moderate-core WPCs showed the decreased hinge-fracture mode (40 % and 10 %, respectively).

4.3.3 Coextruded Core-Shell Composites

4.3.3.1 Morphology

Figure 4.5 shows SEM micrographs for the cross sections (Figure 4.5(a) and (b)) and the laterally-cut shell surface (Figure 4.5(c) and (d)) of strong-core coextruded WPC with 40% GF-filled shell. More magnified image (Figure 4.5(b)) of cross section shows more frequent existence of GF fillers in shell (40% GF) region than that in core (20% GF) region. When it

comes to filler alignment in the shell layer, the alignment of GF fillers in polymer matrix is the same as coextrusion profile direction, which is apparently shown in Figure 4.5(d).

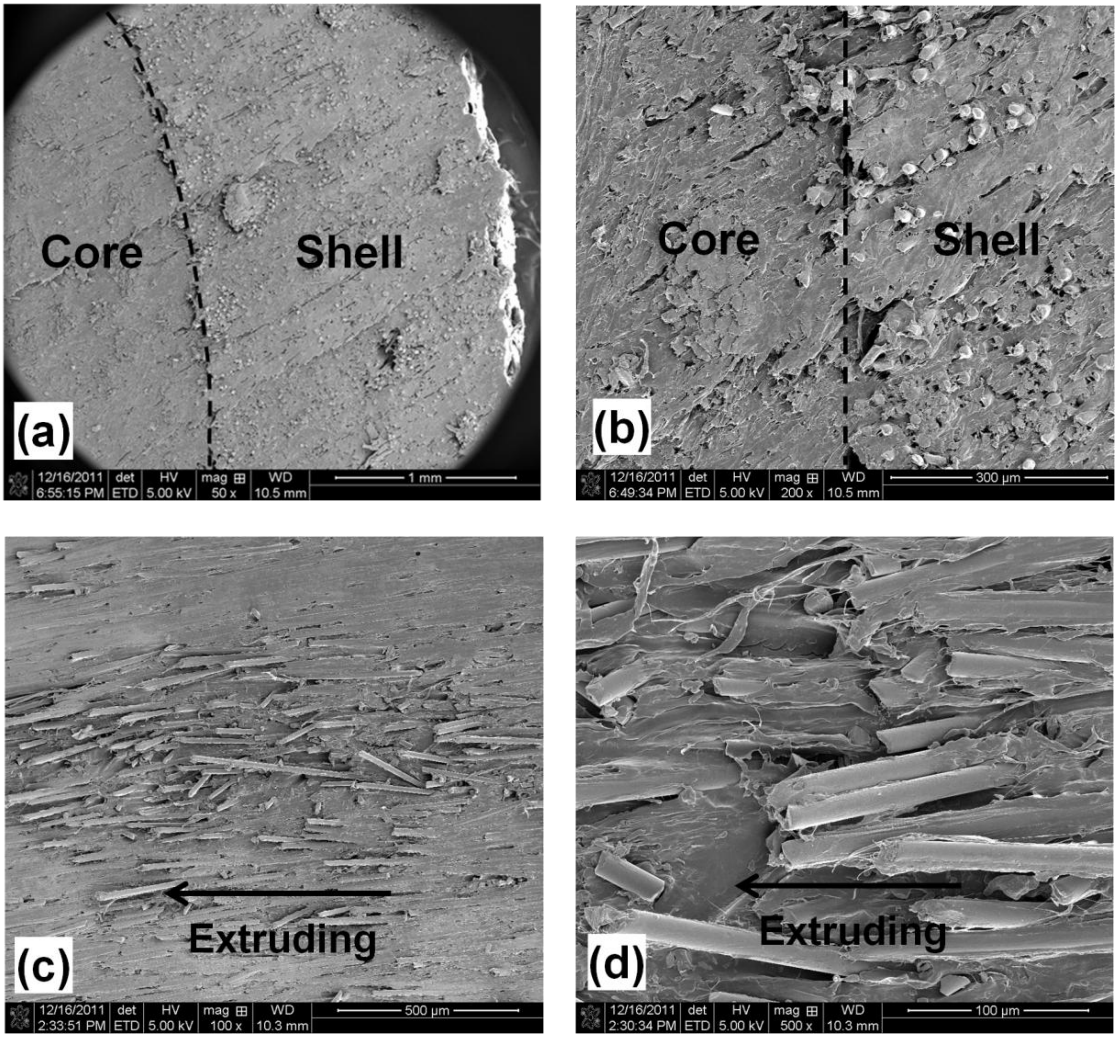

Figure 4.5 SEM micrographs for cross section (a and b) and top view (c and d) of strong-core coextruded WPC with 40% GF shell.

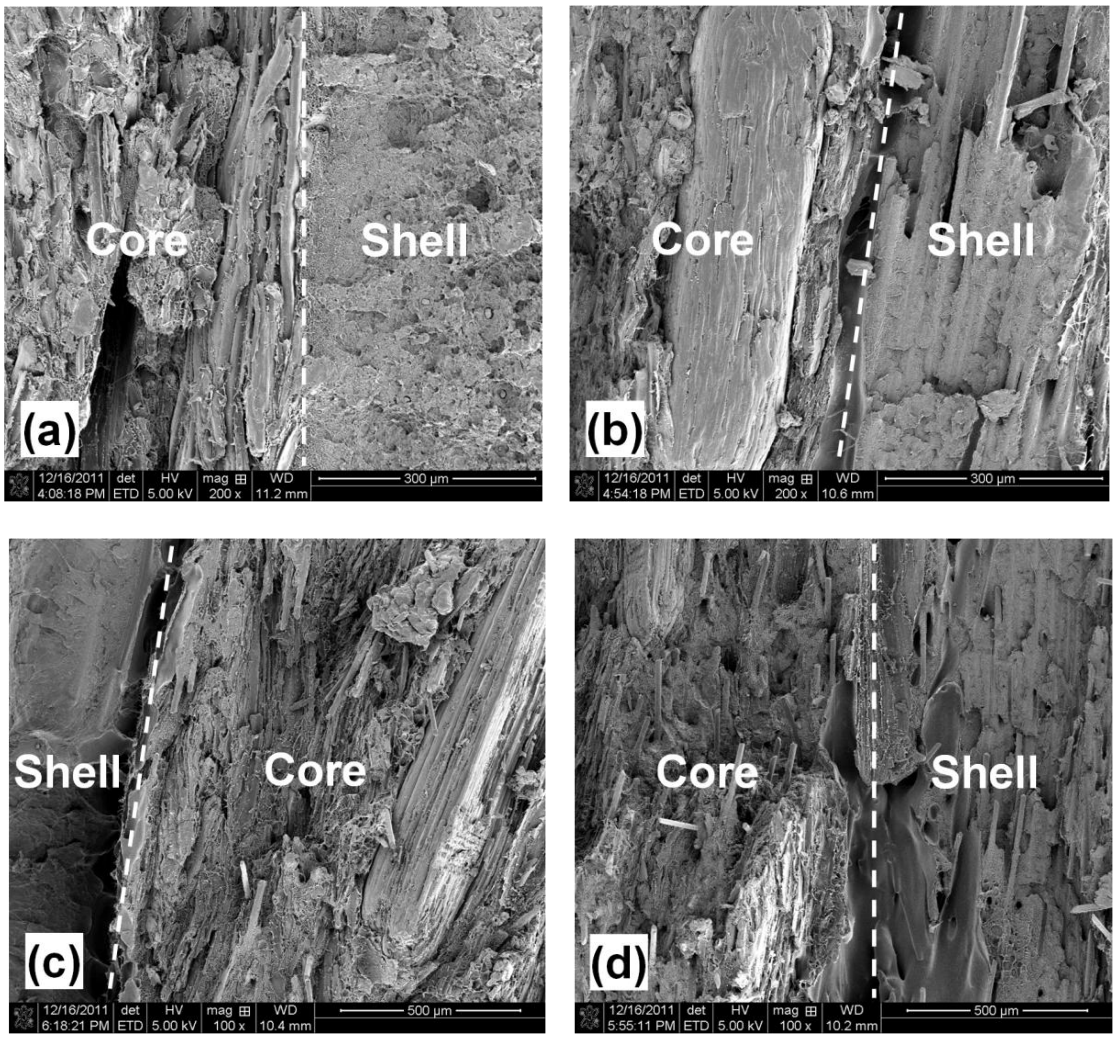

Figure 4.6 SEM micrographs of coextruded WPCs: moderate core with PE shell (a) and with 40% GF shell (b); strong core with PE shell (c) and with 40% GF shell (d).

Impact fractured morphologies for moderate- and strong-core coextruded composites are shown in Figure 4.6. Moderate core with WF filler (left) and HDPE-only shell (right) are clearly seen in Figure 4.6(a) and also, moderate core with WF filler (left) and 40% GF-filled shell (right) are observed in Figure 4.6(b).

As shown in the right section of Figure 4.6(b), the direction of GF filler alignments in the 40% GF-filled shell layer is parallel to that of impact testing direction and this means that it is hard to expect an improved impact property in coextruded composites by the addition of GF filler into the shell layer. Strong core with WF/GF-filled shell (right) and HDPE-only shell (left) are differentiated from each other in Figure 4.6(c) and strong core with WF/GF-filled shell (left) and 40% GF-filled shell (right) in Figure 4.6(d) are discerned by the existence of WF. Though some interfacial gaps between core and shell layers were observed, their bonding condition looks reliable.

4.3.3.2 Mechanical Property

Measured mechanical properties (MOE, MOR, and impact strength) for coextruded composites with three different core qualities are summarized in Table 4.2. Summary plots of the data as a function of the corresponding shell and core properties are shown in Figures 4.8, 4.9, and 4.10, respectively for MOE, MOR, and impact strength. Also, in the figures, the plots of all-core and all-shell properties are illustrated as comparisons.

For each mechanical property, the two lines of all-core and all-shell composites formed upper and lower bonds, respectively. The core property was constant for each coextruded composite system, while the shell property increased with the increase of GF content in the shell layer. The intersections represented the points where core and shell had the same property values. When the coextruded composite systems changed from weak to moderate and strong cores, the intersection points shifted toward higher property value points.

Table 4.2 Mechanical properties of coextruded composites with different core quality (weak, moderate, and strong) and shell thickness including various GF content in shell layer.

GF content[a] (%)	Shell Thickness (mm)	Weak Core			Moderate Core			Strong Core		
		MOE (GPa)	MOR (MPa)	IM (kJ/m^2)	MOE (GPa)	MOR (MPa)	IM (kJ/m^2)	MOE (GPa)	MOR (MPa)	IM (kJ/m^2)
0	0.8	1.88	21.42	7.14	2.85	31.57	N.A.	3.66	43.19	N.A.
	1.0	1.77	21.52	8.56	2.76	31.40	7.26	3.20	38.41	6.73
	1.2	1.66	21.25	10.42	2.56	32.31	9.27	2.41	29.92	9.25
	1.4	1.60	20.60	12.65	2.60	32.60	N.A.	2.45	33.34	10.92
	1.6	1.56	20.99	15.89	2.27	28.51	11.42	2.26	30.67	13.51
10	0.8	2.16	25.68	5.52	2.99	32.76	6.22	3.65	42.98	6.78
	1.0	2.07	25.49	7.42	2.94	33.76	5.37	3.43	41.96	8.04
	1.2	1.96	25.36	8.24	2.60	32.53	7.99	3.11	40.58	8.56
	1.4	2.11	25.54	8.00	2.77	34.53	N.A.	2.81	37.64	10.50
	1.6	2.08	26.89	11.44	2.57	32.53	7.59	2.90	37.85	11.74
15	0.8	2.18	23.79	6.50	3.14	34.19	4.77	3.88	45.72	7.61
	1.0	2.31	25.87	7.79	3.08	36.02	5.31	3.68	45.02	8.29
	1.2	2.40	28.75	9.30	2.86	35.52	5.71	3.54	44.36	9.20
	1.4	2.46	29.81	8.00	2.79	34.40	N.A.	3.42	42.86	10.22
	1.6	2.51	31.42	11.61	2.90	35.90	7.67	3.30	42.78	11.78
20	0.8	2.38	24.68	6.71	3.22	34.50	7.35	4.12	47.27	7.08
	1.0	2.55	27.62	7.26	3.20	35.69	5.40	3.92	47.74	8.29
	1.2	2.66	30.55	8.36	3.06	36.49	9.64	3.88	47.86	9.21
	1.4	2.77	32.46	7.22	3.14	37.28	N.A.	3.77	46.50	9.35
	1.6	2.70	32.79	11.61	3.24	38.24	7.74	3.64	42.65	11.81
30	0.8	2.94	31.21	7.22	3.55	36.32	5.18	4.49	51.75	N.A.
	1.0	3.13	34.48	8.03	3.66	38.90	5.33	4.62	52.55	10.03
	1.2	3.34	36.62	8.24	3.80	43.14	5.83	4.73	53.84	8.99
	1.4	3.55	38.65	9.75	3.93	44.51	N.A.	4.86	54.33	10.14
	1.6	3.83	39.34	11.98	4.11	46.85	8.06	5.03	54.83	11.96
40	0.8	3.46	34.70	8.48	3.97	41.86	4.60	4.84	53.34	N.A.
	1.0	3.44	35.65	6.61	4.06	43.00	5.89	4.98	53.95	8.35
	1.2	3.70	36.49	8.11	4.13	44.87	6.40	5.12	56.26	8.94
	1.4	3.95	39.71	9.24	4.32	46.96	8.83	5.27	57.71	10.32
	1.6	4.66	42.49	12.47	5.09	55.60	8.59	5.41	58.70	12.20

[a] The filler content was based on the total composite weight.

For each composite system, composite modulus increased with the increase of shell modulus at a given shell thickness. When the shell modulus was less than the core modulus, the increase of shell thickness led to reduced composite modulus. For example, when the sell thickness was doubled from 0.8 to 1.6 mm, modulus for composites with pure HDPE-shell was reduced from 1.88 to 1.56 GPa for weak core, from 2.85 to 2.27 GPa for moderate core, and from 3.66 to 2.26 GPa for strong core, respectively. Thus, thinner shell should be preferred for this system. When the shell modulus was higher than the core modulus, the opposite is true. The increase of shell thickness led to increased composite modulus. For example, when the sell thickness was doubled from 0.8 to 1.6 mm, modulus for composites with 30% GF-filled shell was increased from 2.94 to 3.83 GPa for weak core, from 3.55 to 4.11 GPa for moderate core, and from 4.49 to 5.03 GPa for strong core, respectively. Thus, thick shell should be preferred for this system.

In composite strengths, relatively small strength increases from 30% to 40% GF levels are observed for each composite system. This is because excessive GF fillers in the plastic matrix of the shell layer made GFs broken through fiber-fiber interaction and consequently, led to relatively low strength increases (Fu et al. 1999; Gupta et al. 1989; Thomason 2002). Also, at the thinnest shell thickness (i.e., 0.8 mm), composite strength increases stayed in low level and this is attributed to the GF breakages on the surface of the shell layer resulting from the high shear forces of coextrusion process (Truckenmuller and Fritz 1991).

A fiber shape filler is one of the primary load-carrying elements in composites and thus, structural efficiencies of the fiber filled composites are highly dependent on the fiber alignments in composites (Kacir, Narkis, and Ishai 1975). Typically, GF-filled extruded composite profiles show high percentages of GF filler alignments for extruding direction and when a convergent die

is used, their experimental flexural moduli reach about 90% of the corresponding theoretical maximums (Hine et al. 1997). Dominant GF filler alignments for coextruding direction are observed in the laterally-cut shell surface (Figure 4.5(c)) of GF-filled coextruded composites and therefore, it can be concluded that the GF alignments improved the flexural property of coextruded composites (Figure 4.7 and Figure 4.8).

However, in impact strength, the GF alignments were ineffectively activated. The comparison of coextruded composites with HDPE-only and GF-filled shells (Table 4.2 and Figure 4.9) shows no strength improvements with the increase of GF loading in the shell layer.

4.3.4 Analysis of Composite Property

To statistically evaluate the reliability of the mechanical property (MOE, MOR, and impact strength) improvements for core coextruded composites in the variation of GF content in the shell layer and shell thickness, two-way analysis of variance (ANOVA) method was adopted and tested. ANOVA test results are shown in Table 3 for weak-, moderate-, and strong-core coextruded composites, respectfully. In weak-core coextruded composite, the ANOVA results showed that both GF content and shell thickness had a significant influence on each mechanical property of the composites and also, for the combined effect of GF content and shell thickness, a significant interaction was observed for all mechanical properties. Moderated-core coextruded composite also showed the ANOVA results having significantly different p-values for GF content, shell thickness, and the interaction between GF content and shell thickness. But, the effect of shell thickness for MOE shows 0.0447, which is close to 95% confidence level. In case of strong-core coextruded composites, similar ANOVA test results were observed except for the effect of GF content on impact strength not showing significant influences (P-value = 0.2531).

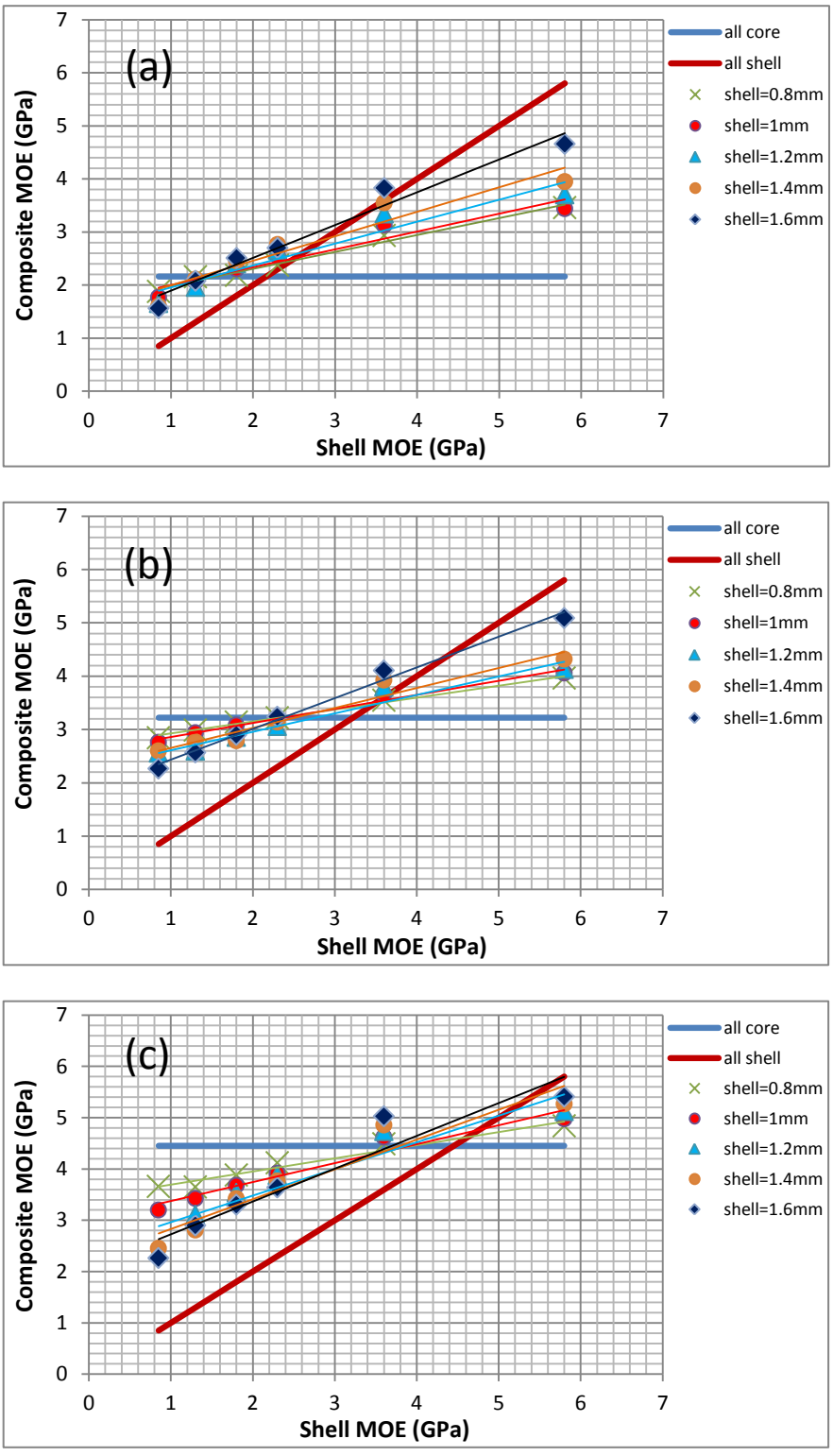

Figure 4.7 Comparison of MOE for coextruded composites with all core- and all shell-composites: (a) weak core, (b) moderate core, and (c) strong core.

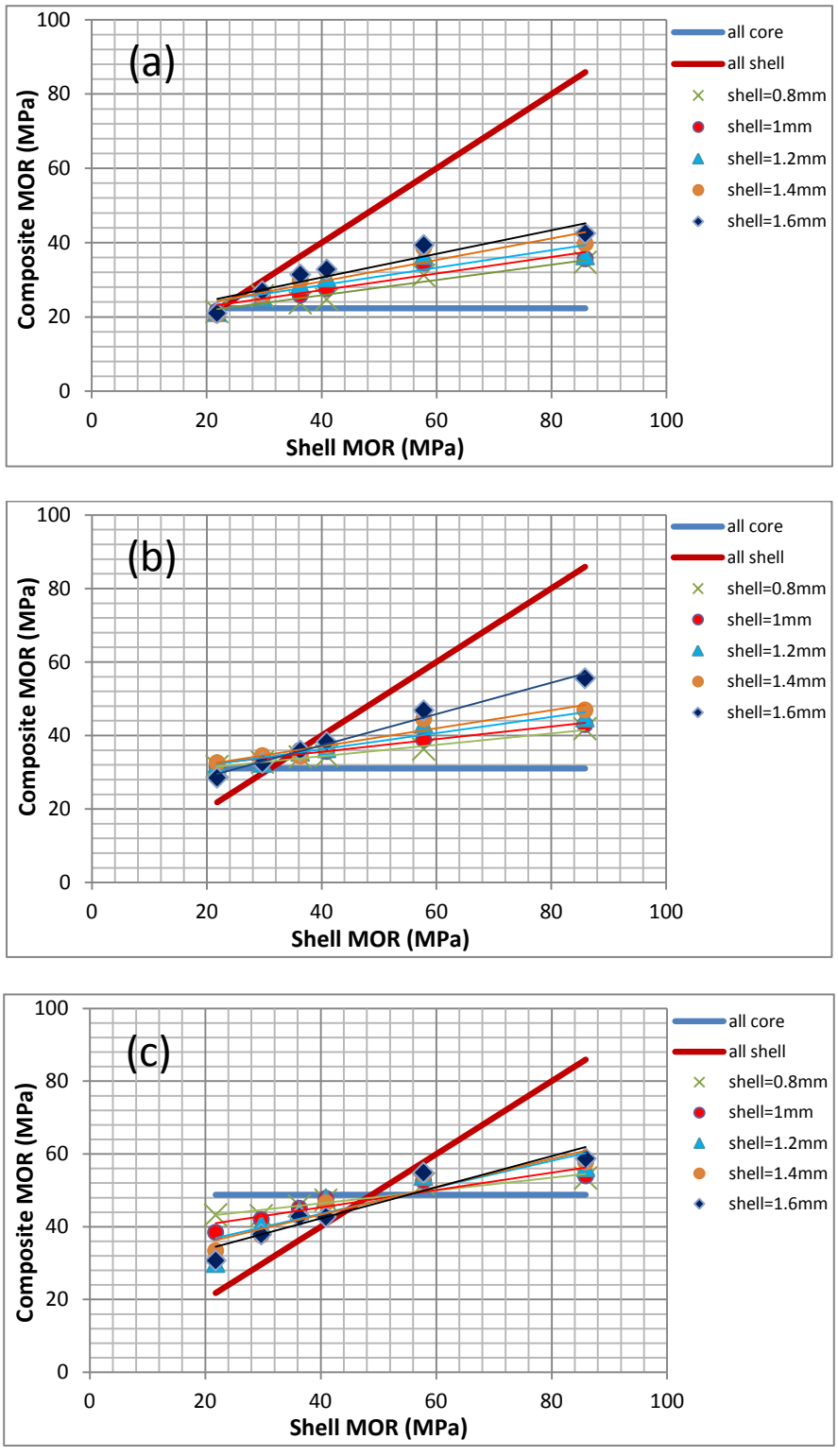

Figure 4.8 Comparison of MOR for coextruded composites with all core- and all shell-composites: (a) weak core, (b) moderate core, and (c) strong core.

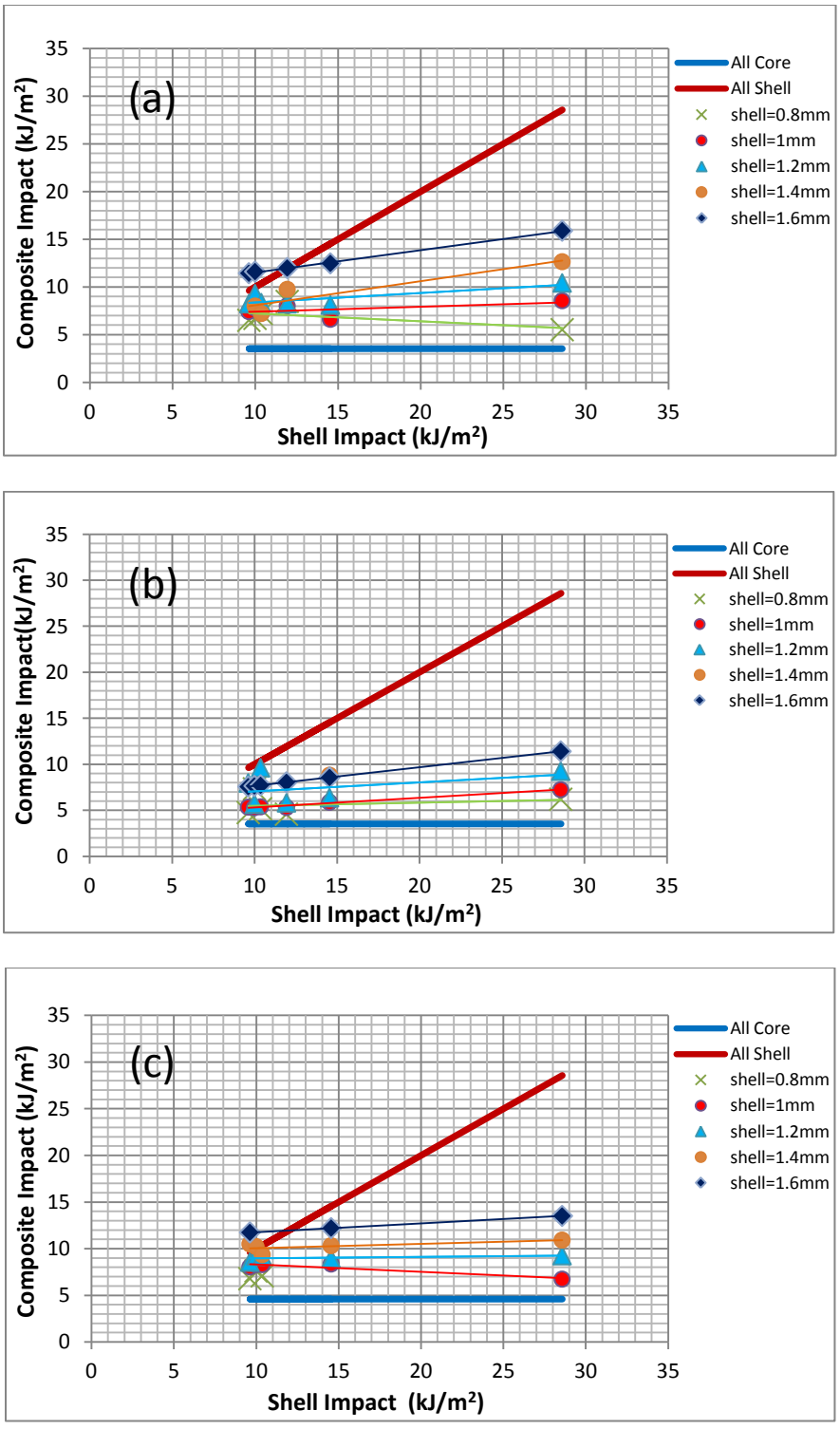

Figure 4.9 Comparison of impact strengths for coextruded composites with all core- and all shell-composites: (a) weak core, (b) moderate core, and (c) strong core.

Table 4.3 Two-way ANOVA tests of the effect of GF content in shell and shell thickness on mechanical properties of different core coextruded composites.

Core Type	Variables	Property		
		MOE[a] (GPa)	MOR (MPa)	IM (kJ/m^2)
Weak	GF	< 0.0001	< 0.0001	< 0.0001
	Thickness	< 0.0001	< 0.0001	< 0.0001
	GF × Thickness	< 0.0001	0.0027	< 0.0001
Moderate	GF	< 0.0001	< 0.0001	< 0.0001
	Thickness	0.0447	< 0.0001	< 0.0001
	GF × Thickness	< 0.0001	< 0.0001	< 0.0001
Strong	GF	< 0.0001	< 0.0001	0.2531
	Thickness	< 0.0001	0.0053	< 0.0001
	GF × Thickness	< 0.0001	< 0.0001	0.0002

[a] The values shown are *p*-values of 2-way ANOVA tests. The *p*-values smaller than 0.05 indicate significant influences of the corresponding treatments on each property at the 95% confidence level.

4.4 CONCLUSIONS

The effects of various GF contents in a shell layer and shell thickness changes on the flexural and impact properties of coextruded WPCs in combination with three core systems (low, moderate, and strong) were studied in this work.

GF fillers in the shell layer behaved as an effective reinforcement for the whole core-coextruded composites with the increase of GF content. The comparisons of flexural property of coextruded composites with different core qualities show that GF reinforcements were optimized at high GF loading levels. Also, GF alignments in the shell layer of the coextruded systems as shown in SEM micrographs played an important role in determining the flexural property. Since GFs were well bonded to the plastic matrix in the shell layer, perpendicularly-aligned GFs to the applied flexural stress effectively improved the flexural property of coextruded composites with GF-filled shell. However, in impact testing, the GF alignment was ineffectively activated and led to no strength improvements.

For the effect of shell thickness, the flexural property of the whole composites increased with the increase of shell MOE and MOR at a given shell thickness. When the flexural property of shell was less than that of core, the increase of shell thickness led to reduced flexural property. Thus, thinner shell should be preferred for this system. On the other hand, when the flexural property of shell was higher than that of core, the opposite was true. Thus, thick shell should be preferred for this system.

4.5 REFERENCES

Charles, A.H. 2000. *Modern Plastics Handbook*: McGraw-Hill.

DiBenedetto, A.T. 2001. Tailing of interfaces in glass fiber reinforced polymer composites: a review. *Materials Science and Engineering: A* 302: 74-82.

Fu, S.-Y., and B. Lauke. 1996. Effect of fiber length and fiber orientation distributions on the tensile strength of short-fiber-reinforced polymers. *Composites Science and Technology* 56: 1179-90.

Fu, S.Y., B. Lauke, E. Mader, X. Hu, and C.Y. Yue. 1999. Fracture resistance of short-glass-fiber-reinforced and short-carbon-fiber-reinforced polypropylene under Charpy impact load and its dependence on processing. *Journal of Materials Processing Technology* 90: 501-7.

Ghaus, M.R., and S. Hamid. 2008. Glass-fiber-reinforced wood/plastic composties. *Journal of Vinyl and Additive Technology* 14: 39-42.

Gupta, V.B., R.K. Mittal, P.K. Sharma, G. Mennig, and J. Wolters. 1989. Some Studies on Glass Fiber-Reinforced Polypropylene .1. Reduction in Fiber Length during Processing. *Polymer Composites* 10: 8-15.

Hine, P.J., S.W. Tsui, P.D. Coates, I.M. Ward, and R.A. Duckett. 1997. Measuring the development of fibre orientation during the melt extrusion of short glass fibre reinforced polypropylene. *Composites Part a-Applied Science and Manufacturing* 28: 949-58.

Jiang, H.H., D.P. Kamdem, B. Bezubic, and P. Ruede. 2003. Mechanical properties of poly(vinyl chloride)/wood flour/glass fiber hybrid composites. *Journal of Vinyl & Additive Technology* 9: 138-45.

Jiang, L., M.P. Wolcott, J.W. Zhang, and K. Englund. 2007. Flexural properties of surface reinforced wood/plastic deck board. *Polymer Engineering and Science* 47: 281-8.

Jin, S., and L.M. Matuana. 2010. Wood/plastic composites co-extruded with multi-walled carbon nanotube-filled rigid poly(vinyl chloride) cap layer. *Polymer International* 59: 648-57.

Kacir, L., M. Narkis, and O. Ishai. 1975. Oriented Short Glass-Fiber Composites .1. Preparation and Statistical-Analysis of Aligned Fiber Mats. *Polymer Engineering and Science* 15: 525-31.

Kim, B.-J., and Q.L. Wu. 2012. Mechanical and Physical Properties of Core-Shell Structured Wood Plastic Composites: Effect of Shells with Hybrid Mineral and Wood Fillers. *Composite Part B, In review*.

Nunez, A.J., P.C. Sturm, J.M. Kenny, M.I. Aranguren, N.E. Marcovich, and M.M. Reboredo. 2003. Mechanical characterization of polypropylene-wood flour composites. *Journal of Applied Polymer Science* 88: 1420-8.

Rothon, R.N. 1999. Mineral fillers in thermoplastics: Filler manufacture and characterisation. *Mineral Fillers in Thermoplastics I* 139: 67-107.

Shakeri, A., and M. Raghimi. 2010. Studies on Mechanical Performance and Water Absorption of Recycled Newspaper/Glass Fiber-reinforced Polypropylene Hybrid Composites. *Journal of Reinforced Plastics and Composites* 29: 994-1005.

Stark, N.M., and L.M. Matuana. 2007. *Coating WPCs using co-extrusion to improve durability*. In *Conference for Coating Wood and Wood Composites: Designing for Durability*, 1-12. Seattle, WA,.

Thomason, J.L. 2002. The influence of fibre length and concentration on the properties of glass fibre reinforced polypropylene: 5. Injection moulded long and short fibre PP. *Composites Part a-Applied Science and Manufacturing* 33: 1641-52.

Thwe, M.M., and K. Liao. 2002. Effects of environmental aging on the mechanical properties of bamboo-glass fiber reinforced polymer matrix hybrid composites. *Composites Part a-Applied Science and Manufacturing* 33: 43-52.

Truckenmuller, F., and H.G. Fritz. 1991. Injection-Molding of Long Fiber-Reinforced Thermoplastics - a Comparison of Extruded and Pultruded Materials with Direct Addition of Roving Strands. *Polymer Engineering and Science* 31: 1316-29.

Tselios, C., D. Bikiaris, P. Savidis, C. Panaviotou, and A. Larena. 1999. Glass-fiber reinforcement of in situ compatibilized propylene/polyethylene blends. *Journal of Materials Science* 34: 385-94.

Tungjitpornkull, S., K. Chaochanchaikul, and N. Sombatsompop. 2007. Mechanical characterization of E-chopped strand glass fiber reinforced Wood/PVC composites. *Journal of Thermoplastic Composite Materials* 20: 535-50.

Velmurugan, R., and V. Manikandan. 2007. Mechanical properties of palmyra/glass fiber hybrid composites. *Composites Part a-Applied Science and Manufacturing* 38: 2216-26.

Wypych, G. 2010. *Handbook of fillers*, 3th ed: ChemTec Publishing.

Xanthos, M. 2005. *Functional fillers for plastics*: Wiley-Vch Co.

Yao, F., and Q.L. Wu. 2010. Coextruded Polyethylene and Wood-Flour Composite: Effect of Shell Thickness, Wood Loading, and Core Quality. *Journal of Applied Polymer Science* 118: 3594-601.

CHAPTER 5 SOUND TRANSMISSION PROPERTIES OF MINERAL FILLED HIGH DENSITY POLYETHYLENE (HDPE) AND WOOD-HDPE COMPOSITES

5.1 INTRODUCTION

Noise is an unwanted sound which is accompanied by industrial machinery and high speed transportations (Jayaraman 2005; Yilmaz 2009). For example, noise level near a highway amounts to the 70 dB level, and the level is increased up to the 80 dB level at heavily used urban road intersections (Kotzen and English 1999). Excessive noises frequently affect people by fatigue, reduced working efficiency and health system disorders (Suzanne et al. 2006). Various barrier materials including concrete, brick, metal, plastic, wood and composites have been used to reduce the noise levels. Among the materials, viscoelastic polymer materials show great potential for dampening sound and vibration. However, most polymer materials have lower elastic modulus and surface density, leading to poor sound insulating performances when solely used as sound barriers (Wang et al. 2011).

Significant work has recently been done to investigate acoustic properties of filled plastic composites. Among the studies, Lee *et al*. (Lee et al. 2010) investigated the tensile and sound transmission loss (TL) properties of composites made of acrylonitrile butadiene styrene (ABS) and carbon-black. It was shown that 5% carbon-black filled composite had more than 10% TL increase compared with unfilled controls. Also, the composites with a high elastic modulus showed higher TL than the materials with a low elastic modulus. It was suggested that increasing tensile modulus through reinforcing the composite structure could be an effective technique for blocking the sound energy. Lee *et al*. (Lee et al. 2008) studied the sound insulation effects of carbon-nanotube (CNT) filled ABS composites. As CNT content in ABS composites increased, the TL values were improved. At the frequency level of 3400 Hz, the average TL values of

composites with 15 vol.% of CNT were 21.7% higher than that of ABS-only composite. It was also found that the increased stiffness from the use of CNTs played more important role on the TL improvement of CNT-filled composites compared with original TL mass law. Costana *et al*. (Cotana et al. 2007) evaluated TL properties of concrete composites filled with different densities of pumice, lapillus and rubber. In here, composite compositions made a noticeable influence on the TL properties. e.g., TL values of lapillus/pumice mixture filled composites were higher than those of lapillus-only and pumice-only filled composites. Among mixtures, the lapillus/pumice filled composite showed higher TL value compared with the pumice/rubber filled composite. This was due to the density changes of composites with different densities of fillers. Wang *et al*. (Wang et al. 2011) studied TL of laminated mica-filled poly (vinyl chloride) composites. In their study, increased TL and resonance frequency were reported with the increase of mica content. They suggested that stiffness and surface density were important factors influencing on the TL properties of mica filled composites and the sound insulation properties of the composites were well described by stiffness and mass law.

Wood plastic composites (WPCs), as new generation green composites, offer advantages in relatively light weight, excellent recyclability, low toxicity and high thermal stability. Thus, their application as noise barrier uses can offer a competitive alternative to the conventional noise barriers. For this purpose, acoustic properties of WPCs, influenced by composite formulations need to be fully understood.

The objectives of this study were firstly to develop an experimental procedure for studying sound transmission properties of solid plastic and wood plastic composites using an impedance tube method and secondly to investigate the effect of mineral type and loading levels on TL properties of the composites in comparison with various corresponding TL predictions.

5.2 THEORETICAL APPROACH

5.2.1 Impedance Tube

The impedance tube system for sound transmission measurements is schematically illustrated in Figure 5.1 (Top). TL measurement is done through four microphones positioned at up and down streams of a test sample in Figure 5.1 (Bottom). In this system, sound pressures at the four measurement locations x_1 to x_4 can be expressed as super-positions of positive and negative directed plane waves ($\pm jkx$) (Olivieri, Bolton, and Yoo 2007; Song and Bolton 2000):

$$\begin{cases} P_1 = Ae^{-jkx_1} + Be^{jkx_1} \\ P_2 = Ae^{-jkx_2} + Be^{jkx_2} \\ P_3 = Ce^{-jkx_3} + De^{jkx_3} \\ P_4 = Ce^{-jkx_4} + De^{jkx_4} \end{cases} \tag{5.1}$$

Where, k is the wave number in ambient air and A to D are complex plane wave coefficients, representing the noise amplitudes. This equation can be rearranged to solve the respective coefficients in terms of the four sound pressures (P_1 to P_4) as:

$$\begin{cases} A = \dfrac{j(P_1 e^{jkx_2} - P_2 e^{jkx_1})}{2\sin k(x_1 - x_2)} \\ B = \dfrac{j(P_2 e^{-jkx_1} - P_1 e^{-jkx_2})}{2\sin k(x_1 - x_2)} \\ C = \dfrac{j(P_3 e^{jkx_4} - P_4 e^{jkx_3})}{2\sin k(x_3 - x_4)} \\ D = \dfrac{j(P_4 e^{-jkx_3} - P_3 e^{-jkx_4})}{2\sin k(x_3 - x_4)} \end{cases} \tag{5.2}$$

Therefore, by measuring the sound pressures at locations x_1 to x_4, the coefficients (A to D) are determined and these coefficients provide the input data for subsequent transfer matrix calculations (Olivieri, Bolton, and Yoo 2007; Song and Bolton 2000; Yousefzadeh et al. 2008).

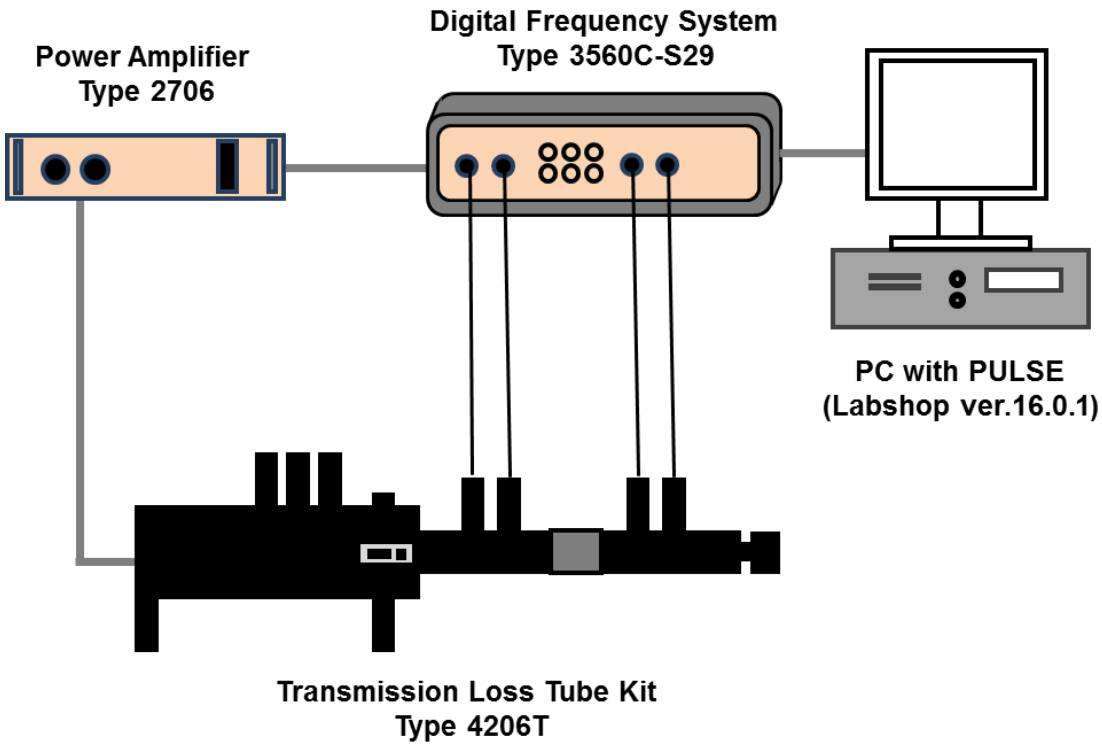

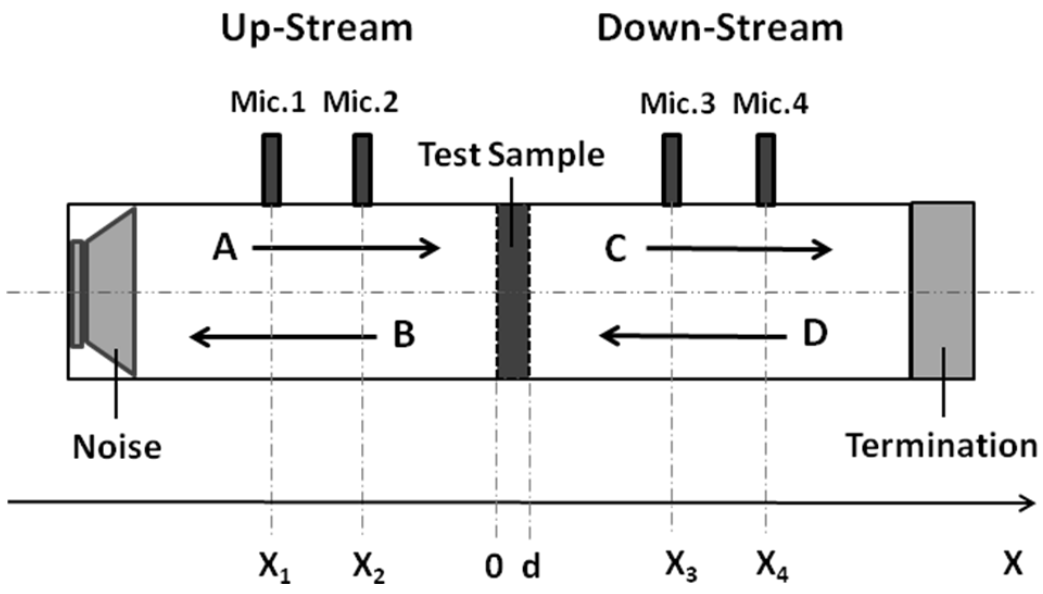

Figure 5.1 Schematic diagram of hardware setup (top) and the TL measurement in an impedance tube (bottom).

The transfer matrix, relating with sound pressures (P) and particle velocities (V) at the two surfaces (front and rear) of the test sample, extending from x=*0* (front) to x=*d* (rear), has the following form (Olivieri, Bolton, and Yoo 2006, 2007):

$$\begin{bmatrix} P \\ V \end{bmatrix}_{x=0} = \begin{bmatrix} T_{11} & T_{12} \\ T_{21} & T_{22} \end{bmatrix} \begin{bmatrix} P \\ V \end{bmatrix}_{x=d} \tag{5.3}$$

Where, T_{ij} are frequency-dependent quantities, related to the acoustical properties of the test sample. Thus, the P and V at the two surfaces of the test sample can be effectively expressed by the positive and negative plane wave components ($\pm jkx$ and complex coefficients):

$$P\big|_{x=0} = A + B \tag{5.4a}$$

$$V\big|_{x=0} = \frac{A - B}{\rho_0 c} \tag{5.4b}$$

$$P\big|_{x=d} = Ce^{-jkd} + De^{jkd} \tag{5.4c}$$

$$V\big|_{x=d} = \frac{Ce^{-jkd} - De^{jkd}}{\rho_0 c} \tag{5.4d}$$

Where, ρ_0 is ambient air density and c is sound speed in air. When the plane wave components are known, based on measurements of the complex pressures at the four locations, the P and V values at the two surfaces of the test sample can be determined. However, Eq. (5.3) represents two equations for four unknowns (i.e., T_{11}, T_{12}, T_{21} and T_{22}). Thus, in order to solve the transfer matrix elements, two additional equations are required. The additional equations are generated by making one more measurement after changing the termination of the impedance tube from open to close. In a matrix form, the result of the two independent measurements (open and close) is expressed as (Song and Bolton 2000):

$$\begin{bmatrix} P_O & P_C \\ V_O & V_C \end{bmatrix}_{x=0} = \begin{bmatrix} T_{11} & T_{12} \\ T_{21} & T_{22} \end{bmatrix} \begin{bmatrix} P_O & P_C \\ V_O & V_C \end{bmatrix}_{x=d} \tag{5.5}$$

Where, the subscripts, *O* (open) and *C* (close) on *P* and *V* denote the two different termination conditions. This approach is referred to as a two-load method (Munjal 1987; Olivieri, Bolton, and Yoo 2006; Song and Bolton 2000) and the above transfer matrix elements are easily calculated by inverting the latter expression to obtain

$$\begin{bmatrix} T_{11} & T_{12} \\ T_{21} & T_{22} \end{bmatrix} = \frac{1}{P_O\big|_{x=d} V_C\big|_{x=d} - P_C\big|_{x=d} V_O\big|_{x=d}} \times \begin{bmatrix} P_O\big|_{x=0} V_C\big|_{x=d} - P_C\big|_{x=0} V_O\big|_{x=d} & -P_O\big|_{x=0} P_C\big|_{x=d} + P_C\big|_{x=0} P_O\big|_{x=d} \\ V_O\big|_{x=0} V_C\big|_{x=d} - V_C\big|_{x=0} V_O\big|_{x=d} & -P_O\big|_{x=d} V_C\big|_{x=0} + P_C\big|_{x=d} V_O\big|_{x=0} \end{bmatrix} \tag{5.6}$$

Pierce (Pierce 1981) suggested that for symmetrical systems, $T_{11} = T_{22}$. Olivieri et al. (Olivieri, Bolton, and Yoo 2006) further reported that for symmetric homogeneous and isotropic porous material, when $T_{11} = T_{22}$, it is possible to get the reciprocal nature of the layer to generate two additional equations without one more measurement:

$$T_{11} = T_{22} \tag{5.7a}$$

$$T_{11}T_{22} - T_{12}T_{21} = 1 \tag{5.7b}$$

By combining Eqs. (5.3), (5.7a) and (5.7b), the transfer matrix elements for a test sample satisfying the above conditions can be expressed directly by the sound pressures (*P*) and particle velocities (*V*) at the two surfaces of the test sample for one termination condition:

$$\begin{bmatrix} T_{11} & T_{12} \\ T_{21} & T_{22} \end{bmatrix} = \frac{1}{P\big|_{x=0} V\big|_{x=d} + P\big|_{x=d} V\big|_{x=0}} \times \begin{bmatrix} P\big|_{x=d} V\big|_{x=d} + P\big|_{x=0} V\big|_{x=0} & P\big|_{x=0}^2 - P\big|_{x=d}^2 \\ V\big|_{x=0}^2 - V\big|_{x=d}^2 & P\big|_{x=d} V\big|_{x=d} + P\big|_{x=0} V\big|_{x=0} \end{bmatrix} \tag{5.8}$$

This approach is called as a one-load method, differed from the two-load method using two measurements (Song and Bolton 2000). Once the transfer matrix elements of the test sample are obtained by using either the one- or two-load methods, all of the other acoustical properties can be acquired.

When a depth (d) of a test sample backed by an anechoic termination is considered, it can be assumed that $D=0$, the P and V at the two surfaces of the test sample can be expressed as:

$$P\big|_{x=0} = 1 + R_a \tag{5.9a}$$

$$V\big|_{x=0} = \frac{1 + R_a}{\rho_0 c} \tag{5.9b}$$

$$P\big|_{x=d} = T_a e^{-jkd} \tag{5.9c}$$

$$V\big|_{x=d} = \frac{T_a e^{-jkd}}{\rho_0 c} \tag{5.9d}$$

Where, reflection coefficient (R_a) = B/A and transmission coefficient (T_a) = C/A for an anechoic termination. After substituting Eqs. (5.9a), (5.9b), (5.9c) and (5.9d) into Eq. (5.3), R_a and T_a can be expressed as, respectively:

$$R_a = \frac{T_{11} + \dfrac{T_{12}}{\rho_0 c} - \rho_0 c T_{21} - T_{22}}{T_{11} + \dfrac{T_{12}}{\rho_0 c} + \rho_0 c T_{21} + T_{22}} \tag{5.10a}$$

$$T_a = \frac{2e^{jkd}}{T_{11} + \dfrac{T_{12}}{\rho_0 c} + T_{21} + T_{22}} \tag{5.10b}$$

The normal incident TL of a sample can be calculated from Eq. (5.10b) as:

$$TL_{normal}(dB) = 10 \log_{10} \frac{1}{\left|T_a\right|^2} \tag{5.11}$$

Where, the subscript, *normal* means that the sample is exposed to a normally incident sound wave field. When the same ambient air is on the two surfaces of the sample, $\left|T_a\right|^2$ is the normal incident power transmission coefficient for the sample with an anechoic termination. This TL is typically determined according to standard procedures (ASTM 2002), where the sample is exposed to a diffuse sound field. In this study using a perfectly anechoic termination

(i.e., *D=0*) as mentioned above, the *TL* can be also expressed as (Olivieri, Bolton, and Yoo 2007; Wang, He, and Geng 2008):

$$TL_{normal}(dB) = 10\log_{10}\left(\left|\frac{A^{(anechoic)}}{C^{(anechoic)}}\right|^2\right) \tag{5.12}$$

When Eqs. (5.9a), (5.9b), (5.9c) and (5.9d) with a perfectly anechoic termination (i.e., *D=0*) are substituted into Eq. (5.3), the *TL* is calculated to be:

$$TL_{normal}(dB) = 10\log_{10}\left(\left|\frac{1}{4}\right|T_{11} + \frac{T_{12}}{\rho_0 c} + \rho_0 c T_{21} + T_{22}\Big|^2\right) \tag{5.13}$$

Eq. (5.13) is incorporated in the B&K acoustic testing program to compute the TL values of test samples. In general, the TL is more easily expressed in a logarithmic form as:

$$TL_{normal}(dB) = 10\log_{10}\left(\frac{I_i}{I_t}\right) \tag{5.14}$$

Where, I_i is the incident sound intensity on the surface of the sample, and I_t is the transmitted sound intensity through the sample.

5.2.2 Mass Law

When incident sound waves hit a sample, the test sample vibrates due to the changes of ambient sound pressures. This vibration energy dissipates in and out of the sample during sound transmission process and the dissipation increases with the increase of the sample mass. This relation is called mass law (Lee et al. 2008). In the mass law, the TL value of a sound barrier sample is calculated as (Jones 1979):

$$TL(\theta,\omega) = 10\log_{10}\left\{1+\left(\frac{\omega m\cos\theta}{2\rho c}\right)^2\right\} \tag{5.15}$$

Where, ω, m, θ and ρc are sound angular frequency, surface area density of sample per unit area, angle of incident sound wave and characteristic impedance of medium, respectively. The TL value calculated from the above equation is mainly controlled by ω, m, and θ with a determined ρc value. However, a small scale of experiment using an impedance tube adopts normal sound waves and the angle of the incident sound waves is perpendicular to the test sample ($\theta=0$). Thus, the above TL equation can also be expressed as:

$$TL(dB)_{normal} = 10\log_{10}\left\{1+\left(\frac{\omega m}{2\rho c}\right)^2\right\} \tag{5.16}$$

In Eq. (5.16), $\omega = 2\pi f$ and this can also be expressed as the following equation for the normal incident sound frequency (Folds and Loggins 1977; Lee and Xu 2009):

$$TL_{normal} = 10\log_{10}\left\{1+\left(\frac{\pi f m}{\rho c}\right)^2\right\} \tag{5.17}$$

Where, f represents sound frequency. According to previous researches, the 6 dB TL increase per octave by doubling sample mass is broadly accepted.

5.2.3 Stiffness Law

The typical TL graph is composed of stiffness-controlled region (S-region) in low frequency ranges and mass law-controlled region (M-region) in high frequency ranges with increasing sound frequency (Irwin and Graf 1979). Hence, the stiffer a sound sample is, the higher TL values it shows in the low frequency ranges. According to the definition (Ng and Hui 2008), the stiffness of material can be expressed as:

$$S = \frac{1}{12}\times\left(\frac{Eh^3}{1-\nu^2}\right) \tag{5.18}$$

Where *S*, *E*, *h*, and *v* are stiffness, modulus of elasticity (MOE), sample thickness, and Poisson's ratio of sample, respectively. From Eq. (5.18), it can be noticed that MOE and sample thickness significantly affect the stiffness of materials. The MOE and sample thickness also can lead to the changes of the speed of longitudinal sound wave (C_p) in materials and subsequent sound resonance frequency (R_f). C_p and R_f are expressed as Eq. (5.19) and Eq. (5.20), respectively (Wang et al. 2011):

$$C_p = \frac{E}{m(1-\nu^2)} \tag{5.19}$$

$$R_{f\,ab} = 0.45 C_p h \left[\left(\frac{a}{\sqrt{\pi} r} \right)^2 + \left(\frac{b}{\sqrt{\pi} r} \right)^2 \right] \tag{5.20}$$

Where, *m* in Eq. (5.19) is area density of sample and *r*, *a* and *b* in Eq. (5.20) are radius of sample surface, and integers (1, 2, …) from the order of sound wave resonance, respectively. Berry and Nicolas (Berry and Nicolas 1994) represented the TL with stiffness-controlled region by using Eq. (5.17) and Eq. (5.20) as:

$$TL_{stiffness} = 10 \log_{10} \left\{ \left(\frac{\pi f m}{\rho c} \right)^2 \left[1 - \left(\frac{R_f}{f} \right)^2 \right]^2 \right\} \tag{5.21}$$

Where R_f, *f*, *m* and ρc represent sound resonance frequency, incident sound frequency, area density of sample per unit area and characteristic impedance of medium, respectively.

5.3 EXPERIMENTAL

5.3.1 Materials and Composite Sample Preparation

Materials and formulations of each composite sample for acoustic testing are listed in Table 5.1.

Table 5.1 Materials and formulations of each composite sample for acoustic testing.

Explanation	Formulation and Content	Supplier
Materials	HDPE (HGB 0760)	ExxonMobil Co., TX
	Pine wood flour (100 mesh)	American Wood Fibers, WI
	Precipitated calcium carbonate (PCC)	Domino SugarCompany, LA
	Nanoclay (nanoMax®)	Nanocor Company, TX
PE Composite	1) PCC: 0, 20, 40% + HDPE	Lab blend
	2) Nanoclay: 0, 4, 8% + HDPE	Lab blend
WPC	1) PCC: 0, 20, 40% + wood: 10% + HDPE	Lab WPC blend
	2) Nanoclay: 0, 4, 8% + wood: 10%+ HDPE	Lab WPC blend

Wood flour (WF) was dried at 85°C for 24 hr to reach moisture content level less than 2%. PCC (precipitated calcium carbonate) and clay were also dried at 85°C for 24 hr to prevent from the effects of moisture. PCC used in this experiment had the average sizes of 1.2 μm and each clay level blended with base HDPE matrix was based on the active clay amount, which is included in the nanoMax-HDPE masterbatch. In the first step, a CW Brabender Intelli-torque twin-screw extrusion machine **(**CW Brabender Instruments, South Hackensack, NJ) was used to make HDPE and PCC or clay base blends (HDPE : PCC = 60 : 40; HDPE : clay = 92 : 8). After that, the pellets were diluted with HDPE or blended with WF to meet the pre-determined mixing ratios and then extruded with a Leistritz Micro-27 co-rotating parallel twin-screw extruder (Leistritz Corporation, Allendale, NJ) in the second step. Materials and formulations for sample manufacturing are listed in Table 1. The blending temperature profiles were 155, 165, 175, 180, 180, 180, 180, 175, 170, 160, and 175°C for PCC filled composites and 155, 165, 170, 175, 175, 175, 175, 170, 160, 155, and 170°C for clay filled composites from feeding zone to die. The extruder rotation speed was 60 rpm. The extruded blends were pelletized again and then dried in an oven at 85°C for 24 hr. The prepared pellets were compression molded by using Wabash V200 hot press (Wabash, ID, USA).

Thirty ton compression force was applied to composite plates at 180^{o}C for 10 min and then the plates were cooled down to room temperature under the same pressure. The manufactured composite plates were water-jetted with a milling machine to produce acoustic samples with target size of 29 (diameter) x 9 (thickness) mm.

5.3.2 Mechanical Property Characterization

Three-point flexural test was performed using a model 5582 Instron testing machine (Instron Inc., Norwood, MA) at a crosshead speed of 3 mm/min. Each sample with a size of 125 (length) ×15 (width) ×9 (thickness) mm was prepared from the same compression-molded composite plates as the acoustic samples. Tinius Olsen Mode 1892 impact tester (Tinius Olsen Inc., Horsham, PA) was used to test un-notched Izod impact strength according to the ASTM D256. The samples having 3-mm thickness were prepared for the impact strength. These samples were also acquired from the same compression-molded composite panels as the acoustic samples by cross-cutting.

5.3.3 Acoustic Property Characterization

To measure TL values of prepared acoustic samples, Brüel & Kjær impedance tube instrument composed of power amplifier (Type 2716C), transmission loss tube kit (Type 4206T), signal amplifier (Type 3560C-S29) and pulse FFT analysis program (Labshop ver. 16.01) was used as shown in Figure 5.1(Top). Small tube (500-6400 Hz) set-ups were adopted. Prior to acoustic testing, test samples were sanded around the perimeter such that they fit into the test tube without much lateral force from the tube wall and also, petroleum jelly (Vaseline) was applied to the sample edges to prevent from sound pressure leaks. Final sample dimension and weight were measured and used to calculate sample area density. To get a better TL curves without noise fluctuations, FFT curves were smoothed by 1/3 octave band width.

5.4 RESULTS AND DISCUSSION

5.4.1 Basic Properties of Mineral Filled HDPE and WPC

Densities of clay, PCC and HDPE are, respectively, 1.60, 2.60, and 0.96 g/cm^3 (Kim et al. 2012; Klyosov 2007; Wypych 2010). Thus, the addition of clay and PCC in the HDPE matrix increased the surface area density of the composites for the same sample size (Table 5.2). Pure HDPE had an area density of 8.59 kg/m^2. The density increased to 8.95 kg/m^2 at the 8% clay loading level and to 10.83 kg/m^2 at the 40% PCC level. Wood plastic composites (10% WF) filled with clay and PCC had much similar area densities compared to corresponding HDPE composite with clay and PCC only, respectively. Thus, the use of 10% WF did not alter the composite area density much.

Table 5.2 Mechanical properties (MOE, MOR, and impact strength), stiffness, and area density of mineral filled composites and WPCs as a function of filler content.

System	Filler (%)	MOE[a] (GPa)	MOR (MPa)	Impact Strength (kJ/m^2)	Stiffness of Unit Area ($\times 10^5$N/m^2)	Area Density of Unit Area (kg/m^2)
Clay Only	0	1.20 (0.02)	41.57 (1.21)	No Break	119.05	8.59
	4	1.31 (0.01)	33.17 (0.05)	5.90 (0.11)	129.47	8.79
	8	1.34 (0.05)	30.42 (0.98)	5.18 (0.19)	131.94	8.95
PCC Only	20	1.47 (0.05)	46.20 (0.56)	11.03 (2.35)	144.47	9.75
	40	1.51 (0.04)	32.49 (0.47)	7.00 (0.65)	148.41	10.83
Clay + WF	0 + 10	1.39 (0.03)	37.47 (0.82)	17.98 (0.89)	136.61	8.26
	4 + 10	1.45 (0.06)	37.67 (1.04)	10.19 (2.21)	141.99	8.47
	8 + 10	1.47 (0.06)	33.22 (0.39)	6.58 (1.50)	143.43	8.68
PCC + WF	20 + 10	1.64 (0.05)	37.14 (1.50)	13.50 (2.74)	159.73	9.57
	40 + 10	1.49 (0.04)	34.33 (0.17)	4.37 (0.36)	145.12	10.66

[a] Numbers in parenthesis are standard deviations.

The neat HDPE samples had an MOE value of 1.2 GPa. At the 4 and 8% clay loading levels, the modulus increased to 1.31 GPa and 1.34 GPa, respectively. Early work in this field (Lei et al. 2007) attributed the modulus increase to clay exfoliation to form nano-platelets in the plastic matrix. The extent of exfoliation depends on mixing and the use of coupling agents. PCC filled HDPE also showed higher modulus compared with neat-HDPE, probably due to higher filler content (Kim et al. 2012). The corresponding stiffness for both types of composites also increased with increased clay and PCC loading levels. On the other hand, both bending MOR and impact strength decreased with increased clay and PCC loading levels. Possible particle aggregation in the HDPE matrix, which creates stress concentration at particle-matrix interface led to decreased overall composite strength.

For clay filled WPC, increased clay loading led to some improvement in the bending MOE (e.g., an increment from 1.39 GPa for 0% clay level to 1.47 GPa for 8% clay level), similar to clay-filled HDPE composites. There was an overall modulus value enhancement compared with corresponding HDPE-only composites, showing some synergetic effect of clay and wood fibers. For PCC-filled WPC, MOE was obviously increased at the 20% PCC level compared with PCC-HDPE composite, but at the 40% PCC level, the MOE was somewhat reduced. There was a decreasing trend for strength properties (especially, impact strength) with the increased clay or PCC loading level. The reduced strength properties of filled composite are attributed to the aggregation effect of filler particles in the HDPE matrix (Kim et al. 2012).

5.4.2 General TL Curves of Filled HDPE and WPCs

Figure 5.2 shows a comparison of measured TL-frequency curves for clay (a) and PCC (b) filled HDPE and WPC material.

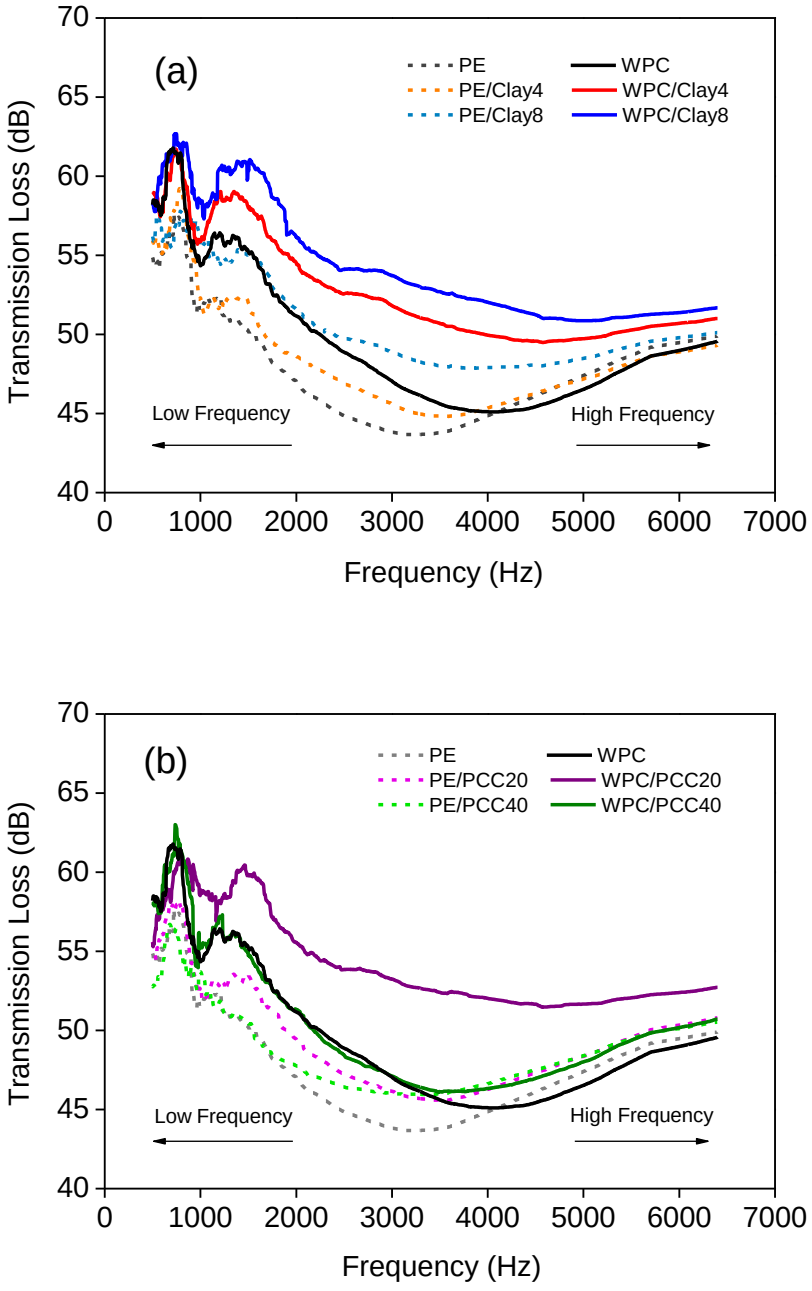

Figure 5.2 Comparisons of TL curves between clay-filled HDPE and WPCs (a) and between PCC filled HDPE and WPCs (b).

The TL curves shifted upwards as clay or PCC level increased, indicating improved TL properties at higher filler loading levels. The area density of clay filled HDPE was only slightly higher than that of neat-HDPE (Table 5.2). The observed TL improvement at higher clay loading levels, especially in a low frequency range, probably indicates the effect of nano-clay in composites. The clay particles, after intercalation and exfoliation, had platelet shapes with thickness in the nanometer range, and they were distributed in the plastic matrix (Ataeefard and Moradian 2011; Gopakumar et al. 2002; Ton-That et al. 2004). The platelets can help deflect sound wave and increase its pathway with energy dissipations as heat, leading to increased TL value (Bharadwaj 2001; Lee et al. 2008; Picard et al. 2007). For PCC filled composites, the addition of PCC in HDPE led to distinctively increased area density and the density increases consequently improved TL values of PCC-filled composites in comparison with neat-HDPE. However, the 40% PCC filled composite showed a lower TL curve in the low frequency range and higher TL curve in the high frequency range, compared with the 20% PCC filled composite as shown in Figure 5.2(b).

The incorporation of 10% WF in the clay and PCC filled composites led to the overall improvements of the composite TL values in comparison with corresponding HDPE composites. The results show a synergistic effect of clay or PCC and wood particles in the composites through blocking/reflecting the sound wave and enhancing composite stiffness. The initial large difference of the observed TL values in the low and middle frequency ranges indicates stiffness controls in the TL of the composites. For PCC-filled composites, composite stiffness was lower at the 40% loading level in comparison with 20% PCC loading. Measured TL values also decreased with PCC loading increases from 20% to 40%.

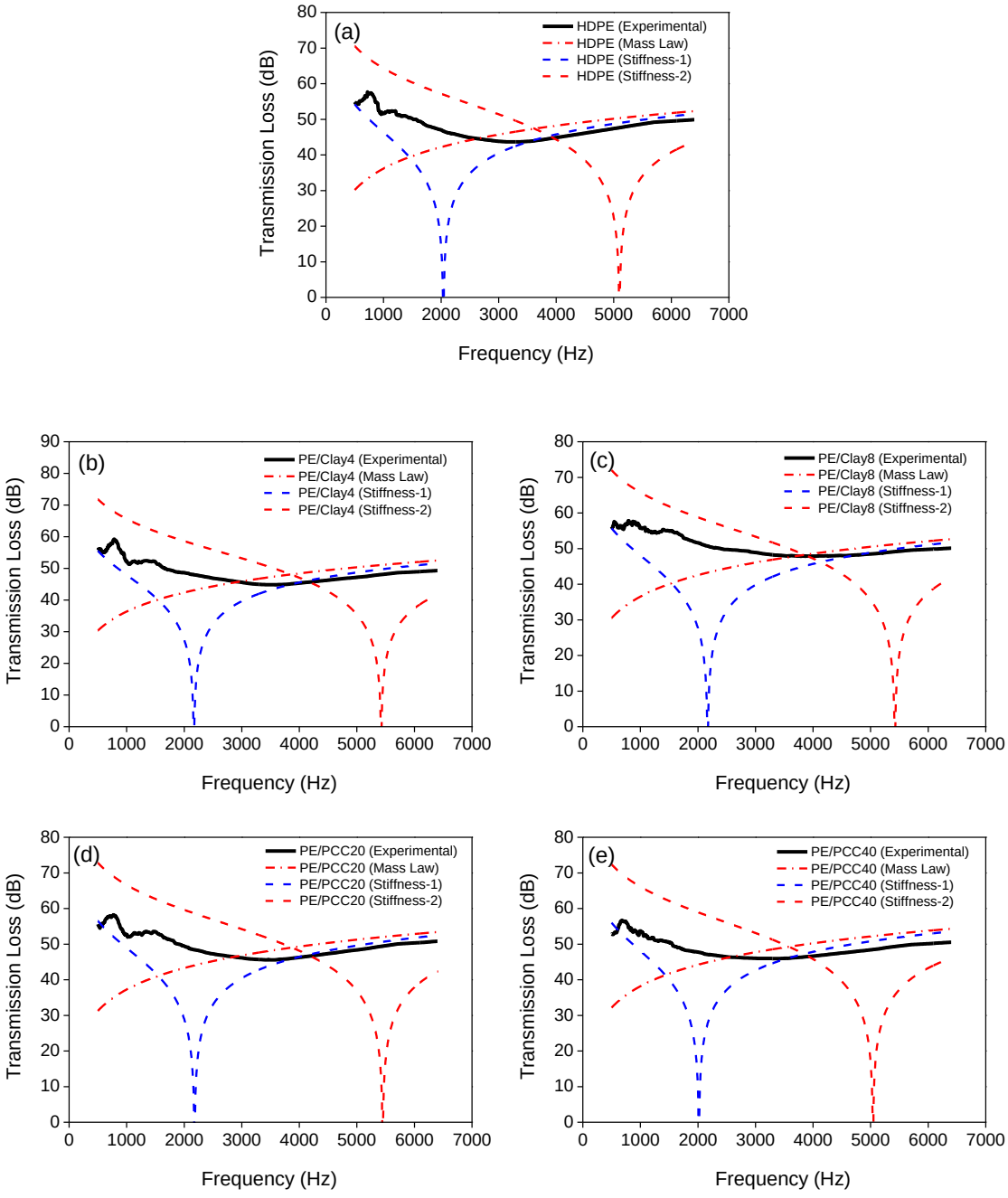

Figure 5.3 Comparisons of experimental TL curves of filled HDPE in comparison with mass and stiffness law TL predictions: (a) HDPE, (b) HDPE/Clay4, (c) HDPE/Clay8, (d) HDPE/PCC20, and (e) HDPE/PCC40.

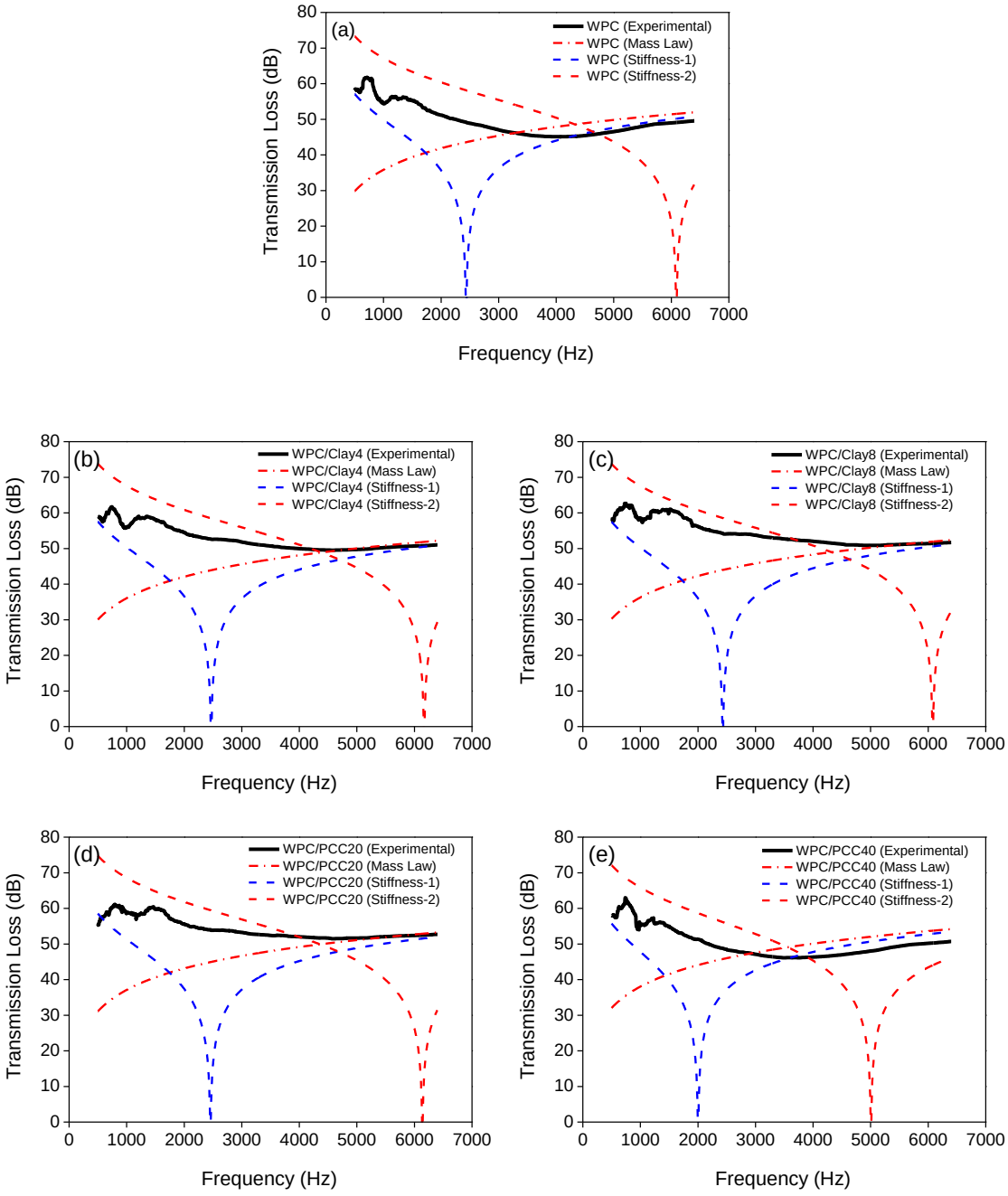

Figure 5.4 Comparisons of experimental TL curves of filled WPCs in comparison with mass and stiffness law TL predictions: (a) WPC, (b) WPC/Clay4, (c) WPC/Clay8, (d) WPC/PCC20, and (e) WPC/PCC40.

5.4.3 Comparison of TL with Mass and Stiffness Law Predictions

Experimental TL curves of clay and PCC filled HDPE and WPCs are shown in Figure 5.3 and Figure 5.4, respectively, in comparison with the corresponding mass law and stiffness law TL prediction lines. The mass law TL equation used was a modified form of Eq. (5.7) (Lee and Xu 2009):

$$TL_{normal} = 20\log_{10}(fm) - 42.5 \tag{5.22}$$

Where, f and m represent sound frequency and area density of sample per unit area, respectively. Stiffness TL equation was adapted from Eq. (5.21) and the first (a=1, and b=1) and second (a=1 and b=2) orders of sound resonance frequencies were used to get two stiffness TL prediction curves (i.e., stiffness-1 and stiffness-2).

There were initial fluctuations in the experimental TL curves at a very low frequency range. The TL values decreased as frequency increased and then increased after passing a certain frequency level (designated as experimental resonance frequency – R_{FE}). The stiffness-1 and stiffness-2 TL curves for each sample have two resonance frequencies R_{FS1} and R_{FS2}, respectively. The mass law TL curves formed linear lines after an initial rapid TL increase at the low frequency range. The effect of filler loading and filler type on the shape of the TL curves seems to be small. A comparison among the experimental, predicted stiffness and mass law TL curves indicates well-defined S-region (left) and M-region (right).

The experimental TL curves of filled HDPE and WPCs (Figures 5.3(a) and 5.4(a)) show similar trends to their corresponding mass law TL predictions for M-region. This result is similar to the previous TL experimental data using mica-filled PVC composites with 1 mm thickness (Wang et al. 2011). However, for S-region, there are some differences between two studies. While the published experimental TL curves had similar features to their corresponding stiffness-

1 TL predictions, the experimental TL curves from the current work are positioned in between the stiffness-1 and stiffness-2 TL predictions. The different experimental TL features in S-region between the two studies may be related with stiffness differences. When the stiffness equation as described in Eq. (5.18) is considered, the stiffness value is significantly affected by the thickness of test sample (i.e., 729 times difference between 1 mm and 9 mm) and the increased sample thickness led to remarkable stiffness value differences. Thus, the increased stiffness values from the test samples with 9-mm thickness resulted in the remarkable TL improvements in the S-region.

The stiffness-1 and stiffness-2 TL curves form two intersection points with the mass law TL curve at two frequency levels, $R_{S1\text{-}M\text{-}IP}$ and $R_{S2\text{-}M\text{-}IP}$, respectively as shown in Figure 5.5 (filled HDPE) and Figure 5.6 (filled WPCs). The experimental TL curves of filled HDPE and WPCs are better approximate to the combined TL predictions from their corresponding stiffness-1 and stiffness-2 TL curves for S-region and Mass Law TL curves for M-region. Table 5.3 shows a comparison of the R_{FE}, R_{FS1}, R_{FS2}, $R_{S1\text{-}M\text{-}IP}$ and $R_{S2\text{-}M\text{-}IP}$ values for various composites. While the experimental R_{FE} values of filled HDPE composites are located between the corresponding $R_{S1\text{-}M\text{-}IP}$ and $R_{S2\text{-}M\text{-}IP}$ values, those of filled WPCs are more close to the corresponding $R_{S2\text{-}M\text{-}IP}$ values or located to the right side of them. From the above result, it can be noticed that the MOE and stiffness increases of the test samples led to the experimental TL improvements in S-region and these consequently shifted their experimental R_{FE} values to the high frequency range.

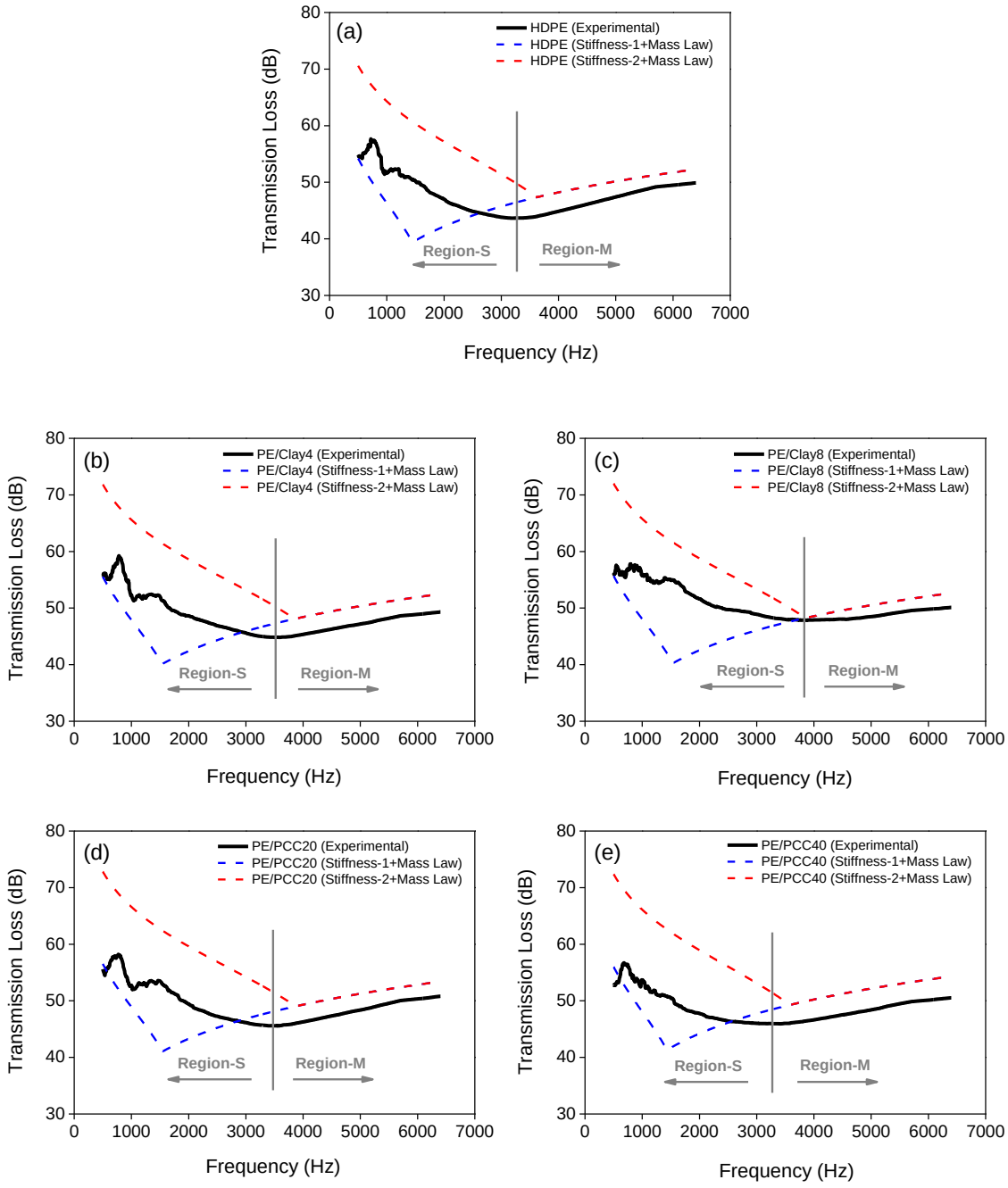

Figure 5.5 Comparisons of experimental TL curves of filled HDPE in comparison with combined TL predictions: (a) HDPE, (b) HDPE/Clay4, (c) HDPE/Clay8, (d) HDPE/PCC20, and (e) HDPE/PCC40.

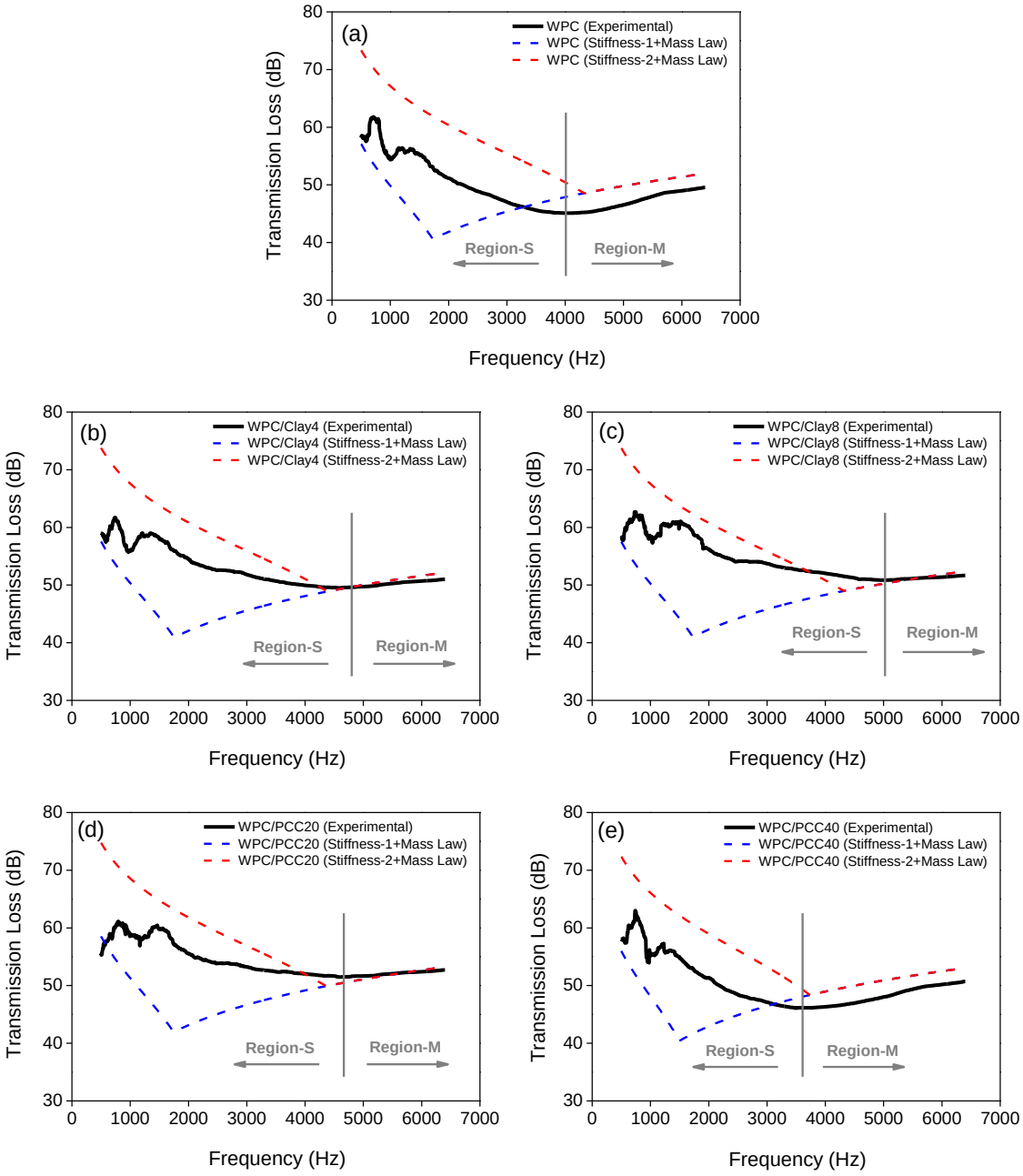

Figure 5.6 Comparisons of experimental TL curves of filled WPCs in comparison with combined TL predictions: (a) WPC, (b) WPC/Clay4, (c) WPC/Clay8, (d) WPC/PCC20, and (e) WPC/PCC40.

Table 5.3 Summary of sound transmission property of filled HDPE and WPCs.

Sample Name	Experimental Resonance Frequency R_{FE} (Hz)	Predicted Resonance Frequency		Stiffness-Mass Law Curves Intersection Points	
		R_{FS1} (Hz)	R_{FS2} (Hz)	$R_{S1\text{-}M\text{-}IP}$ (Hz)	$R_{S2\text{-}M\text{-}IP}$ (Hz)
HDPE	3216	2040	5099	1448	3624
HDPE/Clay4	3592	2168	5421	1540	3852
HDPE/Clay8	3792	2169	5422	1540	3852
HDPE/PCC20	3564	2179	5448	1548	3872
HDPE/PCC40	3416	2016	5041	1432	3580
WPC	4080	2435	6087	1728	4324
WPC/Clay4	4572	2467	6169	1752	4380
WPC/Clay8	4980	2432	6079	1728	4320
WPC/PCC20	4588	2455	6138	1744	4360
WPC/PCC40	3524	2002	5006	1424	3556

5.4.4 Effect of Filler Loading Level on Mean TL

For a more comprehensive comparison of the sound insulation ability of clay- and PCC-filled HDPE and WPCs with various filler contents, their averaged TL (A-TL) values in both S-region and M-region are plotted in Figure 5.7. The A-TL values of clay filled HDPE and WPCs increased with increased clay content in both S-region and M-region (Figure 5.7(a)). While the clay filled HDPE had more obviously improved A-TL values only at the 8% clay level, the clay filled WPCs showed enhanced A-TL values even at the 4% clay level, indicating synergistic effect of WF.

The PCC-filled HDPE and WPCs showed their highest A-TL values at the 20% PCC level. At the 20% PCC loading level, the A-TL value in S-region was much improved with the use of 10% WF. This indicates that the stiffness increase in the 20% PCC-filled WPC played a significant role in the observed TL values.

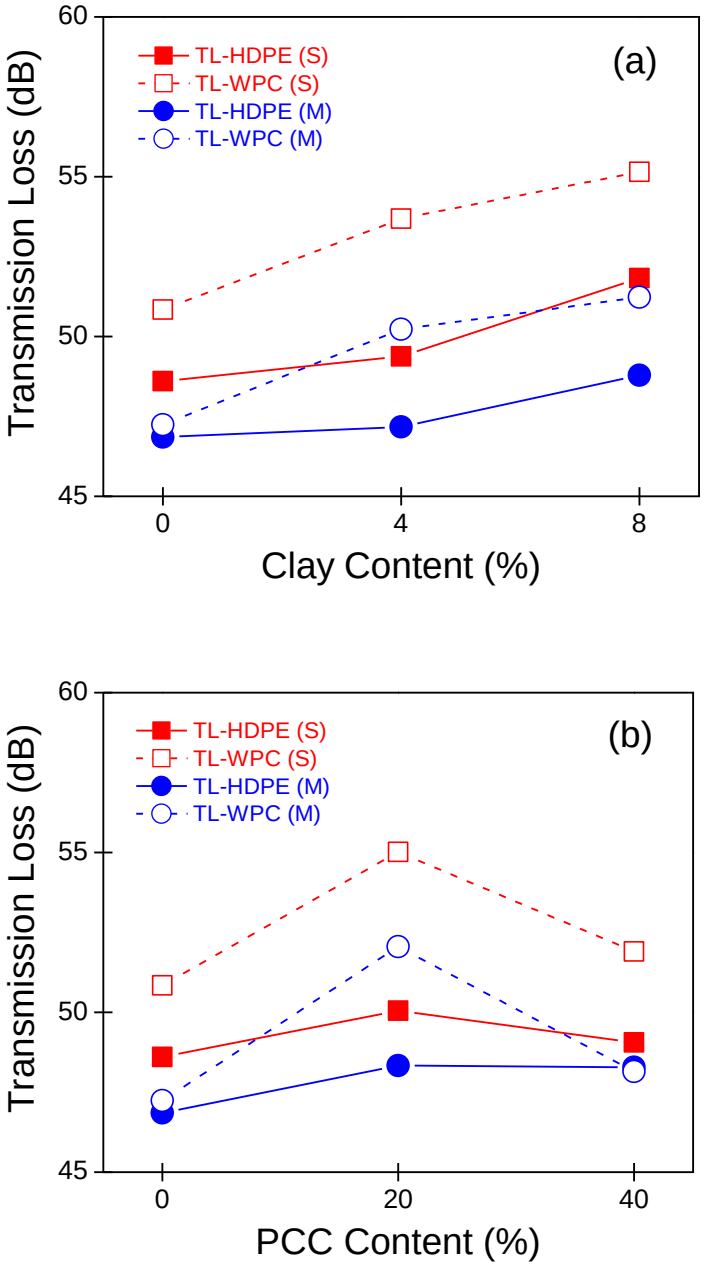

Figure 5.7 Comparisons of Averaged TL values between clay filled HDPE and WPCs (a) and PCC filled HDPE and WPCs (b) in S-region and M-region.

However, with the further increase of PCC contents to the 40% level, the uniformity of composites becomes worse (due to the PCC particle aggregations) and the composite stiffness was decreased, leading to decreased A-TL values. In the M-region, the A-TL values were increased with increased PCC content due to the area density increases of composites.

5.5 CONCLUSIONS

The effect of clay and PCC on mechanical and acoustic properties of HDPE and HDPE based WPC was studied. The experimental TL data of the composites were analyzed with the stiffness and mass laws. The composite modulus generally increased, while the composite strength decreased with increased filler loading level.

The stiffness and surface area density were major factors influencing the sound insulation property of the materials. The experimental TL results show that the addition of clay or PCC and/or WF fillers led to general R_{FE} and TL increases of composites. However, at high filling levels, decreased composite stiffness from filler aggregations led to reduced TL values. The experimental TL curves of filled HDPE and WPCs are approximated with the combined TL predictions from their corresponding stiffness-1 and stiffness-2 TL for S-region and mass law TL for M-region.

5.6 REFERENCES

ASTM. 2002. *ASTM E-90-02 Standard test method for the laboratory measurement of airborne sound transmission loss of building partitions and elements*. West Conshohocken, PA, USA: ASTM International.

Ataeefard, M., and S. Moradian. 2011. Polypropylene/Organoclay Nanocomposites: Effects of Clay Content on Properties. *Polymer-Plastics Technology and Engineering* 50: 732-9.

Berry, A., and J. Nicolas. 1994. Structural Acoustics and Vibration Behavior of Complex Panels. *Applied Acoustics* 43: 185-215.

Bharadwaj, R.K. 2001. Modeling the barrier properties of polymer-layered silicate nanocomposites. *Macromolecules* 34: 9189-92.

Cotana, F., F. Rossi, A. Nicolini, and S. Simoni. 2007. *Acoustic Tests on Original Concrete and Inert Mixture Materials*. In *14th International Congress on Sound & Vibration*. Cairns, Australia.

Folds, D.L., and C.D. Loggins. 1977. Transmission and Reflection of Ultrasonic-Waves in Layered Media. *Journal of the Acoustical Society of America* 62: 1102-9.

Gopakumar, T.G., J.A. Lee, M. Kontopoulou, and J.S. Parent. 2002. Influence of clay exfoliation on the physical properties of montmorillonite/polyethylene composites. *Polymer* 43: 5483-91.

Irwin, J.D., and E.R. Graf. 1979. *Industrial Noise and Vibration Control* Englewood Cliffs, N.J.: Prentice-Hall.

Jayaraman, K.A. 2005. *Acoustical Absorptive Properties of Nowovens*. North Carolina State.

Jones, R.E. 1979. Intercomparisons of Laboratory Determinations of Airborne Sound-Transmission Loss. *Journal of the Acoustical Society of America* 66: 148-64.

Kim, B.J., F. Yao, G.P. Han, and Q.L. Wu. 2012. Performance of Bamboo Plastic Composites With Hybrid Bamboo and Precipitated Calcium Carbonate Fillers. *Polymer Composites* 33: 68-78.

Klyosov, A.A. 2007. *Wood-plastic composites*. Hoboken, New Jersey: John Wiley & Sons Inc.

Kotzen, B., and C. English. 1999. *Environmental Noise Barriers: A guide to their acoustic and visual design*. New York: E & FN Spon.

Lee, C.M., and Y. Xu. 2009. A modified transfer matrix method for prediction of transmission loss of multilayer acoustic materials. *Journal of Sound and Vibration* 326: 290-301.

Lee, J.C., Y.S. Hong, R.G. Nan, M.K. Jang, C.S. Lee, S.H. Ahn, and Y.J. Kang. 2008. Soundproofing effect of nano particle reinforced polymer composites. *Journal of Mechanical Science and Technology* 22: 1468-74.

Lee, J.W., J.C. Lee, J. Pandey, S.H. Ahn, and Y.J. Kang. 2010. Mechanical Properties and Sound Insulation Effect of ABS/Carbon-black Composites. *Journal of Composite Materials* 44: 1701-16.

Lei, Y., Q. Wu, C.M. ClemonS, F. Yao, and Y. Xu. 2007. Influence of nanoclay on properties of HDPE/Wood composites. *Journal of Applied Polymer Science* 106: 3958-66.

Munjal, M.L. 1987. *Acoustics of Ducts and Mufflers*. New York: Wiley-Interscience.

Ng, C.F., and C.K. Hui. 2008. Low frequency sound insulation using stiffness control with honeycomb panels. *Applied Acoustics* 69: 293-301.

Olivieri, O., J.S. Bolton, and T.W. Yoo. 2006. *Measurement of transmission loss of materials using a standing wave tube*. In *Inter-noise 2006*. Honolulu, Hawaii, USA.

Olivieri, O., J.S. Bolton, and T.W. Yoo. 2007. *Measurement of Normal Incidence Transmission Loss and Other Acoustical Properties of Materials Placed in a Standing Wave Tube*. B & K.

Picard, E., A. Vermogen, J.F. Gerard, and E. Espuche. 2007. Barrier properties of nylon 6-montmorillonite nanocomposite membranes prepared by melt blending: Influence of the clay content and dispersion state - Consequences on modelling. *Journal of Membrane Science* 292: 133-44.

Pierce, A.D. 1981. *Acoustics: An introduction to its physical principles and applications*. New York: McGraw-Hill.

Suzanne, D.S., W. N. Sharles, and V.G. Henning. 2006. *Noise and Vibration Control Engineering* 2nd ed: John Willey & Sons, Inc.

Song, B.H., and J.S. Bolton. 2000. A transfer-matrix approach for estimating the characteristic impedance and wave numbers of limp and rigid porous materials. *Journal of the Acoustical Society of America* 107: 1131-52.

Ton-That, M.T., F. Perrin-Sarazin, K.C. Cole, M.N. Bureau, and J. Denault. 2004. Polyolefin nanocomposites: Formulation and development. *Polymer Engineering and Science* 44: 1212-9.

Wang, X., F. You, F.S. Zhang, J. Li, and S.Y. Guo. 2011. Experimental and Theoretic Studies on Sound Transmission Loss of Laminated Mica-Filled Poly(vinyl chloride) Composites. *Journal of Applied Polymer Science* 122: 1427-33.

Wang, Y.S., H. He, and A.L. Geng. 2008. Comparison and application of the experimental methods for multi-layer prediction of acoustical properties of noise control materials in standing wave-duct systems. *Applied Acoustics* 69: 847-57.

Wypych, G. 2010. *Handbook of fillers*, 3rd ed. Ontario, Canada: ChemTec Publishing.

Yilmaz, N.D. 2009. *Acoustic Properties of Biodegradable Nonwovens*. North Carolina State.

Yousefzadeh, M., M. Mahjoob, N. Mohammadi, and A. Shahsavari. 2008. *An experimental study of sound transmission loss (STL) measurement techniques using an impedence tube.* In *Acoustics 2008*, 965-8. Paris, France.

CHAPTER 6 CONCLUSIONS AND FUTURE WORK

6.1 OVERALL CONCLUSIONS

In this dissertation, the effect of mineral fillers including PCC, GF, and clay on properties of structured wood/natural plastic composites was investigated.

The conclusions of this study are as follows:

1) The differences in chemical composition and surface morphology between RBF and GBP led to more effective silane crosslinking on the RBF surfaces. Dry PCC particles showed an agglomerated form with individual particles of about 1.2 micron in diamter, and compounding PCC with R-PP/PE resin helped separate particles. Measured flexural strength and flexural modulus of the PCC-only-filled composites increased significantly from 15 to 30% PCC content levels, while the tensile and impact strength of composites decreased with the addition of PCC. For composites with hybrid bamboo and PCC fillers, tensile and flexural moduli were improved with increasing PCC content. After silane treatment of the bamboo filler, RBF filled composites showed noticeably increased mechanical properties compared to those of GBP filled composites. For modulus values, PCC-bamboo-polymer composites were 3-4 times higher than those of PCC-polymer composites at high PCC levels.
2) Significant differences existed in mechanical, WA/TS and CTE properties between coextruded WPCs with weak and strong core systems as influenced by the shell compositions. In the weak core system with R-PP/HDPE, coextruded composites with a reinforced shell showed significantly improved flexural strengths compared to their core-only composite. In the strong core system made of V-HDPE, the flexural strengths of coextruded WPC were lowered compared with the core-only composite. Impact strengths

were significantly improved for both coextruded systems at low shell filling levels. High level of filler loading in the shell led to some decreases of impact strength in both coextruded systems. The types of impact fracture (i.e., hinge versus complete) varied largely with core quality and filler composition in the shell. WA/TS values of coextruded WPCs with high TPCC content in a shell layer were lower than those of core-only composites and coextruded WPCs with high wood content in the shell layer. The use of high percentage of plastic in a shell layer led to increased overall CTE values for coextruded WPCs. However, increased filler loading in the shell layer led to the decrease of CTE values for resultant coextruded WPC, especially, for the weak core system. Thus, the combination of a relatively weak core (e.g., made of recycled plastics) and a reinforced shell (e.g., with small sized inorganic particles) could be a cost-effective system for coextruded WPC manufacturing.

3) GF fillers in the shell layer behaved as an effective reinforcement for the whole core-coextruded composites with the increase of GF content. The comparisons of flexural property of coextruded composites with different core qualities show that GF reinforcements were optimized at high GF loading levels. Also, GF alignments in the shell layer of the coextruded systems as shown in SEM micrographs played an important role in determining the flexural property. Since GFs were well bonded to the plastic matrix in the shell layer, perpendicularly-aligned GFs to the applied flexural stress effectively improved the flexural property of coextruded composites with GF-filled shell. However, in impact testing, the GF alignment was ineffectively activated and led to no strength increases. For the effect of shell thickness, the flexural property of the whole composites increased with increasing shell property at a given shell thickness. When the

flexural property of shell was less than that of core, the increase of shell thickness led to reduced flexural property. Thus, thinner shell should be preferred for this system. On the other hand, when the flexural property of shell was higher than that of core, the opposite was true. Thus, thick shell should be preferred for this system.

4) The stiffness and surface area density were major factors influencing the sound insulation property of the materials. The experimental TL results show that the addition of clay or PCC and/or WF fillers led to general R_{FE} and TL increases of composites. However, at high filling levels, decreased composite stiffness from filler aggregations led to reduced TL values. The experimental TL curves of filled HDPE and WPCs are approximated with the combined TL predictions from their corresponding stiffness-1 and stiffness-2 TL for S-region and mass law TL for M-region.

6.2 FUTURE WORK

Based on limitations of this study, suggested future studies include:

(1) In PCC filled WPCs, more extensive research on various PCC particle size, shape, and treatment are needed. These further studies could help find the effectiveness of PCC in WPC manufacturing for not only cost reduction but also property improvement.

(2) For mineral-filled coextruded composites, more in-depth experiments are required in a shell filling composition. These include the incorporation of different size, shape, sort, aspect ratio, loading level, and treatment of fillers with various plastics and comparisons with various modeling predictions based on the above filler characteristics are needed. Also, beside conventional properties (flexural, impact, and water absorption), the evaluations for other properties such as surface hardness, scratch resistance, fire/flame resistance, and weathering are required for real applications.

(3) Sound insulation tests for mineral-filled plastic composites and WPCs with hard surface remain at the initial stage. Hence, firstly, additional studies should be performed with respect to the effect of fillers on the acoustic property of filled plastic composites/WPCs. Secondly, further researches for structured composites (layered, hollow, etc) should be followed.

APPENDIX: PERMISSION LETTER

JOHN WILEY AND SONS LICENSE TERMS AND CONDITIONS

Feb 16, 2012

This is a License Agreement between Birm-June Kim ("You") and John Wiley and Sons ("John Wiley and Sons") provided by Copyright Clearance Center ("CCC"). The license consists of your order details, the terms and conditions provided by John Wiley and Sons, and the payment terms and conditions.

All payments must be made in full to CCC. For payment instructions, please see information listed at the bottom of this form.

License Number	2850940339603
License date	Feb 16, 2012
Licensed content publisher	John Wiley and Sons
Licensed content publication	Polymer Composites
Licensed content title	Performance of bamboo plastic composites with hybrid bamboo and precipitated calcium carbonate fillers
Licensed content author	Birm-June Kim,Fei Yao,Guangping Han,Qinglin Wu
Licensed content date	Jan 1, 2012
Start page	68
End page	78
Type of use	Dissertation/Thesis
Requestor type	Author of this Wiley article
Format	Electronic
Portion	Full article
Will you be translating?	No
Order reference number	
Total	0.00 USD
Terms and Conditions	

TERMS AND CONDITIONS

WITH RESPECT TO THE MATERIALS OR THE ACCURACY OF ANY INFORMATION CONTAINED IN THE MATERIALS, INCLUDING, WITHOUT LIMITATION, ANY IMPLIED WARRANTY OF MERCHANTABILITY, ACCURACY, SATISFACTORY QUALITY, FITNESS FOR A PARTICULAR PURPOSE, USABILITY, INTEGRATION OR NON-INFRINGEMENT AND ALL SUCH WARRANTIES ARE HEREBY EXCLUDED BY WILEY AND ITS LICENSORS AND WAIVED BY YOU.

6. WILEY shall have the right to terminate this Agreement immediately upon breach of this Agreement by you.

7. You shall indemnify, defend and hold harmless WILEY, its Licensors and their respective directors, officers, agents and employees, from and against any actual or threatened claims, demands, causes of action or proceedings arising from any breach of this Agreement by you.

8. IN NO EVENT SHALL WILEY OR ITS LICENSORS BE LIABLE TO YOU OR ANY OTHER PARTY OR ANY OTHER PERSON OR ENTITY FOR ANY SPECIAL, CONSEQUENTIAL, INCIDENTAL, INDIRECT, EXEMPLARY OR PUNITIVE DAMAGES, HOWEVER CAUSED, ARISING OUT OF OR IN CONNECTION WITH THE DOWNLOADING, PROVISIONING, VIEWING OR USE OF THE MATERIALS REGARDLESS OF THE FORM OF ACTION, WHETHER FOR BREACH OF CONTRACT, BREACH OF WARRANTY, TORT, NEGLIGENCE, INFRINGEMENT OR OTHERWISE (INCLUDING, WITHOUT LIMITATION, DAMAGES BASED ON LOSS OF PROFITS, DATA, FILES, USE, BUSINESS OPPORTUNITY OR CLAIMS OF THIRD PARTIES), AND WHETHER OR NOT THE PARTY HAS BEEN ADVISED OF THE POSSIBILITY OF SUCH DAMAGES. THIS LIMITATION SHALL APPLY NOTWITHSTANDING ANY FAILURE OF ESSENTIAL PURPOSE OF ANY LIMITED REMEDY PROVIDED HEREIN.

9. Should any provision of this Agreement be held by a court of competent jurisdiction to be illegal, invalid, or unenforceable, that provision shall be deemed amended to achieve as nearly as possible the same economic effect as the original provision, and the legality, validity and enforceability of the remaining provisions of this Agreement shall not be affected or impaired thereby.

10. The failure of either party to enforce any term or condition of this Agreement shall not constitute a waiver of either party's right to enforce each and every term and condition of this Agreement. No breach under this agreement shall be deemed waived or excused by either party unless such waiver or consent is in writing signed by the party granting such waiver or consent. The waiver by or consent of a party to a breach of any provision of this Agreement shall not operate or be construed as a waiver of or consent to any other or subsequent breach by such other party.

11. This Agreement may not be assigned (including by operation of law or otherwise) by you without WILEY's prior written consent.

12. Any fee required for this permission shall be non-refundable after thirty (30) days from receipt.

13. These terms and conditions together with CCC’s Billing and Payment terms and conditions (which are incorporated herein) form the entire agreement between you and WILEY concerning this licensing transaction and (in the absence of fraud) supersedes all prior agreements and representations of the parties, oral or written. This Agreement may not be amended except in writing signed by both parties. This Agreement shall be

binding upon and inure to the benefit of the parties' successors, legal representatives, and authorized assigns.

14. In the event of any conflict between your obligations established by these terms and conditions and those established by CCC's Billing and Payment terms and conditions, these terms and conditions shall prevail.

15. WILEY expressly reserves all rights not specifically granted in the combination of (i) the license details provided by you and accepted in the course of this licensing transaction, (ii) these terms and conditions and (iii) CCC's Billing and Payment terms and conditions.

16. This Agreement will be void if the Type of Use, Format, Circulation, or Requestor Type was misrepresented during the licensing process.

17. This Agreement shall be governed by and construed in accordance with the laws of the State of New York, USA, without regards to such state's conflict of law rules. Any legal action, suit or proceeding arising out of or relating to these Terms and Conditions or the breach thereof shall be instituted in a court of competent jurisdiction in New York County in the State of New York in the United States of America and each party hereby consents and submits to the personal jurisdiction of such court, waives any objection to venue in such court and consents to service of process by registered or certified mail, return receipt requested, at the last known address of such party.

Wiley Open Access Terms and Conditions

All research articles published in Wiley Open Access journals are fully open access: immediately freely available to read, download and share. Articles are published under the terms of the Creative Commons Attribution Non Commercial License. which permits use, distribution and reproduction in any medium, provided the original work is properly cited and is not used for commercial purposes. The license is subject to the Wiley Open Access terms and conditions:
Wiley Open Access articles are protected by copyright and are posted to repositories and websites in accordance with the terms of the Creative Commons Attribution Non Commercial License. At the time of deposit, Wiley Open Access articles include all changes made during peer review, copyediting, and publishing. Repositories and websites that host the article are responsible for incorporating any publisher-supplied amendments or retractions issued subsequently.
Wiley Open Access articles are also available without charge on Wiley's publishing platform, **Wiley Online Library** or any successor sites.

Use by non-commercial users

For non-commercial and non-promotional purposes individual users may access, download, copy, display and redistribute to colleagues Wiley Open Access articles, as well as adapt, translate, text- and data-mine the content subject to the following conditions:

- The authors' moral rights are not compromised. These rights include the right of "paternity" (also known as "attribution" - the right for the author to be identified as such) and "integrity" (the right for the author not to have the work altered in such a way that the

author's reputation or integrity may be impugned).

- Where content in the article is identified as belonging to a third party, it is the obligation of the user to ensure that any reuse complies with the copyright policies of the owner of that content.
- If article content is copied, downloaded or otherwise reused for non-commercial research and education purposes, a link to the appropriate bibliographic citation (authors, journal, article title, volume, issue, page numbers, DOI and the link to the definitive published version on Wiley Online Library) should be maintained. Copyright notices and disclaimers must not be deleted.
- Any translations, for which a prior translation agreement with Wiley has not been agreed, must prominently display the statement: "This is an unofficial translation of an article that appeared in a Wiley publication. The publisher has not endorsed this translation."

Use by commercial "for-profit" organisations

Use of Wiley Open Access articles for commercial, promotional, or marketing purposes requires further explicit permission from Wiley and will be subject to a fee. Commercial purposes include:

- Copying or downloading of articles, or linking to such articles for further redistribution, sale or licensing;
- Copying, downloading or posting by a site or service that incorporates advertising with such content;
- The inclusion or incorporation of article content in other works or services (other than normal quotations with an appropriate citation) that is then available for sale or licensing, for a fee (for example, a compilation produced for marketing purposes, inclusion in a sales pack)
- Use of article content (other than normal quotations with appropriate citation) by for-profit organisations for promotional purposes
- Linking to article content in e-mails redistributed for promotional, marketing or educational purposes;
- Use for the purposes of monetary reward by means of sale, resale, licence, loan, transfer or other form of commercial exploitation such as marketing products
- Print reprints of Wiley Open Access articles can be purchased from: corporatesales@wiley.com

Other Terms and Conditions:

BY CLICKING ON THE "I AGREE..." BOX, YOU ACKNOWLEDGE THAT YOU HAVE READ AND FULLY UNDERSTAND EACH OF THE SECTIONS OF AND PROVISIONS SET FORTH IN THIS AGREEMENT AND THAT YOU ARE IN AGREEMENT WITH AND ARE WILLING TO ACCEPT ALL OF YOUR OBLIGATIONS AS SET FORTH IN THIS AGREEMENT.

v1.7

If you would like to pay for this license now, please remit this license along with your payment made payable to "COPYRIGHT CLEARANCE CENTER" otherwise you will be invoiced within 48 hours of the license date. Payment should be in the form of a check or money order referencing your account number and this invoice number RLNK500721103.
Once you receive your invoice for this order, you may pay your invoice by credit card. Please follow instructions provided at that time.

Make Payment To:
Copyright Clearance Center
Dept 001
P.O. Box 843006
Boston, MA 02284-3006

For suggestions or comments regarding this order, contact RightsLink Customer Support: customercare@copyright.com or +1-877-622-5543 (toll free in the US) or +1-978-646-2777.

Gratis licenses (referencing $0 in the Total field) are free. Please retain this printable license for your reference. No payment is required.

VITA

Birm-June Kim was born in Seoul, South Korea. He attended Kookmin University, where he received his Bachelor of Science degree in Forest Products and Biotechnology in February 1997. After that, he joined South Korean Army and worked there as a signal officer until September 2000. He returned to research field and continued his study at the Graduate School of Seoul National University and received his Master of Science degree in Environmental Materials Science in February 2004. Afterwards, in August 2008, he attended Louisiana State University for his doctoral program in the School of Renewable Natural Resources and continued his research. Birm-June Kim will receive the degree of Doctor of Philosophy in May 2012.